Control and Operation of HVDC Connected Offshore Windfarm with Particular Emphasis on Faults and Black Start

Lei Shi

A thesis presented in fulfilment of the requirements for the degree of

Doctor of Philosophy

Department of Electronic and Electrical Engineering

University of Strathclyde, Glasgow, UK

October 2020

This thesis is the result of the author's original research. It has been composed by the author and has not been previously submitted for examination which has led to the award of a degree.

Signed: Date:

Acknowledgements

I would like to express my gratitude to all those who helped me during my life in UK. The PhD program is an unforgotten experience for me.

First and foremost, I would like to express my sincerest gratitude to my supervisor, Professor Lie Xu, who encouraged and inspired me during the most difficult time in my PhD life. His profound knowledge, rigorous research attitude and research enthusiasm will benefit me for life. I would like to express my heartfelt thanks to him again and hope our cooperation will go well in the future research.

My special gratitude goes to, Dr. Grain P Adam and Dr. Rui Li who gave me valuable comments and suggestions for my research. I would like to thank Dr. Derrick Holliday, Dr. Agusti Egea Alvarez, and other colleagues in PEDEC research group for all the help and advices.

Grateful acknowledgement is made to my friends, Wang Xiang, Yujie Lu, Kai Huang, Ding Zhou, Yin Chen, Xiaozuo Huang, Deyang Guo Shuren Wang Yuan Lu and Yiran Jing, for all concerns and companies in the past time.

Finally, I would like to express my most gratitude to my family, for their support during my PhD journey.

Abstract

High voltage direct current (HVDC) technology has been identified as a preferred choice for long-distance offshore wind power transmission. However, compared with conventional onshore networks, the dynamic behaviour and operation of power electronic based offshore network is significantly different, especially during offshore grid disturbances. Thus, to ensure a secure and reliable power transmission, this thesis investigates the different fault characteristics of HVDC connected offshore windfarm systems and proposes several fault rides through control and system recovery schemes.

The first topic discussed in this thesis is the offshore AC fault ride through operation. When modular multilevel converter (MMC) based HVDC connection is used for offshore windfarm system, the responses of both the offshore MMC station and wind turbine (WT) converters need to be carefully designed to ensure their safety operation during offshore AC faults. Maintain balanced and controlled current contribution to offshore AC grid during asymmetrical AC fault is possible, but it has several drawbacks such as increased risk of protection failure due to the absence of sufficient fault currents, and the inability of post-fault AC voltage recovery. Therefore, based on a detailed sequence network analysis, an enhanced control strategy is proposed during offshore asymmetrical faults to exploit the induced negative sequence and zero sequence voltages to facilitate controlled injection of negative sequence current while avoiding excessive overvoltage in the healthy phases. By adopting the proposed control, the AC fault current can be well regulated and the voltage restoration after fault clearance can be achieved as demonstrated by detailed simulation studies.

After the evaluation of offshore AC faults, the second research topic of this thesis moves to the offshore DC fault ride through operation. In a multi-terminal DC (MTDC) grid that connects multiple offshore windfarms, continued operation in an effort to

retain large proportion of power transfer during a DC fault is very important for critical power corridors. Partially selective protection which only installs fast acting DC circuit breakers (DCCBs) in limited cable locations while the main protection uses cheap DC disconnectors and AC circuit breakers (ACCBs), is a cost-effective solution. However, such protection scheme requires significant modifications to WTs control in order to retain the offshore AC network to ensure fast system recovery after fault isolation. Detailed analysis reveals that the sudden MMC blocking or opening of ACCBs due to the DC fault clearance can cause significant over-voltage and over-frequency in the offshore AC grid, which could necessitate immediate shutdown of the wind farm and damage the offshore infrastructure. To tackle these issues, an enhanced control for wind turbine (WT) converters is proposed to facilitate seamless transition of the WT converters between grid following and forming modes to maintain the offshore AC grid stable when the control from the offshore MMC is lost. The viability of the proposed control is demonstrated in wider context of partially selective DC fault protection in a meshed DC grid. The proposed control method ensures the continuous control of the offshore AC networks and enables the fast power transfer restoration.

Finally, a black start service aiming to support the onshore power networks restoration provided by the diode rectifier (DR) based HVDC connected windfarm is studied. A new frequency-AC voltage (*f*-*V*) droop control of WT converters is proposed to dynamically regulate the offshore AC voltage to ensure the DC voltage of the DR-HVDC link remains in the safe range when the active power consumption by the onshore network varies during black start. The detailed sequential black start is demonstrated, including DR-HVDC link energization, onshore AC voltage build-up and load pick up. Comprehensive simulation results confirm the validity of the proposed black start scheme using DR-HVDC connected offshore wind farms.

List of Abbreviations

CCSC	Circulating Current Suppression Controller
DR	Diode Rectifier
DR-HVDC	Diode Rectifier HVDC
DCCBs	DC Circuit Breakers
DCSWs	DC Switches
EU	European Union
FBSM	Full Bridge Submodule
GSC	Generator-Side Converter
HBSM	Half Bridge Submodule
HVAC	High Voltage Alternating Current
HVDC	High Voltage Direct Current
IGBT	Insulated Gate Bipolar Transistor
LCC	Line Commutated Converter
LSC	Line-Side Converter Modular
MMC	Modular Multilevel Converter
MTDC	Multi-Terminal HVDC
PCC	Point of Common Coupling
PLL	Phase Locked Loop
PMSG	Permanent Magnet Synchronous Generator
PWM	Pulse Width Modulation
PR	Proportional Resonance
PIR	Pre-insert Resistor
VSC	Voltage Source Converter
WT	Wind Turbine

SM	Submodules

List of Symbols

MMC modelling symbols

V_{sm}	Output voltage of the SM
j	Phase $j=a,b,c$
v_{uj}	Upper arm voltages
v_{lj}	Low arm voltages
i_{uj}	Upper arm currents
i_{lj}	Low arm currents
i_j	Phase currents
i_{jcm}	Common mode currents
e_j	inner emf
E_j	MMC three-phase terminal voltage
V_{dc}	DC voltage of the MMC
L_{arm}	Arm inductance
i_{dc}	DC current of MMC
θ	Angle between reference of rotation frame and phase A voltage
ω	Offshore grid voltage angular velocity
ς	Damping ratio
I_{pcc}	Current flowing from the WTs to the PCC bus
I_{MMC}	Current following into the offshore MMC station
C	The MMC equivalent AC capacitance seen at the PCC point

Sequence network symbols

E_{MMC}^{j}	Phase j $(j=a,b,c)$ voltage of the offshore MMC station

I_{MMC}^{j}	Phase *j (j=a,b,c)* current of the offshore MMC station
E_{WT}^{j}	Phase *j (j=a,b,c)* voltage of the WTs
I_{WT}^{j}	Phase *j (j=a,b,c)* current of the WTs
V_{F}^{j}	Phase *j (j=a,b,c)* voltage at fault point
I_{F}^{j}	Phase *j (j=a,b,c)* current at fault point
Z_{MMC}	Equivalent impedances on the offshore MMC
Z_{WT}	Equivalent impedances on the offshore WTs
Z_{F}	Fault impedance
$\mathbf{E}_{WT}^{abc}$	Column vectors of the aggregate windfarm converter voltages in time domain
$\mathbf{E}_{MMC}^{abc}$	Column vectors of the offshore MMC voltages in time domain
$\mathbf{V}_{F}^{abc}$	Column vectors of the fault point voltages in time domain
$\mathbf{I}_{WT}^{abc}$	Column vectors of the aggregate windfarm converter currents in time domain
$\mathbf{I}_{MMC}^{abc}$	Column vectors of the offshore MMC currents in time domain
$\mathbf{I}_{F}^{abc}$	Column vectors of the fault point currents in time domain
Z_{MMC}	Column vectors of MMC impedance in time domain
Z_{WT}	Column vectors of WTs impedance in time domain
$\mathbf{E}_{WT}^{+-0}$	Column vectors of the aggregate windfarm converter voltages in sequence domain
$\mathbf{E}_{MMC}^{+-0}$	Column vectors of the offshore MMC voltages in sequence domain
$\mathbf{V}_{F}^{+-0}$	Column vectors of the fault point voltages in sequence domain

$\mathbf{I}_{WT}^{+-0}$	Column vectors of the aggregate windfarm converter currents in sequence domain
$\mathbf{I}_{MMC}^{+-0}$	Column vectors of the offshore MMC currents in sequence domain
$\mathbf{I}_{F}^{+-0}$	Column vectors of the fault point currents in sequence domain

MMC connected offshore windfarm symbols

I_{MMC}	MMC grid side currents
E_{MMC}	MMC grid side voltages
I_{WT}	WTs grid side currents
E_{WT}	WTs grid side voltages
I_{CBx}	Current flows ACCB *x (with x=1-4)*

Meshed DC grid symbols

I_{dcx}	DC current on terminal *x (with x=1-4)*
V_{dcx}	DC voltage on terminal *x (with x=1-4)*
I_{Cxy}	Cable current from terminal *x* to *y* (*with x=1-4 and y=1-4)*
I_{dmax}	Maximum current limit for *d*-axis current
I_{dmax_v}	Maximum current limit for *d*-axis current imposed by passive V_{ac} controller
I_{qmax}	Maximum current limit for *q*-axis current
I_{qmax_v}	Maximum current limit for *q*-axis current imposed by passive V_{ac} controller
K_f	Droop coefficient between current and frequency
ω	Voltage angular frequency of offshore AC voltages

DR-HVDC connected offshore windfarm symbols

V_{dWT}	WT *d*-axis voltage
V_{qWT}	WT *q*-axis voltage
ω_{WT}	WT voltages angular frequency
V_{dcDR}	DR-HVDC link DC voltage
n	Rectifier transformer turns ratio
X_T	Leakage reactance of the DR transformer
I_{dcDR}	DR-HVDC link DC current
P_{DR}	DR-HVDC link DC power
k_Q	Droop gain between offshore WT reactive power and frequency
Q_{WT}	Reactive power of individual WT
V_{pcc}	Offshore PCC voltage
Q_{DR}	Reactive power consumed by the DR station
$P_{onshore}$	Onshore MMC AC power
P_{WT}	WT power

List of Figures

List of Tables

Table of Contents

Chapter 1

Introduction and Research Background

1.1 Offshore wind development

Due to increased environmental concerns, depletion of fossil fuels and to achieve net-zero carbon emission target, renewable power generation has gained huge growth globally. According to the 2020 Global Status Report [1], the total installed renewable power capacity was around 2588 GW by 2019, maintaining a more than 8% average growth rate over the previous five years.

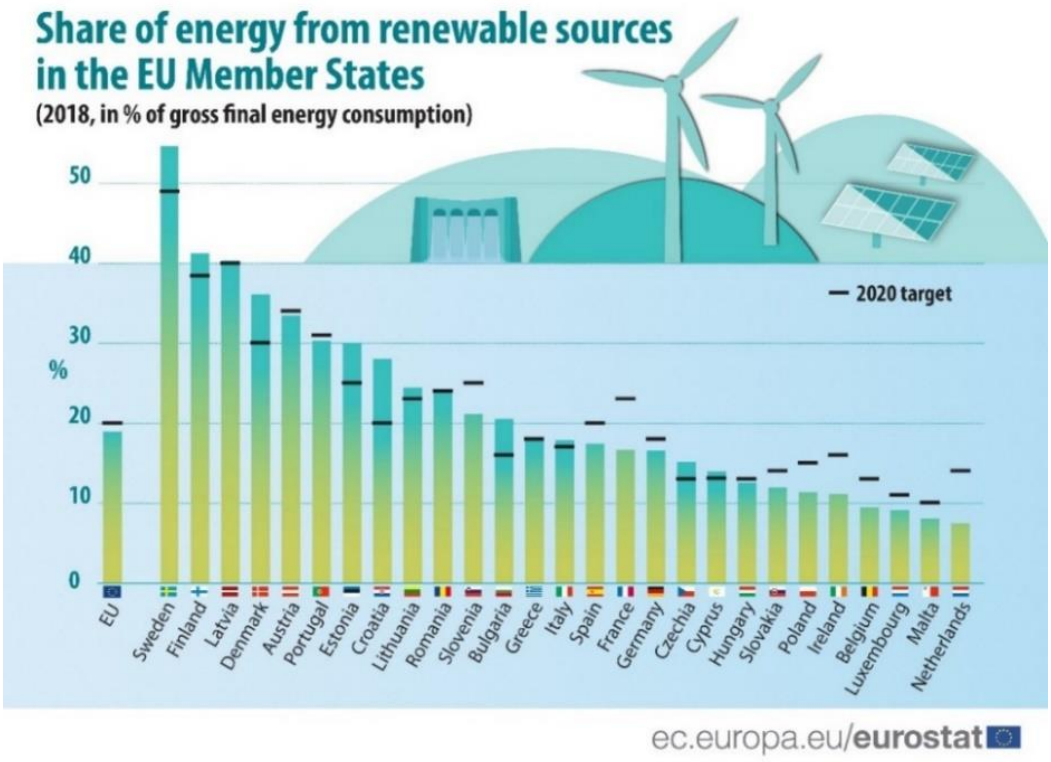

Fig. 1.1 Share of energy from renewable sources in the EU member states [2]

The European Commission has recently proposed a target of at least 32% energy consumed in the European Union (EU) to be from renewable energy sources (RESs) by 2030 [3]. According to European Environment Agency, renewable energy consumption in 2018 reaches 18% of total energy consumption and 16 EU member states reached or exceeded their own national renewable energy action plans, as shown in Fig. 1.

Due to the advantage of low environment impact and more consistent wind resources, offshore wind energy shows great promise to be a major electricity source in the near future and has grown rapidly [4, 5]. In 2019, EU connected 3,623 MW of net offshore wind power capacity, which reaches a new record in annual offshore installation and the cumulative installed capacity reaches 22,072 MW. Among the EU members, the United Kingdom leads the offshore installations in 2019 (1,764 MW in total), followed by Germany (1,111 MW) and Demark (374 MW) [6].

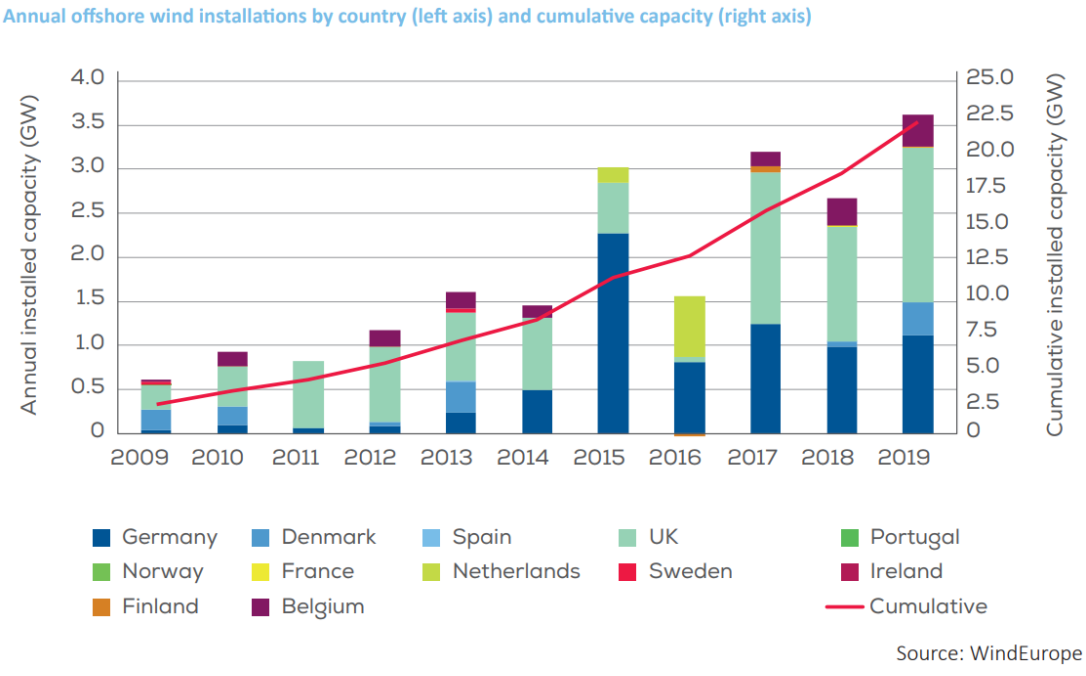

Fig. 1.2 Annual offshore wind installation in EU country

To date（2020）, the largest offshore wind farm in operation around the world is the Hornsea One with a capacity of 1218 MW, composed of 174 wind turbines rated at 7 MW provided by SIEMENS Gamesa [7]. To reduce the total investment cost of offshore windfarms, the power rating of offshore wind turbines has significantly increased in recent years. The average power rating of offshore WTs installed in 2019 was 7.8 MW, 15% larger than that in 2018 and the largest WTs reaches 14 MW with the rotor diameter of 222 m constructed by SIEMENS [8].

1.2 Offshore wind power transmission solutions

High voltage AC (HVAC) and HVDC are the two technologies that have been employed as the main energy corridor connecting large offshore windfarms to the main grids. This section will give a brief introduction on both technologies and their respective advantages and drawbacks.

1.2.1 Offshore system topologies

HVAC is a well-established transmission technology and has been used in many projects (e.g., Hornsea One). Fig. 1.3 shows the typical topology of HVAC connected offshore wind farms, which consists of generator assets, transmission assets and onshore grid [9]. WTs in offshore wind farms are connected through different array cables (typically 33 kV or 66 kV) to the point of common coupling (PCC) as an initial collection grid. Then, step-up transformer installed at offshore substation boosts the AC voltage from collection level to transmission level, e.g. 132 kV or 220 kV. Depending on the cable length, reactive power compensation may have to be used which are usually installed on onshore substation to compensate required reactive power for HVAC cables. Finally, wind power is exported to onshore grid through the

subsea three-phase AC cables.

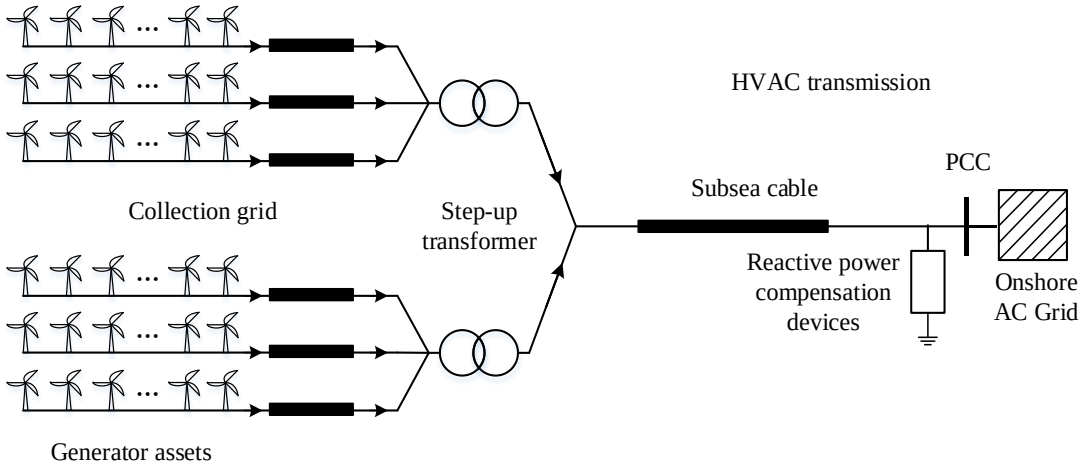

Fig. 1.3 Layout of the HVAC connected offshore wind farms.

HVDC technology is an alternative solution for offshore wind power transmission and has already been employed in a number of projects, e.g. DolWin 1 [10]. Fig. 1.4 shows a typical layout of a HVDC connected offshore windfarm. Similar to the HVAC, WTs are connected through different array cables with voltage rated at 33 kV or 66 kV to the PCC for collection. Step-up transformers further boost the AC voltage to around 200 kV and then connects to a converter transformer and HVDC rectifier to convert the offshore AC power to DC power, which is transmitted to onshore through HVDC cables. Then the DC power is converted to AC power by a DC-AC converter and exported to onshore AC grid.

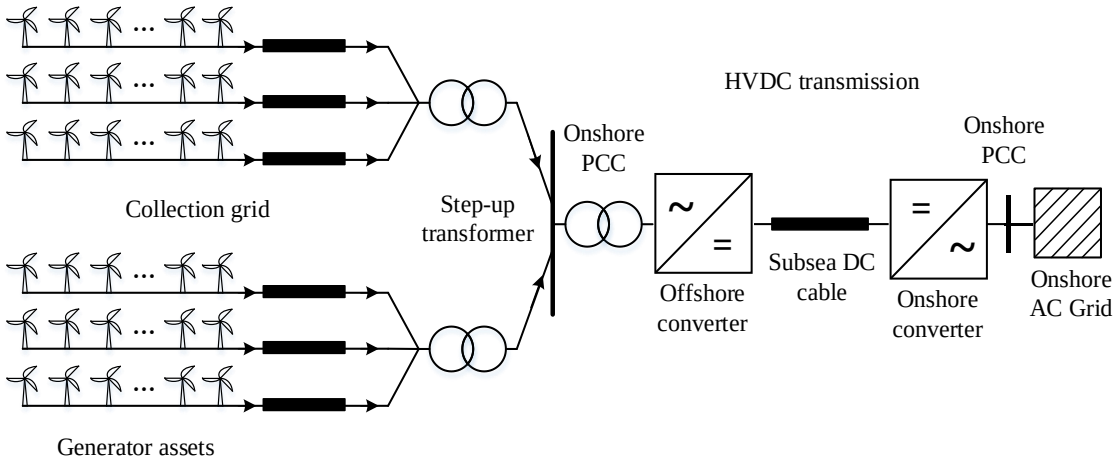

Fig. 1.4 Layout of the HVDC connected offshore wind farms.

1.2.2 Comparison between HVAC and HVDC system

HVAC system as a conventional power transmission system, has been widely used in near-shore windfarm system due to its simple structure with low investment cost. However, as the offshore AC grid and onshore power system are synchronously coupled, faults can propagate on both sides which could lead to system failures [11-14]. In addition, due to high capacitance of the HVAC cables, system resonances between the onshore and offshore AC grids and the charging current for long AC cables reduce the transmission capability and increase power losses which limits the HVAC system application for long distance offshore system application [15].

References [13] compare the costs on HVAC and HVDC transmission system for offshore wind farm connecting. As shown in Fig. 1.5, the total cost for the HVDC transmission system is lower than the HVAC system when the distance is over the breakeven distance.

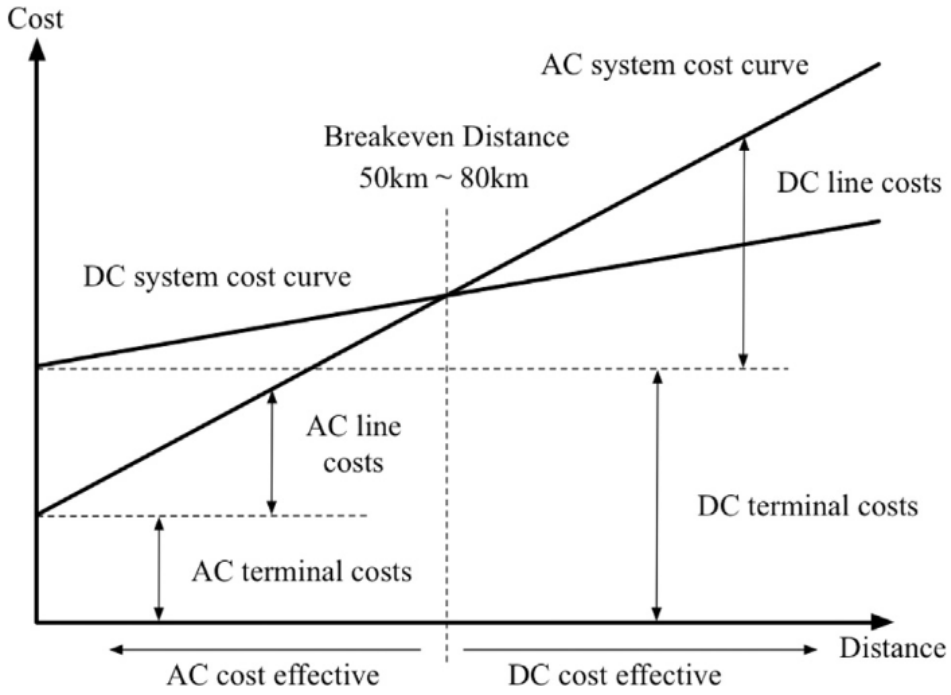

Fig. 1.5 Cost comparison of HVDC and HVAC transmission systems [13].

However, HVDC system, which utilizes the advanced power electronics devices can effectively decouple the onshore AC and offshore AC system. The interaction between onshore and offshore system during system transient can be minimized. Also, as no charging current in DC cable, the technically maximum transmitted power is largely independent with the transmission distance and the overall losses is lower than HVAC system. Besides, the voltage source convert (VSC) based HVDC system can provide the voltage regulation capability which can be utilized to support the onshore during grid disturbances and establish the offshore AC voltage and frequency. This simplify the offshore WTs controller design. Such features make VSC based HVDC system more attractive for connecting future large offshore wind power plants over long distances[11-13].

1.3 Research motivation

The future large-scale offshore windfarms transmission system is normally planned far from shore due to the limited space availability in near-shore and more stable wind resources in offshore. Such system should have very high reliability due to the long restoration time and high maintenance cost. Moreover, the commercially used VSC-HVDC connected offshore windfarm system is mainly constructed with power electronics devices and the offshore network is formed by the HVDC converter and WT converters. Compared with traditional power system, such converter based system has no rotating machines and is extremely vulnerable to overcurrent and overvoltage in the event of a network fault [16]. On the other side, adequate fault current contribution from converters would help fault detection and fault isolation. Thus, the system control and protection algorithm during offshore grid disturbances need to be elaborated.

For offshore AC system, the fault characteristics are mainly dominated by converter control algorithm. So far, the symmetrical AC fault has been studied in several research work and reported that the existing converter control (grid forming and grid feeding [17]) can successfully ride through the severe symmetrical AC fault with limited fault current injection to prevent the converter damage [18, 19]. However, the situation becomes more challenging for offshore asymmetric faults in terms of negative sequence voltage/current control algorithm provision from both the HVDC and WT converters as it has shown that inadequate setting of negative sequence currents for the offshore HVDC grid forming converter could lead to problematic behaviours and thus, need further investigation[10, 20].

DC fault protection is another major technical obstacle that prevent the development of offshore HVDC based windfarm and has drawn significant attention

from academia and industry [21-23]. In addition, serval studies and projects concluded that the multi-terminal DC network can increase the offshore wind power reliability by reducing the overall downtimes of "loss of infeed" and can provide links between different area to lower the system investment and operation cost [24-26]. Among the different DC fault clearance strategy [27, 28], the partially selective protection which only installs the expensive and large footprint DC circuit breakers (DCCBs) in limited cable locations while the main protection uses cheap DC disconnectors and AC circuit breakers (ACCBs), can be a cost-effective solution [29]. However, as the offshore AC network is usually controlled by the offshore HVDC converter, the offshore system voltage regulation ability would deteriorate if the HVDC station is lost during DC faults due to either converter blocking or the opening of the main offshore ACCBs. This could potentially lead to the shutdown of the complete offshore system and a prolonged system recovery process [30, 31]. Thus, a special concern needs to be taken when designing the WT control and protection scheme such that the offshore AC system can be retained in such events to ensure fast system restoration after DC fault clearance.

Moreover, the increasing penetration of renewable energy and the gradual reduction of conventional power generation potentially increase the risk of wide-area blackouts, especially in strongly linked networks [32]. Large HVDC connected offshore windfarms as a more stable energy compared with other renewable sources has been proposed to provide fast black start services (e.g. the ENTSO-E requires the renewable energy sources to provide the black start service to AC system) [4, 16, 33]. The technical challenges associated with different stages of energization when HVDC connected offshore windfarms are used for black start have been identified and discussed in [33-35]. DR-HVDC system has recently been proposed for integrating large offshore windfarms due to its lower transmission losses and total investment cost compared to VSC (e.g. MMC) based systems. However, the potentials in using

offshore wind farms connected to DR-HVDC system for black start of onshore networks have not been explored, especially considering the distinctive features of WT control in such a system.

1.4 Author's publications

[1] L. Shi, G. P. Adam, R. Li and L. Xu, "Control of Offshore MMC During Asymmetric Offshore AC Faults for Wind Power Transmission," in *IEEE Journal of Emerging and Selected Topics in Power Electronics*, vol. 8, no. 2, pp. 1074-1083, June 2020, doi: 10.1109/JESTPE.2019.2930399.

Abstract: The adoptions of medium-voltage in AC collection networks of large DC connected wind farms significantly increase the AC current magnitudes during normal and fault conditions. Controlling fault currents at zero during asymmetric AC faults is possible, but it has several drawbacks such as increased risk of protection mal-operation due to absence of fault currents, which also tends to prevent the recovery of AC voltage in post-fault. Therefore, this paper presents an enhanced control strategy that exploits the induced negative sequence voltages to facilitate controlled injection of negative sequence currents during asymmetric AC faults. The proposed control not only defines a safe level of fault current in the offshore AC network but also instigates immediate recovery of the AC voltage following clearance of AC faults, which avoid protection mal-operation. In addition, the positive sequence voltage set-point of the offshore modular multilevel converter (MMC) is actively controlled by considering the negative and zero sequence voltages, which effectively avoids the excessive overvoltage in the healthy phases during asymmetrical AC faults. The theoretical basis of the proposed control scheme is described, and its technical viability is assessed using simulations.

[2] L. Shi, G. P. Adam, R. Li and L. Xu, "Enhanced Control of Offshore Wind Farms Connected to MTDC Network Using Partially Selective DC Fault Protection," in *IEEE Journal of Emerging and Selected Topics in Power Electronics*, doi: 10.1109/JESTPE.2020.2985129.

Abstract: In recent years, several DC fault clearance schemes have emerged, in which reduced number of fast acting DC circuit breakers (DCCBs) and AC circuit breakers (ACCBs) are used to clear DC faults. In offshore DC grids, such approach entails opening of the ACCBs that connect the wind farms to the offshore HVDC stations which control offshore AC voltages and frequencies, potentially leading to uncontrolled offshore voltage and frequency. Existing studies show that the loss of offshore converter due to blocking or sudden opening of ACCBs can cause significant over-voltage and over-frequency in the offshore AC grid, which could necessitate immediate shutdown of the wind farm. An enhanced control for wind turbine converters (WTCs) of the offshore wind farm is proposed to enable retention of AC voltage and frequency control when the offshore converter is lost, in which seamless transition of the WTCs between grid following and forming modes is facilitated. The viability of the proposed control is demonstrated in wider context of partially selective DC fault protection in an illustrative meshed DC grid, which includes detailed implementations of DC fault clearance, system restart and power transfer resumption. The presented simulation results confirm the effectiveness of the proposed WTC control in preventing excessive rise of offshore AC voltage and frequency and facilitating DC fault ride-through using reduced number of DCCBs.

[3] L. Shi, R. Li, L. Xu and G. P. Adam, "Enhanced Control of DR-HVDC Connected

Offshore Wind Farms for Black Start," in *IEEE Transactions on Power Delivery* (under review)

Abstract: The use of diode rectifier (DR) HVDC connected offshore wind farms to provide black start service for onshore AC grid is investigated in this paper. A new frequency-AC voltage (*f- V*) droop control of wind turbine converters is proposed to dynamically regulate the offshore AC voltage according to the offshore frequency to ensure the DC voltage of the DR-HVDC link remains in the safe range. By utilizing the active power-reactive power-frequency (*P-Q-f*) coupling characteristics of DR-HVDC systems, the proposed control enables WTs to automatically detect the operation condition of the DR-HVDC link without communication to balance the offshore and onshore power. In the event of onshore grid faults during black start, the proposed control automatically reduces the offshore AC voltage and overvoltage of the HVDC link is thus avoided. When certain WTs' available wind power is low, the power required by onshore loads is redistributed among WTs with the proposed control and the DC voltage of DR-HVDC link is largely unaffected. Black start of the onshore AC grid using the DR-HVDC connected wind farm is demonstrated, including DR-HVDC link energization, onshore AC voltage build-up and load pick up. Comprehensive simulation results confirm the validity of the proposed black start scheme.

[4] L. Shi, G. P. Adam, R. Li and L. Xu, "Interoperability assessment of MMC and DRU connected offshore windfarms in meshed multi-terminal DC grids," *8th Renewable Power Generation Conference (RPG 2019)*, Shanghai, China, 2019, pp. 1-7, doi: 10.1049/cp.2019.0341.

Abstract: In the last decade, a number of academic and industry studies have identified

diode rectifier unit (DRU) as a potential replacement for offshore modular multilevel converter (MMC) of DC connected offshore windfarms. However, side-by-side operation of DRU and MMC connected windfarms in multi-terminal DC grid will present new operational challenges. Therefore, this paper will study the interoperability of a minimum meshed DC grid, which includes MMC and DRU connected offshore windfarms. To identify any potential issues that may arise from introduction of DRU, the system performance during onshore AC faults are simulated using PSCAD models. Simulation results show that the DRU connected windfarm exhibits different behaviours with the MMC based equivalent but does not adversely impact the DC grid performance. Instead, the use of DRU improves DC grid performance with its inherent sensitivity of active power transmission to DC voltage variation.

1.5 Thesis organization

This thesis is organised as follows:

Chapter 2 presents a general overview of HVDC systems connected offshore windfarms, including the configuration, system control and operation. System fault ride-through and black start services provided by offshore windfarm systems are also reviewed. Based on the review, several potential issues which have not been well addressed in literature are identified and discussed.

Chapter 3 presents the behaviours of MMC connected offshore windfarm system and theoretical analysis during offshore asymmetrical faults. Based on the analysis and potential issues, an enhanced AC voltage control is proposed to instigate immediate recovery of the AC voltage following clearance of AC faults, while avoiding overcurrent protection mal-operation with defined WT fault current contributions.

PSCAD simulations are provided to verify the effectiveness of the proposed control strategy.

Chapter 4 investigates DC fault handling strategies for MMC based meshed DC grid. Considering the use of partially selective DC fault protection scheme, the problems when the offshore MMC station is suddenly blocked during DC faults or the ACCBs in offshore AC grid suddenly open for fault clearance operation are analysed. An enhanced control for WT LSCs is then proposed to enable the retention of AC voltage and frequency control and provide the support during system recovery sequence. The viability and application of the proposed control is demonstrated using simulations.

Chapter 5 studies the use of DR-HVDC connected offshore wind farms for black start of onshore power networks. A WT frequency-AC voltage (f-V) droop control is proposed to dynamically regulate the offshore AC voltage to maintain the DC voltage of the DR-HVDC link in a safe range while keeps the power balance between the onshore and offshore grids during black start. Detailed sequential energization process of the DR-HVDC link and onshore AC network as well as load pick up are demonstrated through PSCAD simulations.

Chapter 6 draws the conclusions of the research and recommends further works.

Chapter 2
HVDC Connected Offshore Windfarm Systems

As discussed in Chapter 1, HVDC transmission system is the most suitable technology to connect future large offshore windfarms over long-distance. At present, a number of projects have already been in operation and the control and operation of HVDC systems and offshore wind farms have been extensively studied. This chapter provides a general overview of the different configurations, fault ride-through operation and the black start operation of HVDC connected offshore wind farm systems.

2.1 Configuration of HVDC system for offshore wind power transmission

For connecting large offshore windfarms, the HVDC transmission structures can be designed as point-to-point links, parallel configurations and multi-terminal systems depending on different technical, geographical and economic requirements [36]. In addition, referring to the different types of offshore HVDC converters, HVDC transmission converter topologies can be classified as line commutated converter (LCC) -HVDC, VSC-HVDC, and DR-HVDC systems. Thus, this section will briefly introduce the possible different system topologies.

2.1.1 Point-to-point HVDC link

The point-to-point HVDC system has the simplest structure, which consists of an offshore rectifier station, which converts the offshore AC power into DC, and an onshore inverter which converts the DC power back to AC, then exports to onshore AC network. In the following subsections, the point-to-point configuration is introduced considering the use of different rectifier topologies.

a) LCC based HVDC

LCC, also known as current source converter, has been widely used in HVDC systems for onshore bulk power transmission due to its advantages of large capacity, high reliability and low power losses [37]. LCC uses thyristor valves and is usually arranged in a 12-pulse bridge configuration, as shown in Fig. 2.1. The 12-pulse bridge is formed of two 6-pulse bridges connected in series on DC side and in parallel on AC side through a star-star-delta transformer. Under such connections, harmonic currents (especially the 5^{th} and 7^{th}) generated by the thyristor bridges during operation are effectively eliminated on the common AC side. However, using LCC-HVDC for offshore wind power transmission has the following challenges:

- It needs an external voltage source for its commutation, which may require additional auxiliary equipment to establish a stable offshore network or the needs of WTs to form the offshore network.
- Large footprint and heavily weighted passive filters are required to eliminate harmonics and compensate reactive power consumption of LCC, which poses a big challenge for offshore platforms.
- It is vulnerable to commutation failure during onshore AC network disturbance, which would interrupt power transmission.

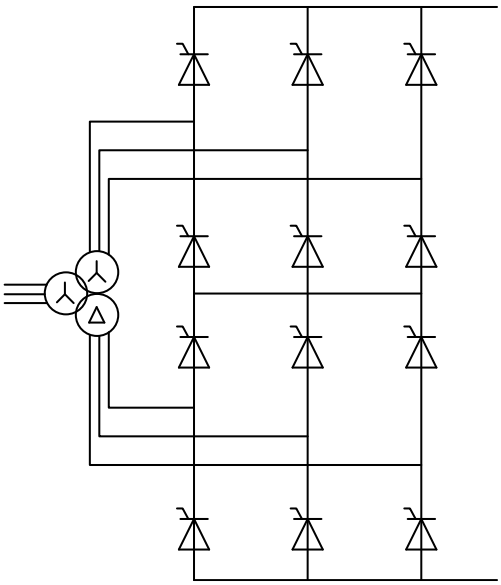

Fig. 2.1 Twelve-pulse bridge of LCC

b) VSC based HVDC

VSC-HVDC uses self-commutated insulated-gate-bipolar-transistors (IGBTs), which can be switched on and off at any time independent of the AC grid voltage and current [11]. Comparing with LCC-HVDC, VSC-HVDC offers the following advantages for offshore applications:

- Offshore VSC station can form offshore AC network voltages and start-up offshore WTs.
- VSC can independently control its active and reactive power and generates less harmonics. Thus, only small filters (or even no filter) are required. This leads to compact offshore converter station designs.

These features make VSC-HVDC more attractive for connecting offshore wind farms. Fig. 2.2 illustrates the basic two-level VSC circuit which consists of six IGBT switches, three-phase reactors and AC harmonic filters. Pulse-width-modulation (PWM) with high switching frequency is employed to synthesize a sinusoidal AC

voltage output. The main limitations of two-level VSC for offshore application are summarized as [11]:

- High switching frequency results in high power losses.
- Filters are required to reduce AC and DC harmonics.
- Large numbers of IGBTs are connected in series to withstand high DC voltage leading to significant technical challenges of voltage sharing.
- DC link capacitors' discharge leads to high fault current during DC faults.

To overcome the limitation of the 2-level VSC for high voltage application, MMC which was first proposed in 2003 [38] has been widely adopted in commercial projects and has been extensively studied in academia and industry.

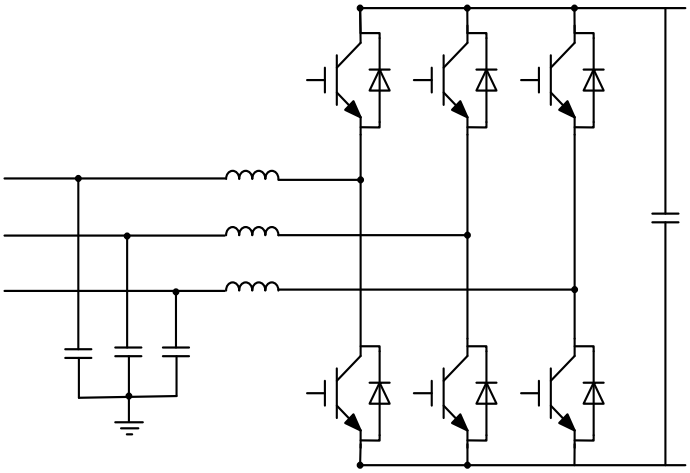

Fig. 2.2 Two-level VSC.

Fig. 2.3 a) illustrates the basic structure of an MMC. It consists of 6 arms and each arm contains a large number of series-connected submodules (SM). Half-bridge SM (HBSM) and full-bridge SM (FBSM), as shown in Fig. 2.3 b) and c) respectively, are two of the main SM configurations used for MMCs. Comparing with the two-level

VSC, MMC has the following advantages [39, 40]:

- Modular design with good scalability to meet high voltage requirements.
- Higher efficiency due to low switching frequency.
- High quality AC output waveforms, leading to small (or even no) AC filters.
- Reduced fault current during DC faults due to distributed DC link capacitors.
- DC fault ride-through capability for some of the SM topologies.

Due to the superior performance in high voltage applications, several MMC connected offshore windfarm projects are in operation, as listed in Table 2.1.

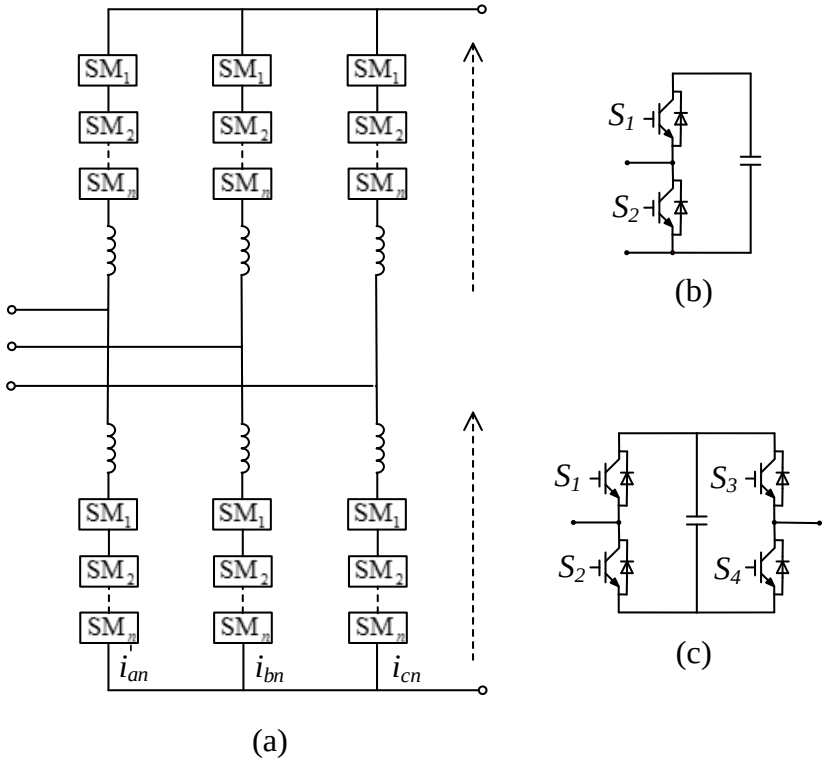

Fig. 2.3 MMC and two submodule topologies: a)MMC configuration b) HB SM and c) FB SM.

Table 2.1 Existing HVDC connected offshore windfarm projects [41]

No.	Project	V_{dc} (kV)	Rated power (MW)	DC cable (km)	Contractor
1	DolWin1	640	800	165	ABB
2	DolWin2	640	900	135	ABB
3	DolWin3	640	900	160	Alstom
4	HelWin1	500	576	130	Siemens
5	HelWin2	640	690	130	Siemens
6	BorWin1	300	400	200	ABB
7	BorWin2	600	800	200	ABB

c) DR-HVDC

DR-HVDC is another promising topology for offshore windfarm integration [42-44]. Fig. 2.4 illustrates the basic structure of a DR-HVDC system, where several DR stations are connected in series on the DC side to boost DC voltage while the AC sides are connected in parallel to the offshore wind farm network. Each DR station consists of a 12-pule bridge, a star-star-delta transformer, and filter banks for providing reactive power compensation. Compared with the previously presented HVDC transmission system, DR-HVDC has the benefits of lower investment, lower space requirement, and higher efficiency. Compared with MMC-HVDC for offshore wind farm connection, the offshore windfarm platforms and transmission losses can be reduced by 30% and 20%, respectively, while the total cost can be reduced by 30% [42, 43]. However, as the uncontrolled diode rectifier cannot provide offshore frequency and voltage control as the MMC counterpart does, WTs must perform more control functions.

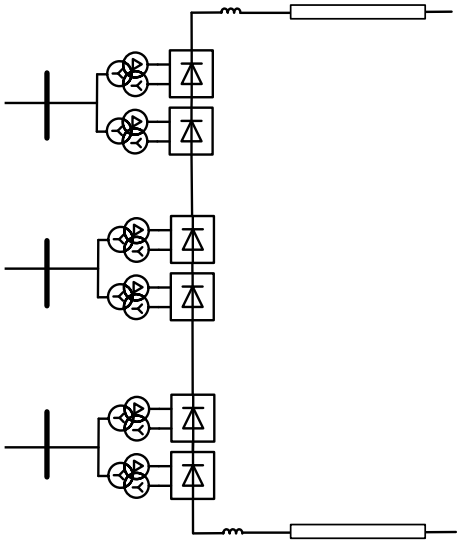

Fig. 2.4 Configuration of DR station

2.1.2 Parallel configurations and MTDC systems

Compared to the simplest and most commonly used point-to-point links, parallel and MTDC configurations increase power transmission capability and system availability but have more complex configurations and high control requirements.

a) Parallel configurations

A parallel connection of offshore windfarm system is illustrated in Fig. 2.5. The offshore windfarm is connected to the offshore AC collectors through offshore AC cables and transformers, and two parallel HVDC links are used to transmit the generated wind power to the onshore sites. With such a configuration, the availability of the system can be improved during fault scenarios. For example, when one HVDC link is out of service due to faults, the majority of the generated power can still be exported to onshore through the other link [45]. In such a parallel arrangement, extra controls need to be allocated to the offshore HVDC stations to allow proper power sharing [46].

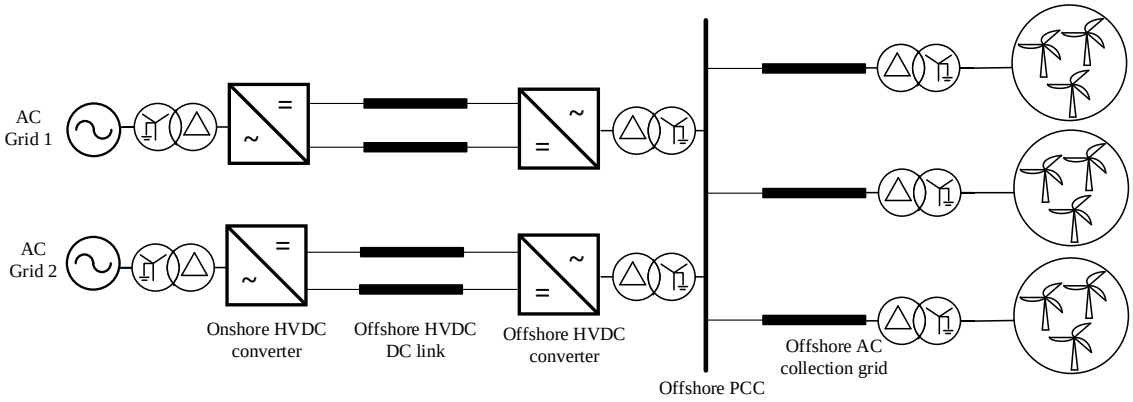

Fig. 2.5 Parallel connection of HVDC links for offshore wind power transmission

b) MTDC configurations

Fig. 2.6 illustrates a 4-terminal meshed MTDC network. Under such a connection, the availability of the system could be enhanced [47]. Various studies have shown that MTDC links improve power exchange flexibility between multiple areas and provide better system redundancy [48, 49]. To ensure stable operation and proper power-sharing, coordinated controls, such as droop control and master-slave control, have been well investigated in literature [50-53]. So far there are several MTDC network are employed (eg. Zhangbei 4-terminal HVDC project and Zhoushan 5-terminal HVDC project in China) [54, 55].

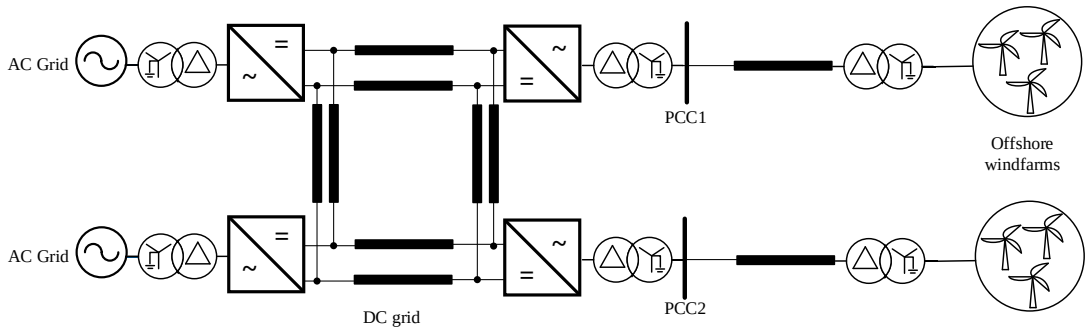

Fig. 2.6 MTDC system configuration

2.2 Control and operation of HVDC systems connected to offshore windfarms

The operation of HVDC connected offshore wind farms will be introduced in this section. In a point-to-point system, the onshore converter usually regulates the DC voltage of the HVDC link and transfers the received active power to onshore grid. For the offshore converter, the system operation mechanism is discussed in two scenarios, i.e., VSC-HVDC system with voltage regulation capability and DR-HVDC system without voltage regulation capability.

2.2.1 VSC-HVDC system

The operation of VSC-HVDC connected offshore windfarm has been well described in [19] with the control scheme illustrated in Fig. 2.7. The offshore MMC station is controlled to resemble an AC voltage source to regulate the offshore AC voltage and frequency. Thus, the control strategy adopted for WTs is the same as onshore AC connected WTs, e.g. the WT generator side converter (GSC) controls the active power generated by WTs to achieve the maximum power output while the line-side converter (LSC) controls the WT DC voltage and reactive power. The generated wind power is automatically absorbed by the offshore HVDC converter and converted to DC power. Thus, the offshore WTs are working under same control scheme as the onshore WTs.

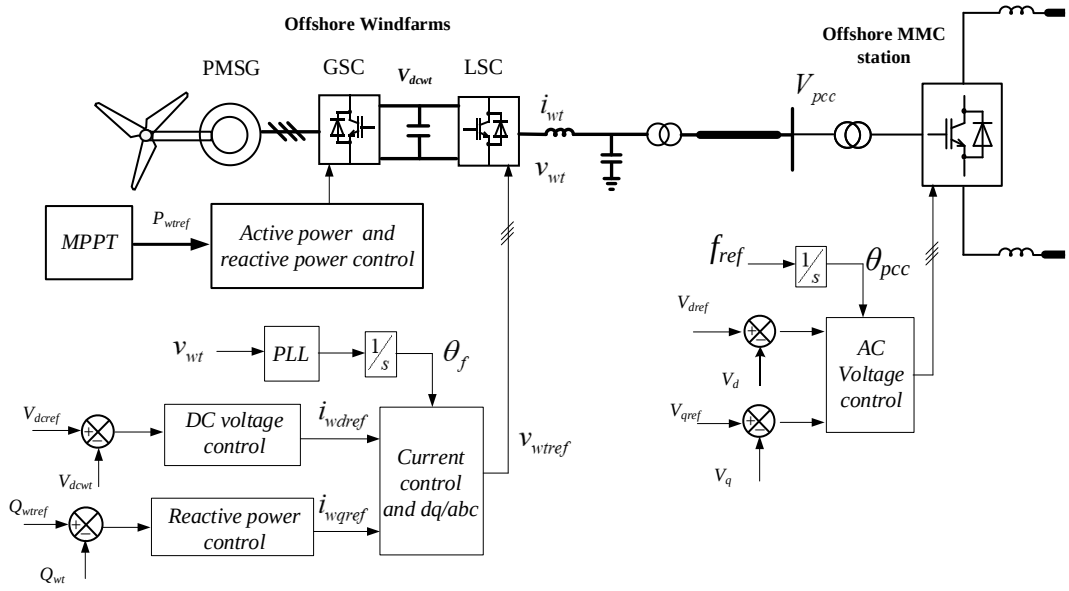

Fig. 2.7 Control diagrams of WTs and VSC-HVDC for offshore wind power transmission

2.2.2 DR-HVDC system

Using DR-HVDC system to connect offshore windfarm is investigated in [56-59]. In [59], the control strategy based on external centralized controllers is proposed, as shown in Fig. 2.8. The WT level control of this solution is similar to that when connected with VSC-HVDC. However, an external centralized controller is required to regulate the offshore frequency and voltage at the PCC, which are shared with all the WTs through communication. Thus, the system performance relies on reliable communication system, which may cause severe issues in the event of communication failure.

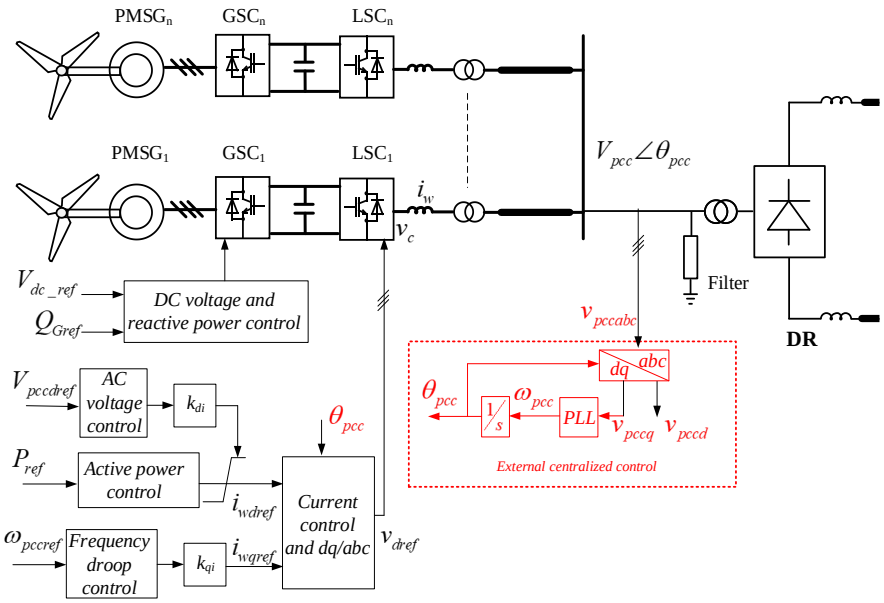

Fig. 2.8 Control and operation of WTs connected with DR-HVDC [41]

To address the communication issue, a distributed PLL based *P*-*V* and *Q*-*f* control is proposed in [58] as illustrated in Fig. 2.9. Such control method enables each WT converter to operate as a grid-forming source and autonomously contribute to the overall offshore voltage and frequency regulation, which provides WTs with plug-and-play capability for easy synchronization to the offshore network.

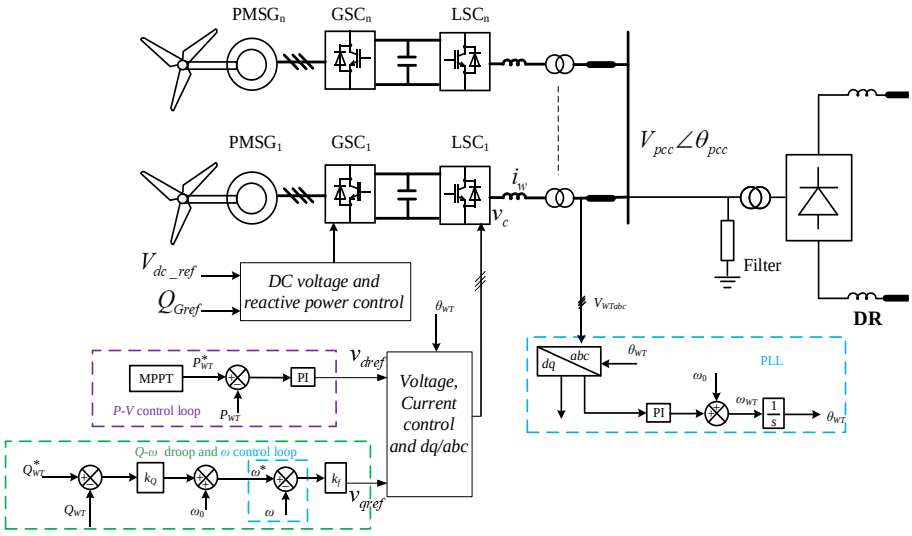

Fig. 2.9 Distributed PLL control for DR-HVDC connected offshore windfarms [40]

2.3 Fault ride-through of offshore windfarm systems

Compared with conventional power systems, the HVDC connected offshore wind farm system is mainly constructed with power electronics converters. Such system is extremely vulnerable to over-current and over-voltage in the event of a network fault [60]. Thus, system control and protection during various faults, including offshore and onshore AC faults, DC faults, are significantly important and need to be carefully considered and designed. Thus, this section reviews some of the existing fault ride-through strategies including converter control and protection strategies.

2.3.1 Offshore AC fault ride through operation

In the event of an offshore symmetrical AC fault, the rapid drop of offshore AC voltage could potentially lead to overcurrent of the offshore converter stations. To limit the fault current, the current-voltage droop method is proposed in [61], which adjusts the output voltage reference according to the measured offshore three-phase currents, as shown in Fig. 2.10. When the currents exceed the pre-defined threshold, the voltage is reduced accordingly to reduce the MMC output currents.

In addition to the direct voltage regulation method [61], the cascaded vector control with inner current loop and outer voltage loop has been proposed [18], which has the capability to limit the overcurrent during offshore AC faults. During offshore AC faults, the output current reference generated by the outer voltage loop will saturate and the current reference fed to the inner current controller is limited by the current limiter as illustrated in Fig. 2.11. Thus, thanks to the fast inner current control loop, the converter currents will be limited to the maximum set value, preventing potential converter overcurrent.

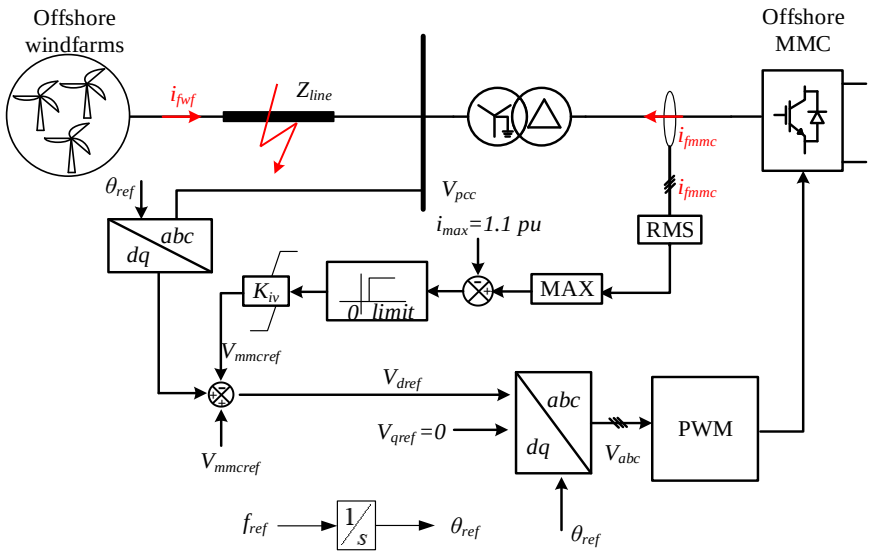

Fig. 2.10 Current-voltage droop control of offshore MMC to ride-through symmetrical offshore AC faults

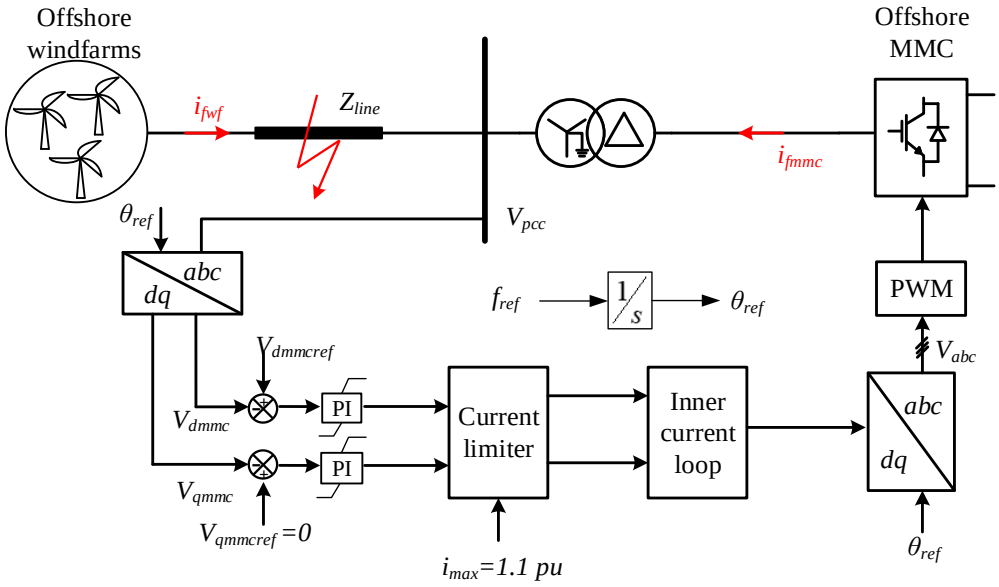

Fig. 2.11 Offshore MMC current limiting control during symmetrical offshore AC faults

In addition to symmetrical faults, system control and operation during asymmetrical offshore AC faults is another challenge for HVDC connected offshore

windfarms operation. During asymmetrical faults, VSCs can exhibit undesirable performance such as output current distortions, DC link voltage oscillations and output power oscillations. To tackled these issues, the use of double-synchronous reference frame for control of conventional VSCs, where the AC voltages and currents are decomposed into positive and negative sequence components, has been used [62-65]. These works have investigated a number of achievable operational objectives by adjusting the negative sequence current reference, as illustrated in Fig. 2.12 to improves VSCs' behaviours during asymmetrical faults. Such control objectives include suppression of negative sequence currents (for maintaining balanced AC currents), nullification of oscillating active power (for prevention of injection of double frequency oscillating power into DC side), etc.

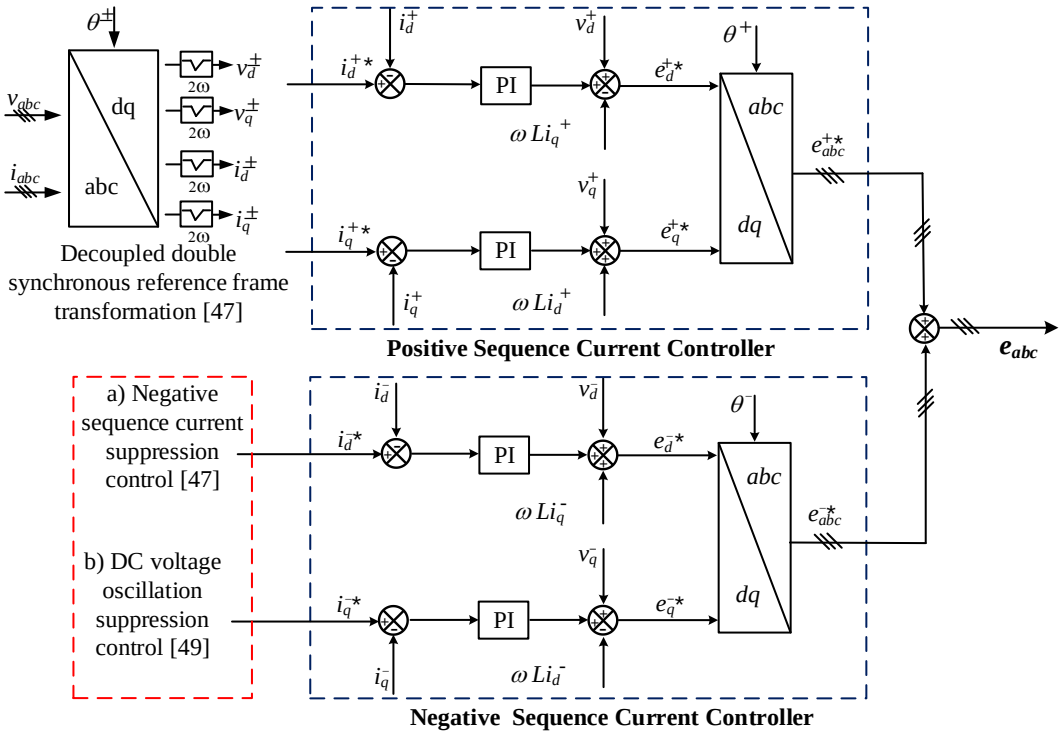

Fig. 2.12 Double-synchronous reference frame control strategy for negative sequence current regulation [62-65].

In addition, reference [66] reports that during asymmetrical fault (single phase to ground and phase to phase to ground), over-voltage may occur in non-faulty phases which could lead to the disconnection of the power generation set. An enhanced dynamic voltage control, which takes both grid positive and negative sequence voltages into consideration to prevent excessive rise of the AC voltage in the healthy phases is proposed to fulfil the German grid code in [66]. Simulation results reveal that the proposed scheme can maintain the voltage magnitudes of the healthy phases around 1.0 pu, while minimizing the voltage depression in the faulty phases. However, the work is based on grid-connected system, while the HVDC connected offshore windfarm system shows different behaviours. Thus, new control and analysis methods are required.

Reference [67] proposes a control strategy for riding through less severe asymmetric AC faults in the offshore network. Both WTs and offshore two-level HVDC converter control their negative sequence current injected into the offshore AC network in order to eliminate the oscillating AC power at their respective filter buses considering the unknow power/voltage reference. Such control objective is achieved by numerically setting the power oscillation term as detailed in [62] to zero to derive the negative sequence current reference. This approach is particularly designed for offshore station and aims to minimize voltage and current ripple for the DC transmission system. Nonetheless, during severe asymmetric AC faults or when the ratio between the negative sequence voltage and the positive sequence voltage exceeds 70%, the negative sequence current controllers of the WTs and offshore HVDC converter need to be disabled to prevent large amount of negative sequence current injection by converters. Consequently, the system loses negative sequence current control, potentially leading to overcurrent.

Unlike two-level VSCs, several studies on the behaviour of modular multilevel

converters (MMCs) under asymmetric AC faults reveal that MMC can be controlled not to inject even harmonic power into DC side thus exhibiting no even harmonic voltage ripples in the DC link when it operates with balanced or unbalanced AC current [68-70]. Studies in [68, 71] reveal that, during asymmetrical AC fault, the circuiting current in MMC contains not only negative sequence double frequency currents but also the zero and positive sequence ones. The zero-sequence currents can flow to DC side and cause DC voltage oscillation. Thus, a zero-sequence suppression control is proposed in [72] to eliminate the DC oscillation. Further studies in [73] use the proportional-resonance (PR) controller successfully suppressed the positive, negative and zero sequence circuiting currents under unbalance fault to improve the MMC internal and external fault ride through behaviours. Therefore, the previous objective for 2-level VSCs of eliminating the oscillating components of the active power during asymmetric faults becomes redundant in MMC cases. The negative sequence current represents an additional degree of freedom in MMCs that could be exploited to optimize overall system transient behaviour in conjunction with other protection considerations.

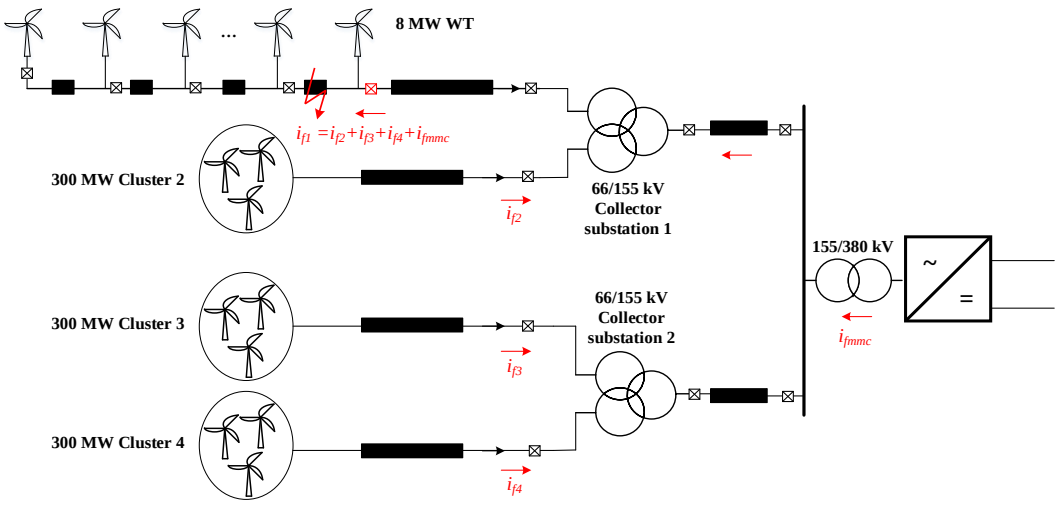

Fig. 2.13 Offshore HVDC connected windfarm system protection

Protection system design is another critical issue for ensuring satisfactory offshore

windfarm fault ride through operation. The fault currents which used to activate some protective relays (e.g. overcurrent relays) is normally provided by synchronous generators in conventional power networks. In contrast, the offshore converters can only provide limited (e.g. 1.2 pu) fault current depending on their designs [74].

References [19, 75, 76] analyse the impact of offshore windfarm system fault current distribution on protection system design during symmetrical fault conditions. It concludes that the converters can successfully trip the over-current relay installed on the WT string level. However, for the collection grid that connects WT string to offshore HVDC station, the performance of overcurrent relay is inadequate, while differential protection can distinguish the fault current. Moreover, fault current contribution from MMC and WTs could result in excessive fault current for faults at WT strings as illustrated in Fig. 2.13 [76]. Thus, reference [56] proposes a voltage-dependent current order limit method, which decreases the maximum current injection when the offshore AC voltage drops below 0.2 pu until the currents contribution from converters down to zero. However, the method neglects the fault currents requirements for the operation of the overcurrent relays. To address this issue, [19] proposes a fault current providing control method, as illustrated in Fig. 2.14. When the fault is detected, the i_{dref} that contributes to active power transfer is reduced to zero (low AC voltage so no active power can be transferred) while the reactive current i_{qref} is gradually ramped up (rather than jumped to the current limited instantly). Thus, the fault current at the faulty point will increase gradually, and excessive fault current can be avoided (so no need to increase the capacity of the circuit breakers in the WT strings)

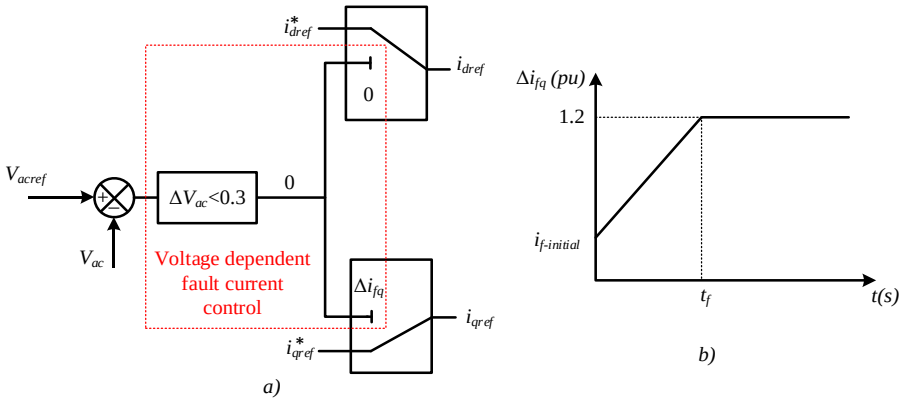

Fig. 2.14 Fault current management scheme [19] a) fault current injection control b) fault current supply

To facilitate the analysis of asymmetrical faults, power circuits are generally decomposed into equivalent positive, negative and zero sequence circuits in conventional power system [77]. Reference [20] adopts controlled current sources to represent VSCs in sequence network when analysing asymmetrical AC faults for offshore windfarm system. However, a fundamental problem of the representation in [20] is the absence of shunt impedances across the current sources in the sequence network, which are necessary for decoupling the current sources from the inductances of the converter transformer and interfacing inductors. This has led to circuit anomaly and resulted in extremely high voltages when negative sequence currents are suppressed as the detailed results presented in [20]. Therefore, the current source representation is abandoned and controlled voltage source equivalent is adopted in [10]. Such an approach is preferred because it does not require any factitious impedance, as pointed out earlier in the current source representation.

In addition to the safe offshore converter operation and protection system, WT GSCs and the generator also need to be properly controlled to ride through faults. Due to the reduced offshore voltage, the active power that can be transmitted by offshore network is significantly reduced. Thus, the surplus power generated by WT will charge

its DC capacitance leading to overvoltage on the DC side. To tackle this issue, the most effective method is installation of energy dissipation units, e.g. DC choppers, to burn the surplus power to maintain the DC voltage [78-80]. However, due to the heat effect, this method can only sustain the WTs for a short period time and thus, extra action from generator side needs to be taken such as pitch control [81, 82] to reduce captured wind power or shut down of WTs for permanent faults.

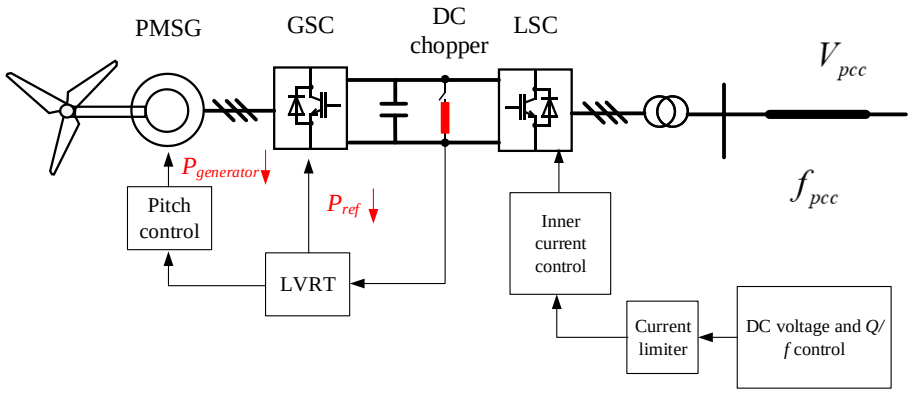

Fig. 2.15 WT fault ride-through operation

2.3.2 Onshore AC fault ride through operation

During onshore AC network faults, the power transmission capability of onshore converters is severely reduced. The continuous power export from the windfarm to the HVDC link leads to power imbalance and results in rapid DC voltage rising of the DC link. To avoid shutdown of the entire system, the excess power has to be dissipated, or the windfarm needs to reduce the exported power.

The energy dissipation unit method as introduced in the last section at (WT level) can also be adopted in such scenario. However, compared with individual WT, the HVDC system needs large rating of DC choppers or dynamic braking resistors at the HVDC link, leading to a significant increase in capital costs.

Power reduction control with the aid of fast communication system is employed in [83-85], as illustrated in Fig. 2.16. When the fault is detected by the onshore converter, the communication system will share the fault signal to each WT to reduce the power generation. However, under such arrangements, the system performance mainly relies on communication reliability and speed, which reduces the robustness of system.

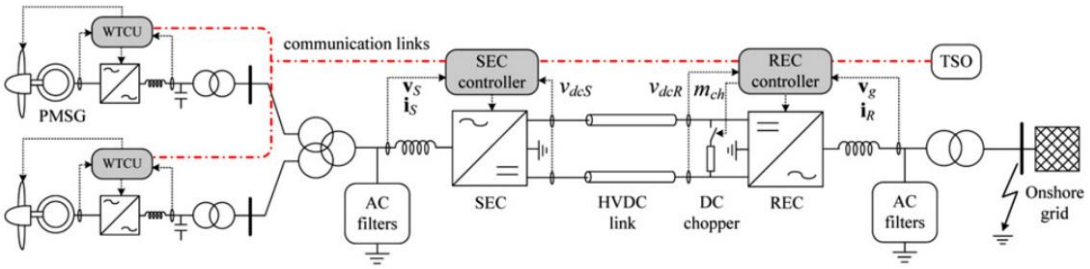

Fig. 2.16 Communication layout of VSC-HVDC connected offshore wind farm for onshore AC fault ride-through [83]

Reference [86] proposes a method that utilizes the system inherence characteristics, e.g. raised DC voltage, to design the V_{dc}-V_{ac} droop control, which can distribute the power stress among local windfarm. During an onshore AC fault, the MMC reduces the offshore AC voltage magnitude according to the raised DC voltage. Then, WT grid side control will hit current limits imposed at outer controllers leading to the power reduction of individual WT. Such control method can effectively reduce the onshore terminal power stress.

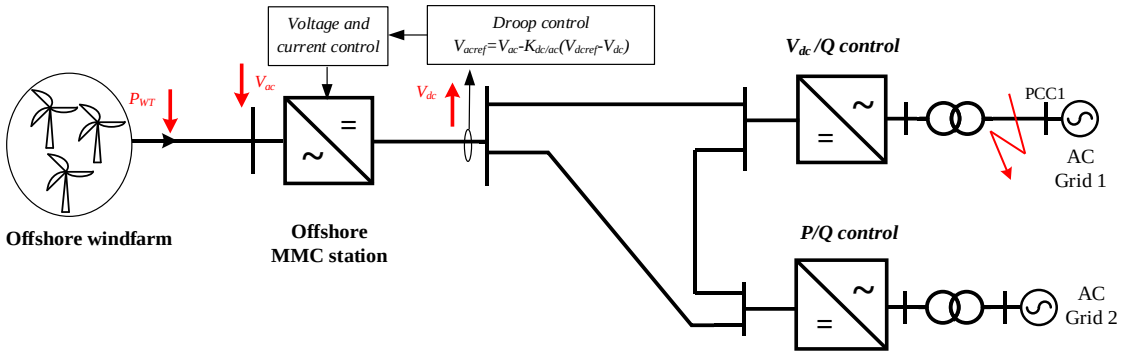

Fig. 2.17 Onshore fault ride-through V_{dc}-V_{ac} droop control

2.3.3 DC fault ride through operation

The DC fault is another key issue for the operation of HVDC connected offshore windfarms [87]. As discussed in previous section, most employed offshore windfarm projects are MMC connected system and thus, the majority of existing DC fault ride-through operations are focused in this field.

Due to the low DC impedance, a DC pole-to-pole fault can result in the collapse of DC voltage within a few milliseconds and large DC fault current due to the capacitor discharging and AC fault current feeding through the freewheeling diodes of the converters. Power electronics devices used in the MMCs have limited overcurrent capability and are extremely vulnerable to the rapidly increased DC fault current [88]. Thus, the protection speed required for DC fault is much faster than that in AC fault. In addition, DC fault current does not have zero crossing, so fault breaking becomes challenging.

The cooperation of ACCBs and fast DC switches (DCSWs) is one of the options used to clear DC fault [54]. When the fault happens on the DC line, the large DC fault current flows through the MMC arms. The internal protection will monitor the fault current and block the converter if the arm current excessed certain threshed, e.g. 2 pu,

to protect the IGBTs [89]. Then, the ACCBs installed on the converter side trip to break the fault current at AC current zero-crossing point. After the fault current from DC side decays to around zero, the installed DCSWs connected at the faulty lines open to isolate the DC fault, as illustrated in Fig. 2.18.

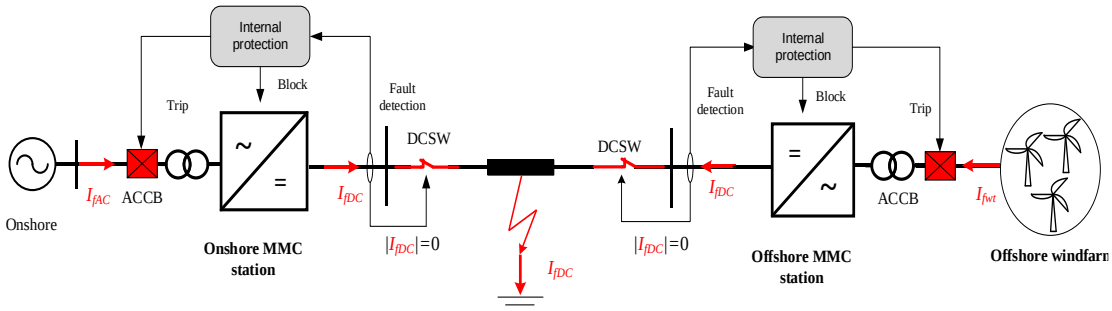

Fig. 2.18 DC fault clearance through ACCBs and DCSWs

Various SM topologies, e.g. FB [90], clamped double [91] and mixed submodules [92], have also been proposed for MMC to block fault current feeding from AC to DC side. Taking the FB SM as an example, when all switches are blocked as shown in Fig. 2.19 a), the capacitor C_{sm} is inserted into the current path in negative polarity to block the fault current following through the freewheeling diode from the AC side. In addition, as FB SM can generate negative voltages as listed in Fig. 2.19 b), it can continue operating during the DC fault as STACOM to support the AC grid side voltage [93]. However, FB-MMC doubles the power electronics devices, which leads to additional power losses and investment costs.

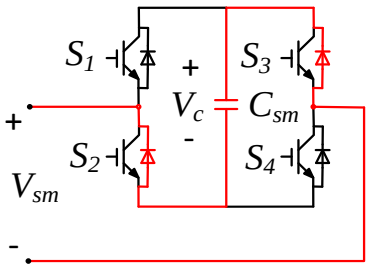

(a) FB SM

Switching state	S1	S2	S3	S4	V_{sm}
I	1	0	0	1	V_c
II	0	1	1	0	$-V_c$
III	1	0	1	0	*0*
IV	0	1	0	1	*0*
Blocked	0	0	0	0	$-V_c$ for DC fault blocking

b) Output voltage of FB SM

Fig. 2.19 FB SM and its operating state

DCCBs are key technologies to enable a fast DC fault isolation. Depending on their configurations, DCCBs can be categorized as mechanical, solid-state and hybrid DCCBs [94]. Fig. 2.20 illustrates a typical mechanical DCCB which composes of a mechanical switch in parallel with surge arrestors and resonance circuits. When the fault is detected, the auxiliary switch activates the LC resonance circuit to superimpose a resonant current to counter the fault current, so an artificially current zero-crossing is created. Thus, the mechanical switch can be opened to isolate the fault. The surge arrestors limit the maximum voltage across the resonant circuit and absorb the energy stored in the DC lines [95].

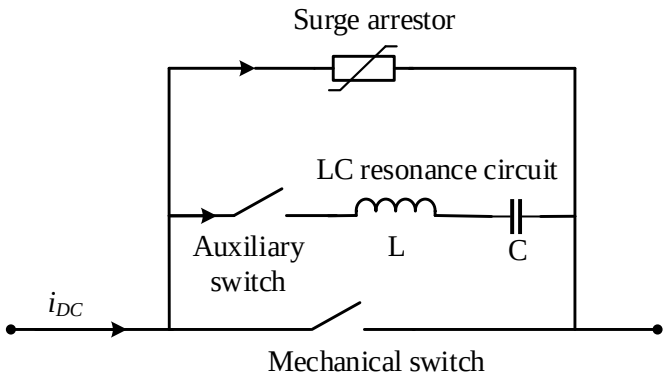

Fig. 2.20 Mechanical DCCB

Fig. 2.21 illustrates a topology for the solid-state DCCBs. As can be seen, the solid-state DCCBs replace the mechanical switch and resonant circuit by series-connected semiconductors. Surge arrestors are connected in parallel with the IGBT main breaker to absorb the energy in DC line and to limit the voltage across the DCCB during fault isolation process. Due to the fast action of IGBTs, the solid-state DCCBs can interrupt the fault in less than 1 ms [94, 96]. However, the high capital cost and on state operation losses hinder its applications.

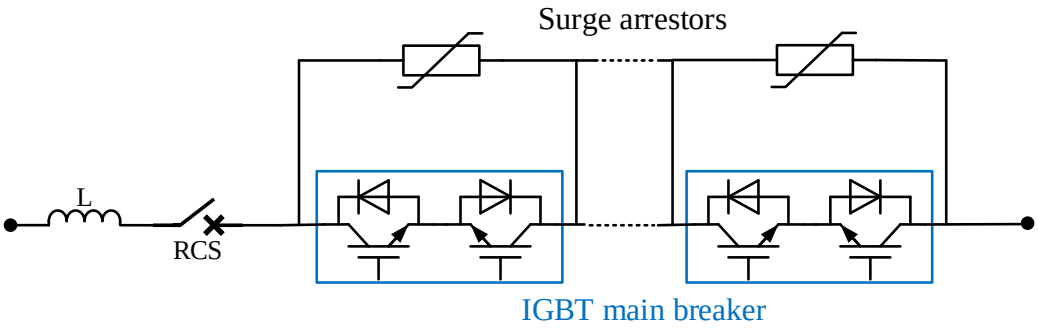

Fig. 2.21 Solid-state DCCB

To improve, the hybrid DCCB topology proposed [97] where a fast disconnector is series connected with an auxiliary breaker constructing the main conduction path while an equivalent solid-state DCCB is parallel connected for fault isolation, as shown in Fig. 2.22. During normal operation, the currents flow through the mechanical switch due to the lower on-state voltage than the solid-state DCCB branch. After fault detection, the auxiliary breaker turns off and the current will commutate to the parallel solid state DCCB branch. Thus, the currents flow to the fast DC disconnector drops to zero and DC disconnectors can be opened. The solid-state DCCB branch can then be turned off to reduce the DC fault current and isolates the fault quickly. Compared with the other two types of DCCBs, the hybrid DCCB can operate at high speed with minimal losses during normal operation. However, the large footprint and high capital cost are the major concerns for vendors that prevent its wide application.

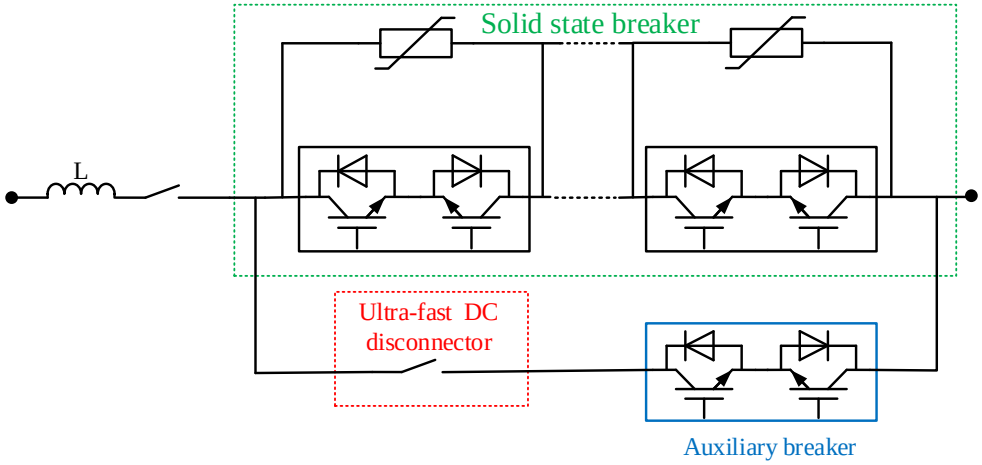

Fig. 2.22 Hybrid DCCB

Serval studies and projects have concluded that MTDC network can potentially increase offshore power transmission system reliability by reducing the overall downtimes of "loss of infeed" and lower overall investment and operation cost [24-26]. DC fault protection is a major technical obstacle that prevents the development of reliable MTDC grids and has drawn significant attention from academia and industry [21-23]. To date, several protection concepts have been proposed to facilitate fault isolation in offshore MTDC networks.

In [27], a "handshaking" DC fault protection method that utilizes ACCBs and fast DC dis-connectors to isolate DC fault and facilitates system restoration in MTDC terminal is proposed, as demonstrated in Fig. 2.23. If currents flowing into the cables through the DCSWs is defined as positive, for the faulty branch, both ends of currents (DCSW 3-2 and DCSW 2-3) are positive, while at the healthy cables, at least one cable current is negative. Then, the fault location can be identified and isolated by opening the corresponding DCSW once the DC fault current decays to zero after all the ACCBs opened. However, such scheme is inadequate for MTDC network, especially for critical power corridors, as it leads to the shutting down of the entire system and system recovery is slow.

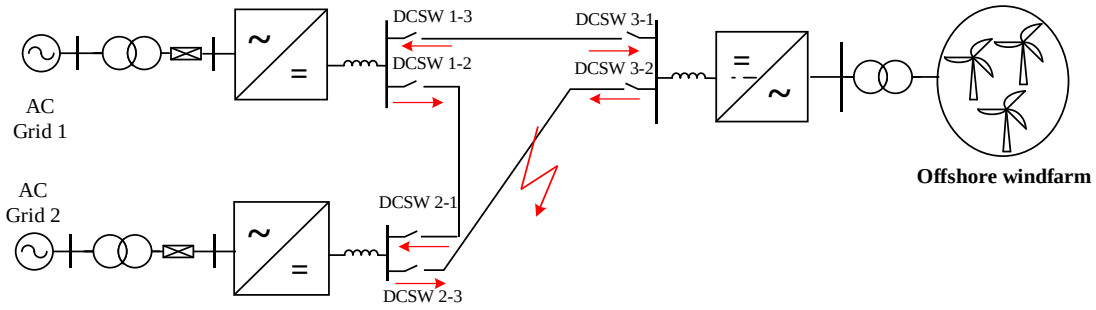

Fig. 2.23 DC fault clearance by ACCBs and DCSW with "Handshaking."

To speed up the fault clearance, a DC fault ride-through method in MTDC grids is investigated in [29], in which a dedicated fault clearance and system restoration sequence is discussed when fault blocking converters such as the FB MMC and high speed DC switches are employed. When a DC fault occurs, the FB SM will be controlled to quickly reduce the DC voltage in order to extinguish the DC fault current. Although the approach demonstrated in [29] can effectively reduce the period of system outage, it still does not facilitate continued operation for the healthy part of the system.

Thus, to minimize power interruption through prevention of total shut down of the DC grid, the uses of different types of DCCBs are investigated in [98-100]. By connecting fast acting solid-state or hybrid DCCBs at both ends of each cable as illustrated in Fig. 2.24, the DC fault can be quickly isolated after a fast fault detection and localization [101]. Thus, interruption of remaining service can be minimized. However, the high cost and weight, and large footprint of full-size DCCBs, particularly for offshore application, increase the total investment cost significantly.

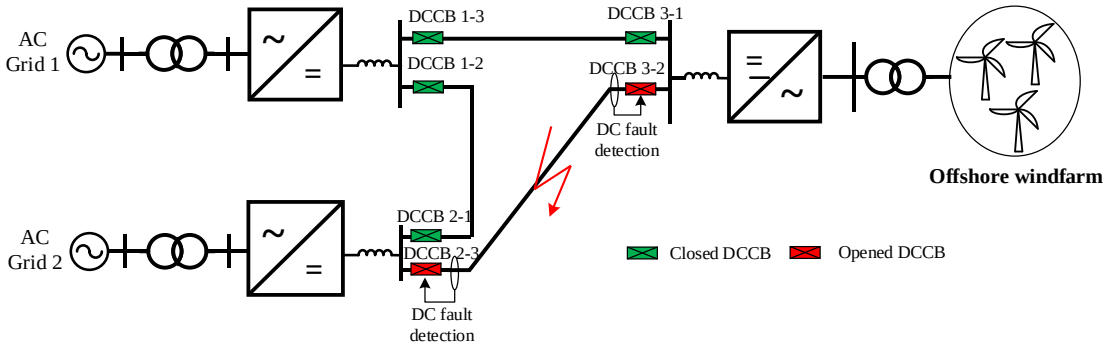

Fig. 2.24 DC fault clearance by DCCBs

Thus, the partial selective protection scheme which uses a combination of reduced number of DCCBs and slow DCSWs to clear DC faults while retaining some of the pre-fault power transfer, could be a cost-effective solution [102]. Such method is achieved by equipping the expensive DCCBs or DC-DC converters [103] at strategic locations which partition the large DC system into a number of small DC network zones. In case the fault happens in one DC network zone, the fast-acting DCCBs will be opened, which acts as a firewall to interrupt the fault propagation. Thus, the healthy system can remain operational. Within each zone, relatively slow and cheap protection equipment (ACCBs with DCSWs) can be used. Nonetheless, the slow partially selective DC fault protection strategy requires significant modifications to WTs control, particularly, to maintain offshore AC voltage and frequency for extended period of time after the blocking of offshore MMC, in order to avoid the protentional issues and provide fast system restoration.

2.4 Black start service provided by offshore windfarms

Massive integration of RESs into power systems increases the risk of wide-area blackouts, especially in strongly linked networks [32]. In August 2019, the deloaded of the Hornsea 1 offshore windfarm in the UK led to blackout across wide areas,

affecting over one million customers [104]. The current practical power system restoration primarily relies on conventional hydro and thermal power plants due to their capability to meet the technical requirements for black start [105]. However, they are characterized by long start-up time.

VSC based HVDC system can be used as a standby facility for black start and system restoration due to its voltage regulation capability [106]. In [107], a field test on the use of VSC-HVDC system to provide the required electrical auxiliary power to start-up a thermal power station is described. Several critical processes were demonstrated during the test such as energizing the large transformer, long overhead line energization (200 km 330kV), and the starting up of large generators (250 MVA). The tests were performed in the Pohivork network in Estland in June 2007 and the lessons learned from the test can be summarized as follows:

- Compared with conventional generators, the AC voltage of VSC HVDC system can be directly controlled with a wide range of 0 pu to 1.1 pu, so adverse impact on the excitation system of the generators can be avoided.
- The soft energization scheme, in which the voltages on lines and transformers are gradually built up, avoids any large inrush current.
- The fast and direct regulation on the frequency can aid the generator governor to damp any generator angle swing after the generator reconnection.

Further studies have investigated the impact of soft energization on traditional AC protection systems due to the low short circuit current contribution of HVDC converters. In [108], it is pointed out that the differential protection could not be used as primary protection due to limited fault current contribution for the 420 kV system but the undervoltage protection would be a good choice after successful system starting up. For lower voltage levels, e.g. 22 kV, the original protections setting is sufficient

due to enough fault current contribution. However, those studies are tested in an island grid to ensure the safety of main AC grid operation. The studies present in [109] extend the black start to a live network. The test was carried out in Danish grid with the Norwegian grid work as only power source to feed the HVDC link. After successfully energizing the 400 kV AC transmission line, several large transformers, a 25 MW boiler are connected, and the synchronization between the live and black started AC grid is executed by the converter. The overall behaviours are satisfactory, but small transients and oscillations were observed after the system reconnection[109].

With the fast development of offshore windfarms and continuously increased penetration of renewable energy, large VSC-HVDC connected offshore windfarms as a more stable energy compared with other renewable sources, are also proposed to provide fast black start service [4, 16]. For example, black start service provided by offshore windfarm has been included in the ENTSO-E network connection requirements as an optional requirement and can be requested by transmission system operators (TSOs) [33].

So far, several studies have been carried out to explore the feasibility of black start operation for offshore windfarm system. Technical challenges associated with different stages of energization when HVDC connected offshore windfarm are used for black start have been identified and discussed in [33-35], including the self-start of offshore windfarms. References [110, 111] propose a start-up method that utilizes an auxiliary generator in offshore platform to energize the offshore WTs, transformers and cables as shown in Fig. 2.25. Detailed analyses on impacts of inrush current on transformers and offshore HVAC and HVDC cables using EMT simulation reveal that the auxiliary generator can successfully power the offshore network with the aid of properly designed pre-insertion resistor (PIR) to limit the transient behaviour. However, such an arrangement adds extra cost and the control and operation for WTs are not addressed.

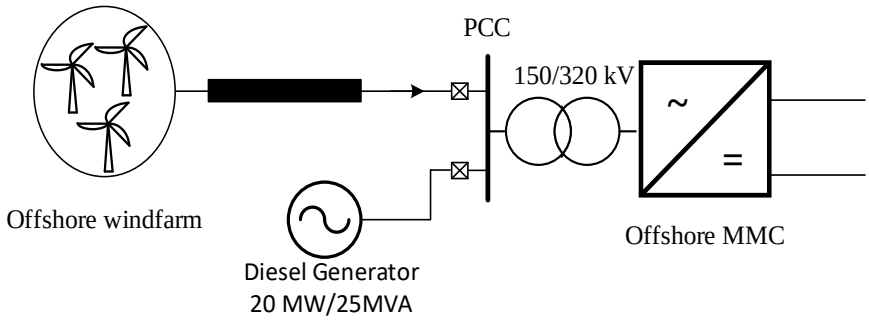

Fig. 2.25 Offshore network start-up with auxiliary diesel generator [111]

In contract, the Type-4 WTs with fully rated power electronics converter can self-start with the aid of internal backup power supply (battery energy storage system) for initial energization and an UPS power source for its auxiliaries and yaw & pitch mechanisms, as illustrated in Fig. 2.26 [33] [112]. Once some WTs can sustain themselves, the next stage requires the synchronization between the WTs in the offshore grid. This stage requires the WTs to operate in grid forming mode to regulate the offshore AC grid voltage while enables the rest of WTs autonomously synchronize to the main AC grid and contribute to voltage and frequency regulation. In addition, [58]has successfully demonstrated a sequential black start scheme for offshore AC network in which each WTs are powered and connected to the AC grid without significant transient to the offshore AC network. However, due to the onshore converter station has to work under grid forming mode, the requirement of regulating DC voltage needs shift to offshore network.

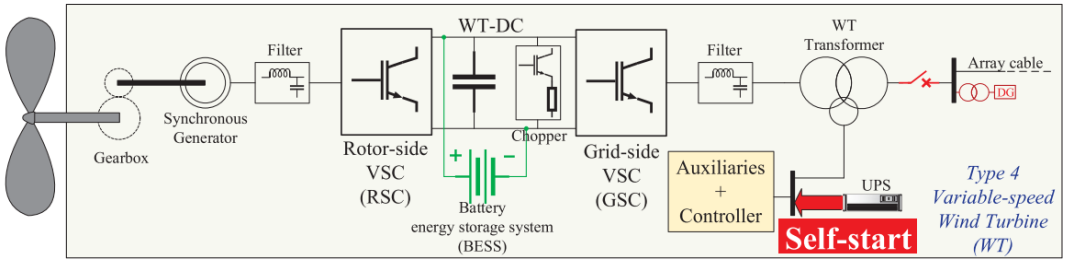

Fig. 2.26 Self-start scheme for Type-4 WT [33]

Reference [34] demonstrates black start using HVDC connected offshore windfarm where the onshore MMC station works under grid forming mode while the offshore MMC station in DC voltage regulation mode. Under such condition, the offshore AC voltages are regulated by the WTs. The detailed energization sequence of the offshore AC network, HVDC link and onshore AC grid is studied. However, the work present in [34] does not consider the detailed charging process of onshore converter and the results presented shows a significant voltage dip in HVDC link and large transient in the offshore and onshore MMC cell voltages and valve currents when the onshore converter is enabled. This issue might be addressed by using a PIR to limit the large infeed current or by adopting active charging method in [113, 114] in which the blocked SMs are bypassed slowly with voltage sorting algorithm.

Hybrid DC transmission system with DR as front-end interfacing converter at offshore may be a good alternative to MMC HVDC system for future offshore windfarms due to its low cost [7-9]. The existing researches for DR-HVDC operation mainly focus on its control, system fault ride-through and start-up operation of the offshore AC system [57, 58, 75, 115], while using DR-HVDC connected offshore windfarm for black start onshore network has not been investigated. In addition, compared with MMC connected offshore windfarm system, the black start operation using DR-HVDC is more challenging such as the issue of DC voltage regulation and power balance between onshore and offshore grids due to the uncontrollable DR station.

2.5 Summary and thesis' contributions

This chapter reviews HVDC connected offshore wind farm configurations, control of HVDC transmission system, FRT operation and black start operation of offshore windfarms. In this chapter, three different offshore HVDC converter topologies, i.e. LCC, VSC and DR are reviewed, and the advantage and disadvantages are compared. Three different offshore windfarm configurations, i.e. point-to-point, parallel connection and MTDC network, are introduced. Various offshore AC ride-through operations including converter control and its impact on protection have been discussed. In addition, the black start services provided by HVDC and windfarm systems are reviewed.

Based on the identified challenges, the main contributions of this thesis are:

- The control and analysis for MMC connected offshore windfarm systems under asymmetrical fault conditions. A detailed sequence analysis is performed to assist in understanding power electronics-based network characteristics under asymmetrical faults. An enhanced offshore MMC control strategy is then proposed to ride-through offshore asymmetrical faults, which helps to define a safety fault current level in offshore AC network while avoiding any excessive overvoltage in healthy phases, and instigating speedy recovery of the AC voltage following clearance of AC faults.
- Control of offshore WTs during DC grid faults. A comprehensive analysis is performed to understand the impact of DC faults on the offshore AC network control and operation. Based on the findings, an enhanced passive voltage control for offshore WT converters is proposed to deal with the situation when the control from the offshore MMC station is lost due to its blocking or sudden

opening of offshore AC circuit breakers during a DC fault. The value and viability of the proposed WT control is demonstrated in a 4-terminal meshed DC network using partially selective DC fault protection method that uses reduced number of DCCBs to facilitate DC fault isolation and ensures system restoration.

- Black start operation using DR connected offshore windfarm systems. To enable the DR-HVDC system to perform black start to onshore grid, a new WT frequency-AC voltage (f-V) droop control is proposed to regulate the DC voltage of the DR-HVDC link in a safe range and keep the power balance between onshore and offshore grid. Such operation method is achieved by dynamically regulating the offshore AC voltage according to the system operation condition considering the DR system characteristics.

Chapter 3
Control and Analysis of MMC connected Offshore Windfarm during Asymmetrical AC faults

For MMC connected offshore windfarm systems, the offshore AC network built up by the offshore MMC station exhibits different characteristics during faults compared with conventional AC systems. To date, offshore asymmetrical faults for such systems have not been properly analysed and how the negative sequence current and voltage for the offshore MMC and WTs converters shall be controlled requires further study. This chapter will briefly introduce the basic control of the offshore MMC and WTs. A theoretical analysis of the system operation during offshore asymmetrical faults with the aid of conventional power system sequence network theory is then carried out. Based on the findings, an enhanced AC fault ride through method is proposed to enable fast post-fault AC voltage recovery while ensures a safe fault current level and prevents any excessive overvoltage in the healthy phases. Validity of the proposed solution is confirmed by numerical simulations in PSCAD.

3.1 MMC connected offshore windfarm system modelling and control

Fig. 3.1 shows the structure of the considered windfarm rated at 1200MW connected through a MMC-HVDC system. The windfarm consists of a large number of Type-4 full size PMSG based WTs. The following section will briefly introduce the modelling and control of offshore system adopted in this thesis.

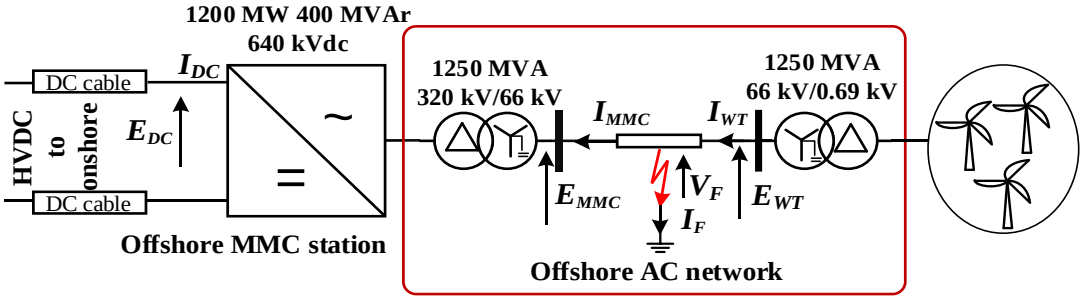

Fig. 3.1 Generic representation of offshore network.

3.1.1 MMC structure

Fig. 3.2 shows a typical structure of a three-phase MMC converter, which is composed with three-phase legs (*a, b, c*) and each phase leg consists of an upper arm and a lower arm. Each arm has one arm inductor and *N* numbers of HB SMs which are used to form the arm voltage denote as v_{ua} and v_{la} for phase *a* in Fig. 3.2. The configuration of the HB SM is also illustrated on the top left of Fig. 3.2 where V_{sm} is the output voltage of the SM.

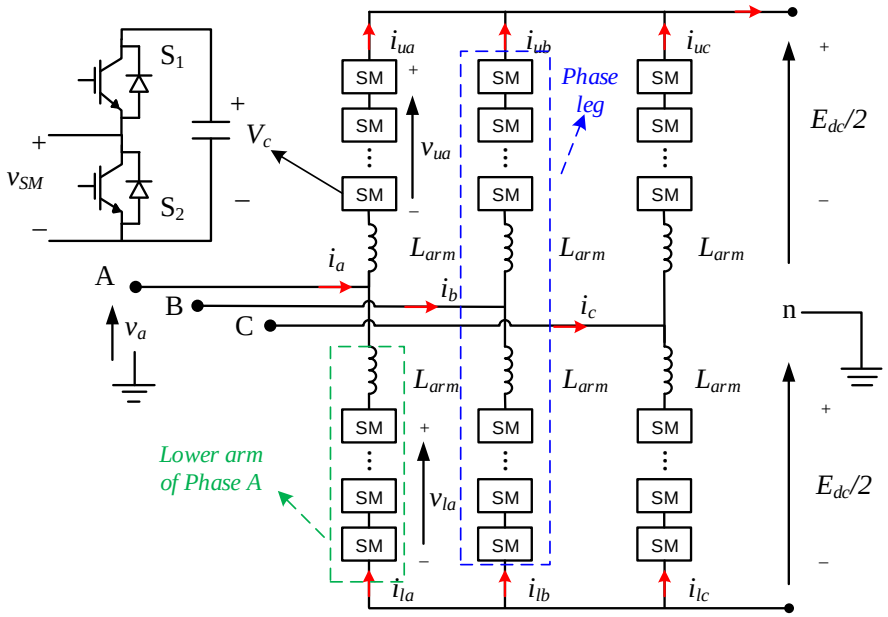

Fig. 3.2 Basic structure of HB SM based MMC

3.1.2 MMC equivalent model

Assuming the SM voltage of MMC is well maintained, the upper and low arm voltages can be equivalent to controllable voltage sources of v_{uj} and v_{lj} (phase j=a,b,c), respectively. To simplify the analysis, the circuit in Fig. 3.2 is converted to a simplified single-phase representation, as shown in Fig. 3.3.

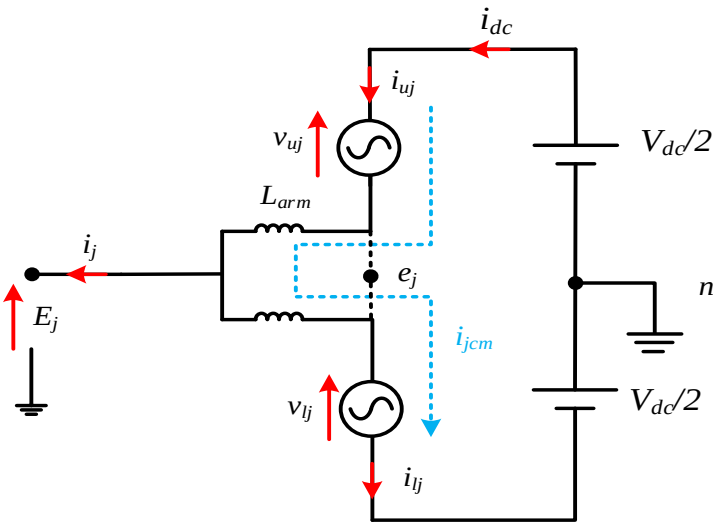

Fig. 3.3 Simplified representation of a single-phase MMC

Applying KCL to Fig. 3.3, the arm currents i_{uj} and i_{lj} can be represented by considering a common mode and a differential mode as:

$$\begin{cases} i_{uj} = \dfrac{i_j}{2} + i_{jcm} \\ i_{lj} = -\dfrac{i_j}{2} + i_{jcm} \end{cases} \tag{3.1}$$

where i_j is the three-phase current (equivalent to the differential mode arm current) and i_{jcm} is the common-mode current in each phase arm.

Taking the neutral point n of the DC link as the reference point, the voltage

equation can be expressed as:

$$\begin{cases} L_{arm}\dfrac{di_{uj}}{dt} = e_j - E_j \\ L_{arm}\dfrac{di_{lj}}{dt} = E_j - e_j \end{cases} \tag{3.2}$$

where e_j is the inner emf generated in phase j and is expressed as:

$$e_j = \frac{V_{dc}}{2} - v_{uj} = -\frac{V_{dc}}{2} + v_{lj} = \frac{v_{lj} - v_{uj}}{2} \tag{3.3}$$

and E_j denotes the three-phase terminal voltage. V_{dc} is the DC voltage of the MMC station and L_{arm} is the arm inductance.

By substituting (3.2) and (3.3) into (3.1), the three-phase voltages can be described as:

$$\frac{L_{arm}}{2}\frac{di_j}{dt} = e_j - E_j \tag{3.4}$$

$$2L_{arm}\frac{di_{jcm}}{dt} = V_{dc} - (v_{lj} + v_{uj}) \tag{3.5}$$

Equation (3.4) indicates that i_j can be regulated by controlling the equivalent inner emf e_j. Thus, the classic current vector control strategy for conventional two-level VSC based on dq coordinates, including an outer power/reactive power controller and an inner current controller can also be used in MMC to control the AC terminal current. According to (3.5), once the desired inner emf e_j which is generated by the current controller is known, the required arm voltages v_{uj} and v_{lj} can also be obtained as:

$$v_{uj} = \frac{V_{dc}}{2} - e_j \tag{3.6}$$

$$v_{lj} = e_j + \frac{V_{dc}}{2} \tag{3.7}$$

Moreover, under steady-state conditions, the common-mode current only contains 1/3 of DC current i_{dc}. Thus, according to the (3.5), the DC voltage is given as:

$$V_{dc} = v_{lj} + v_{uj} \tag{3.8}$$

3.1.3 Double synchronous reference frame vector control for MMC

To facilitate precise control of MMC, the double synchronous reference frame current control is adopted in this thesis. The method as detailed in [62-65] decomposes the three-phase voltages and currents into positive and negative sequence components and then transforms them into two orthogonal planes as 'dq^+' and 'dq^-' that rotate at speed of ω and $-\omega$, respectively as illustrated in Fig. 3.4. In this manner, the positive and negative sequence voltage and current can be controlled independently. It is worth mentioning that, due to the transformer arrangement, zero-sequence voltage and current are normally absent on the converter side.

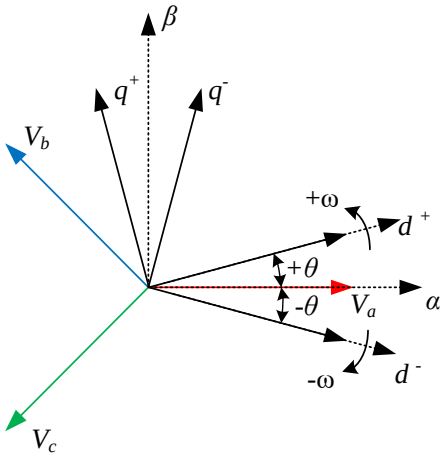

Fig. 3.4 Voltage vector in 'dq^+' and 'dq^-' reference frame

Three-phase variables with no-zero sequence can be decomposed into the positive and negative sequences as:

$$F_{abc}(t) = F_{abc}^{+}(t) + F_{abc}^{-}(t) \tag{3.9}$$

Then, the positive and negative sequences in *abc* frame can be transformed to the relevant dq^+ and dq^- frames as:

$$\mathbf{F}_{dq}^{+} = \mathbf{P}(\theta)\mathbf{F}_{abc}^{+}, \quad \mathbf{F}_{dq}^{-} = \mathbf{P}(-\theta)\mathbf{F}_{abc}^{-} \tag{3.10}$$

where

$$\mathbf{P} = \frac{2}{3}\begin{bmatrix} \cos\theta & \cos(\theta - 2\pi/3) & \cos(\theta + 2\pi/3) \\ -\sin\theta & -\sin(\theta - 2\pi/3) & -\sin(\theta + 2\pi/3) \end{bmatrix} \tag{3.11}$$

and θ is the angle between V_a and *d-axis* as illustrated in Fig. 3.4.

It should be noted that, during grid unbalance condition, the positive sequence and negative sequence are cross-coupled. Thus, notch filters are used to remove the second-order component [75] and the transfer function is:

$$G(s) = \frac{s^2 + 4\omega^2}{s^2 + 4\zeta\omega s + 4\omega^2} \tag{3.12}$$

where s is the Laplace operator, ω is the offshore grid angular velocity and ζ is the damping ratio.

After transforming (3.4) into synchronous dq^+ and dq^- reference frames, the following equations can be obtained:

$$\begin{cases} \frac{1}{2}L_{arm}\frac{di_d^+}{dt} = e_d^+ - v_d^+ + \frac{1}{2}\omega L_{arm} i_q^+ \\ \frac{1}{2}L_{arm}\frac{di_q^+}{dt} = e_q^+ - v_q^+ - \frac{1}{2}\omega L_{arm} i_d^+ \\ \frac{1}{2}L_{arm}\frac{di_d^-}{dt} = e_d^- - v_d^- - \frac{1}{2}\omega L_{arm} i_q^- \\ \frac{1}{2}L_{arm}\frac{di_q^-}{dt} = e_q^- - v_q^- + \frac{1}{2}\omega L_{arm} i_d^- \end{cases} \tag{3.13}$$

where, ω is the angular frequency of the offshore network. Using proportional-integral (PI) regulators, the positive and negative current loops are designed as illustrated in Fig. 3.5.

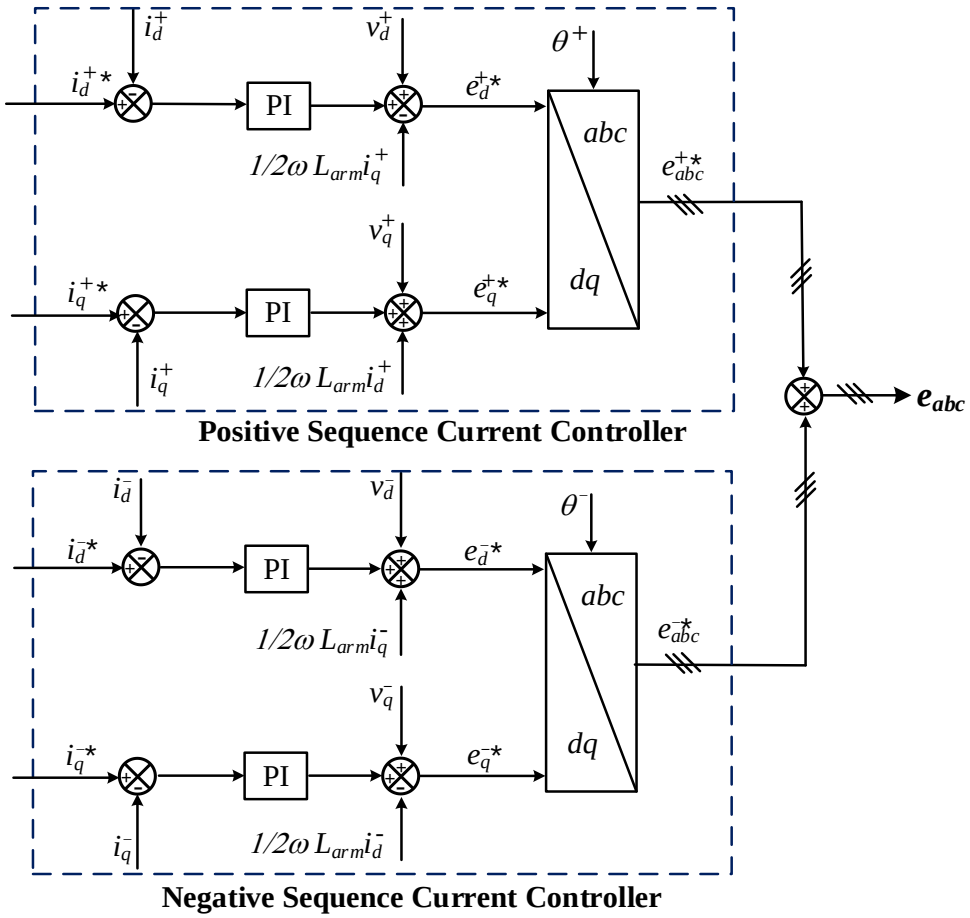

Fig. 3.5 Positive and negative sequence current controllers

3.1.4 Offshore AC voltage control

To analyse the dynamics of offshore voltage, a simplified one-line diagram of the offshore grid is drawn in Fig. 3.6, where I_{pcc} is the current flowing from the WTs to the PCC bus and I_{MMC} is the current following into the offshore MMC station. C represents the equivalent AC capacitance seen at the PCC point.

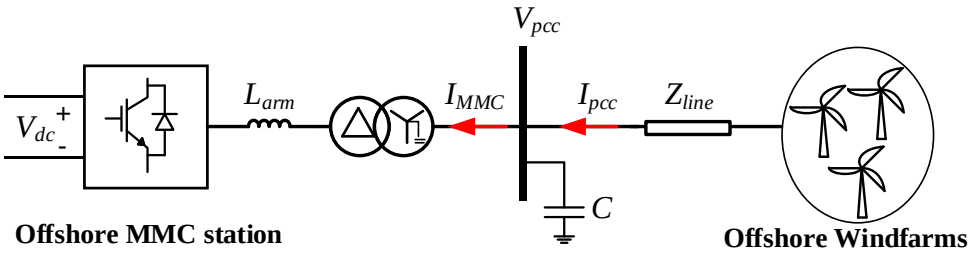

Fig. 3.6 simplified one-line diagram for offshore grid

Appling KCL to Fig. 3.6, the relationship between current and voltage at the PCC can be obtained as:

$$\begin{bmatrix} I_{MMCa} \\ I_{MMCb} \\ I_{MMCc} \end{bmatrix} = \begin{bmatrix} I_{PCCa} \\ I_{PCCb} \\ I_{PCCc} \end{bmatrix} - C\frac{d}{dt}\begin{bmatrix} V_a \\ V_b \\ V_c \end{bmatrix} \tag{3.14}$$

Transforming (3.14) into dq frame yields:

$$\begin{bmatrix} I_{MMCd} \\ I_{MMCq} \end{bmatrix} = \begin{bmatrix} I_{PCCd} \\ I_{PCCq} \end{bmatrix} + \begin{bmatrix} 0 & \omega C \\ -\omega C & 0 \end{bmatrix}\begin{bmatrix} V_q \\ V_d \end{bmatrix} - \begin{bmatrix} C & 0 \\ 0 & C \end{bmatrix}\frac{d}{dt}\begin{bmatrix} V_d \\ V_q \end{bmatrix} \tag{3.15}$$

From (3.15), it can be concluded that the offshore PCC voltage can be regulated by adjusting the current references of the inner current controller. Thus, the positive sequence voltage reference which forms the offshore AC voltage under normal operation can be regulated. For the negative sequence, the current reference normally sets as zero to maintain balance output current.

In addition, the offshore AC grid frequency is also regulated by offshore MMC and is typically fixed, say at 50 Hz. Thus, the phase angle θ is simply derived using the fixed frequency as illustrated in Fig. 3.7 as:

$$\theta = \omega t = 2\pi ft = 100\pi t \tag{3.16}$$

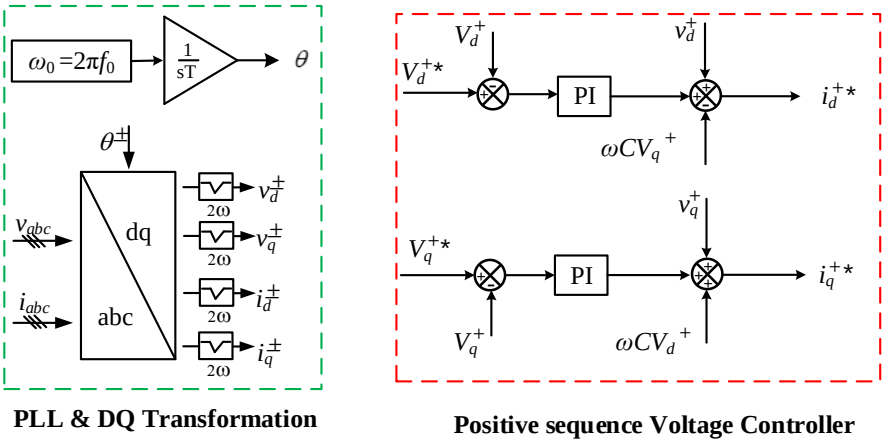

Fig. 3.7 Positive and negative sequence controller

3.1.5 MMC supplemental control

a) Modulation methods

To control the switching of the SMs, the phase-shift PWM [116]and level-shift PWM [117] are commonly used for low or medium voltage. However, for HVDC application, both two modulation techniques become impractical due to the high number of SMs and complexity of the switching decisions. Thus, the nearest level modulation (NLM) [118] is commonly adopted for HVDC applications. As illustrated in Fig. 3.8, at each sampling period, the NLM modulation method selects the number of SMs to be inserted such that the total arm voltage generated by the inserted SMs closely matches the modulation waveform (i.e. the reference arm voltage). Assuming that the SM capacitor voltages are largely balanced, the average SM voltage V_{sm} is:

$$V_{sm} = V_{dc} / N = (v_{lj} + v_{uj}) / N \tag{3.17}$$

Thus, based on the modulation index, the inserted SM numbers at upper arm N_{upper} and lower are N_{lower} can be described as:

$$\begin{cases} N_{upper} = \dfrac{N}{2} - round(\dfrac{e_s}{V_{sm}}) \\ N_{lower} = \dfrac{N}{2} + round(\dfrac{e_s}{V_{sm}}) \end{cases} \tag{3.18}$$

where round means the closest integer.

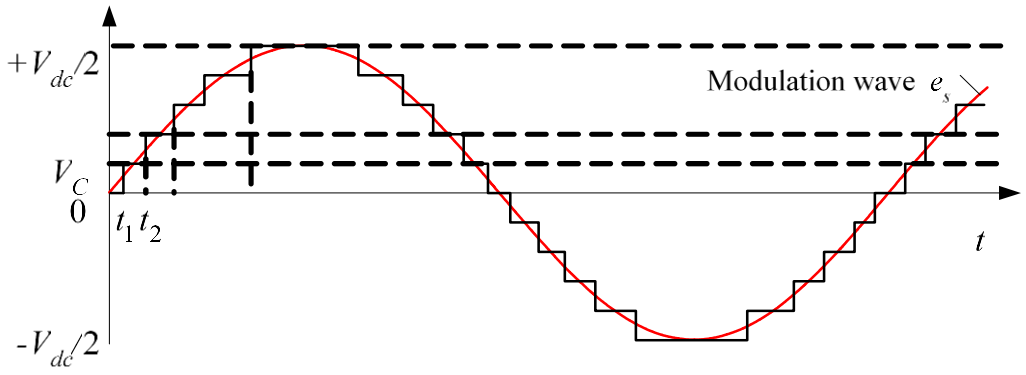

Fig. 3.8 Nearest level modulation

b) Voltage balancing control

To ensure safe operation, the capacitor voltages of all the SMs must be balanced [119]. Depending on the switching state of SM, its capacitor charging or discharging states are listed in Table 3.1. As seen, when the SM capacitor is inserted to the arm (i.e. State 1), the SM capacitor is charged or discharged depending on the arm current direction. Thus, the soring algorithm [120] is used in each sampling period to ensure all SMs capacitor voltages balanced. Specifically, the SMs with lower capacitor voltage will be inserted during the charging cycle, while the SMs with high capacitor

voltage will be inserted during discharging cycle.

Table 3.1 Switching states and capacitor charging and discharging of HBSM

States	S_1	S_2	V_{SM}	i_{SM}	Capacitor status
1	On	Off	V_c	>0	Charging
	On	Off	V_c	<0	Discharging
2	Off	On	0	-	Bypassed
3	Off	Off	-	-	Blocked

Another important aspect of MMC operation is to ensure the stored energies in all the six arms are equally distributed which commonly refers as horizontal (different phase legs) energy balancing control and vertical (upper and lower arms) energy balancing control [121] as illustrated in Fig. 3.9. Such controls have been well understood, and as their operation does not directly affect the proposed method, no further details are provided here.

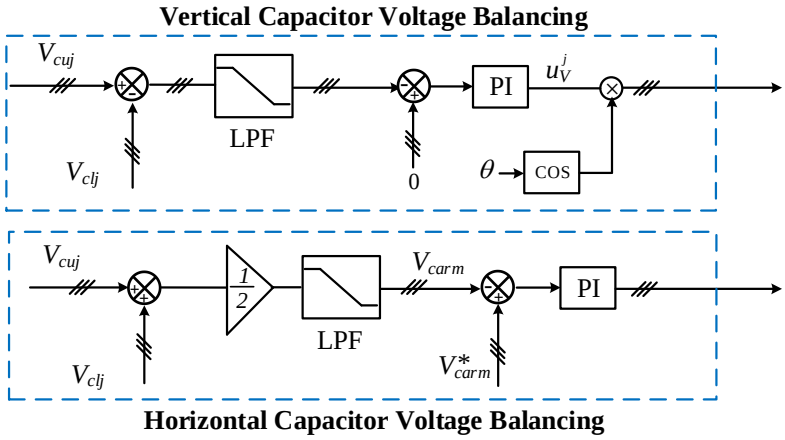

Fig. 3.9 Vertical and horizontal capacitor voltage balancing control

c) Circulating current control

Controlling the circulating current is another key issue for the MMC operation.

This is due to the double frequency power oscillations in the different phases resulting in the second-order harmonic voltage at the SM capacitors. Consequently, 2nd order harmonic voltage can present in each of the three-phase legs with 120 degrees phase shift, resulting in 2nd order harmonic current circulating inside the 3 phase legs. This can increase the converter power losses and lead to extra semiconductor voltage/current stress. The detailed mathematic analysis can be found in [68-70]. To eliminate the circulating current, the PR controller is adopted in this thesis, as illustrated in Fig. 3.10.

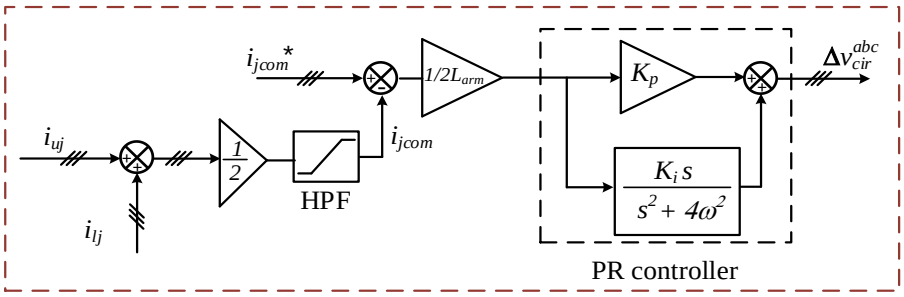

Fig. 3.10 Circulating current suppression controller

The overall control diagram of the offshore MMC is illustrated in Fig. 3.11, with the main control blocks previously described.

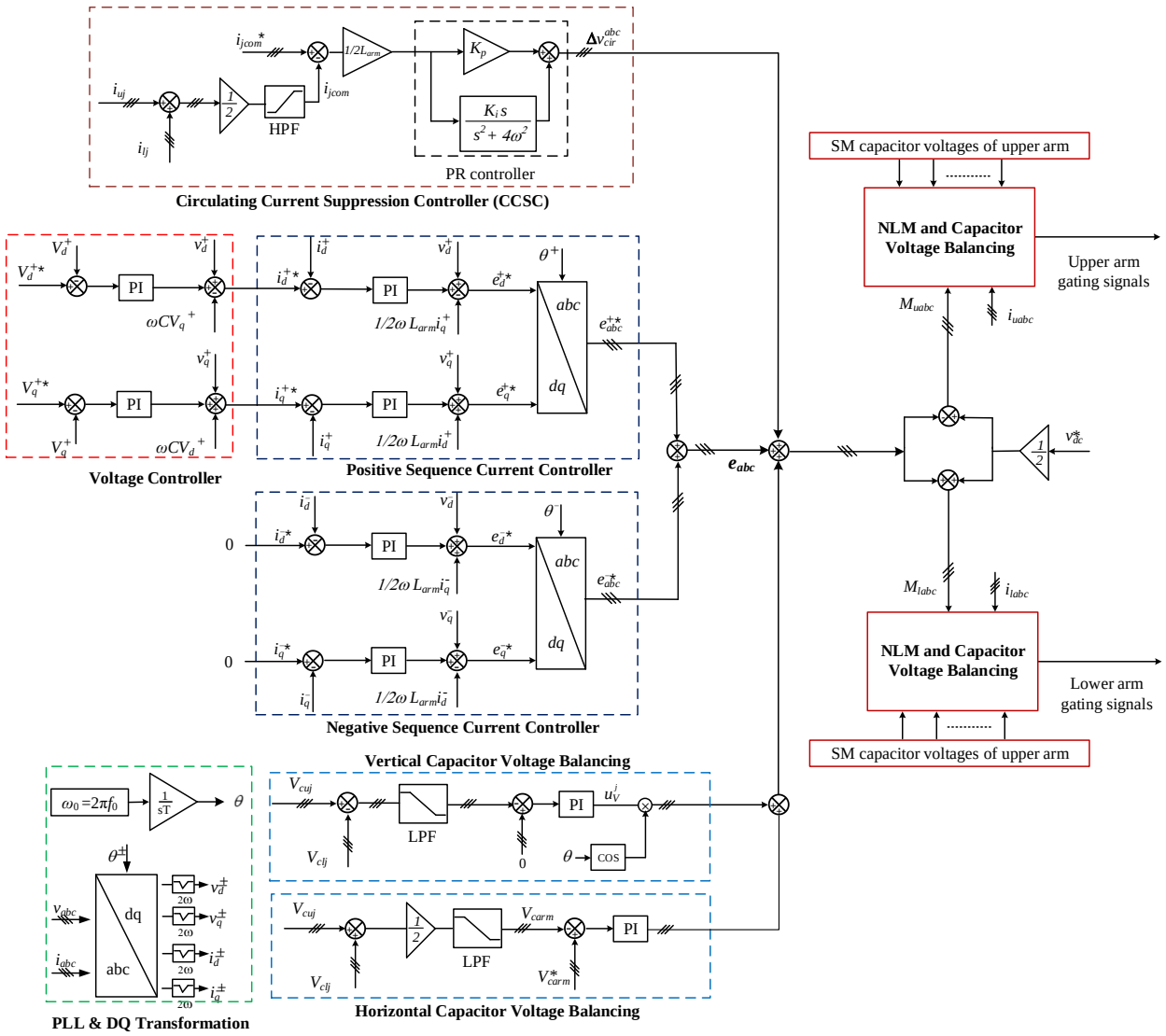

Fig. 3.11 Overall control diagram for offshore MMC station

3.1.6 WTs model and control

For large offshore wind farms containing hundreds of WTs, system modelling and simulation become computationally intensive if each WT is modelled in detail [122]. As this thesis mainly focuses on the offshore AC and DC network dynamics, aggregated and simplified WT systems are used. Thus, the detailed influence factors such as wake effect and variable wind speed are not considered. Instead, each of WT is assumed working under rated power (as quite often, this is the most demanding case

for control). In addition, as the advanced fault ride-through operation for WTs mechanical system has been well documented [123, 124] and is not directly related to the identified problems and the proposed method, the dynamics of the WT mechanical system are not modelled and only the WT LSC connected to a DC source is considered [56, 57, 75, 125]. Fig. 3.12 illustrates the WTs model considered in this thesis.

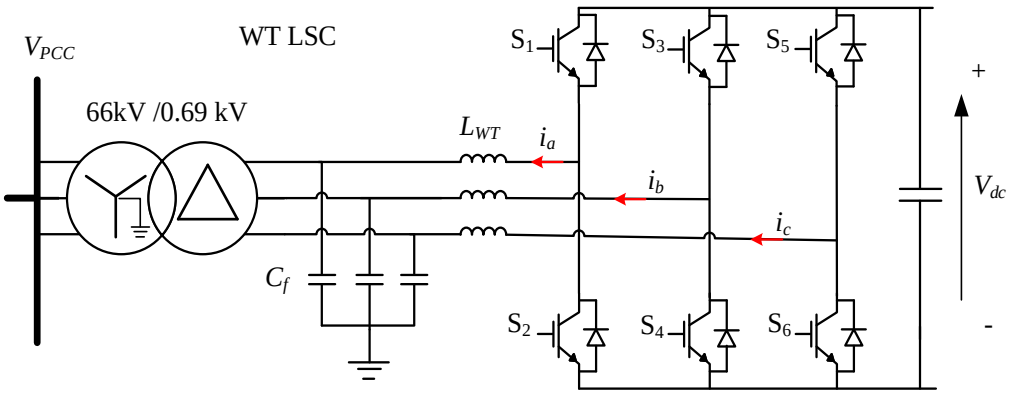

Fig. 3.12 Diagram of WT grid side converter modelling

As the offshore AC network is regulated by the MMC station, the WTs work under grid following mode, and their active and reactive power are controlled in a similar way as those AC connected WTs. Fig. 3.13 illustrated the control diagram in where outer power loops and inner current loops are used. Similar to the offshore MMC, the conventional double synchronous reference frame vector control is adopted for the WT LSC to enable a precisely control of both positive sequence and negative sequence current. The maximum dq^+ current references are set according to the converter current rating to limit the fault current. For the negative sequence current reference, the control target is set as suppressing the negative sequence current to zero.

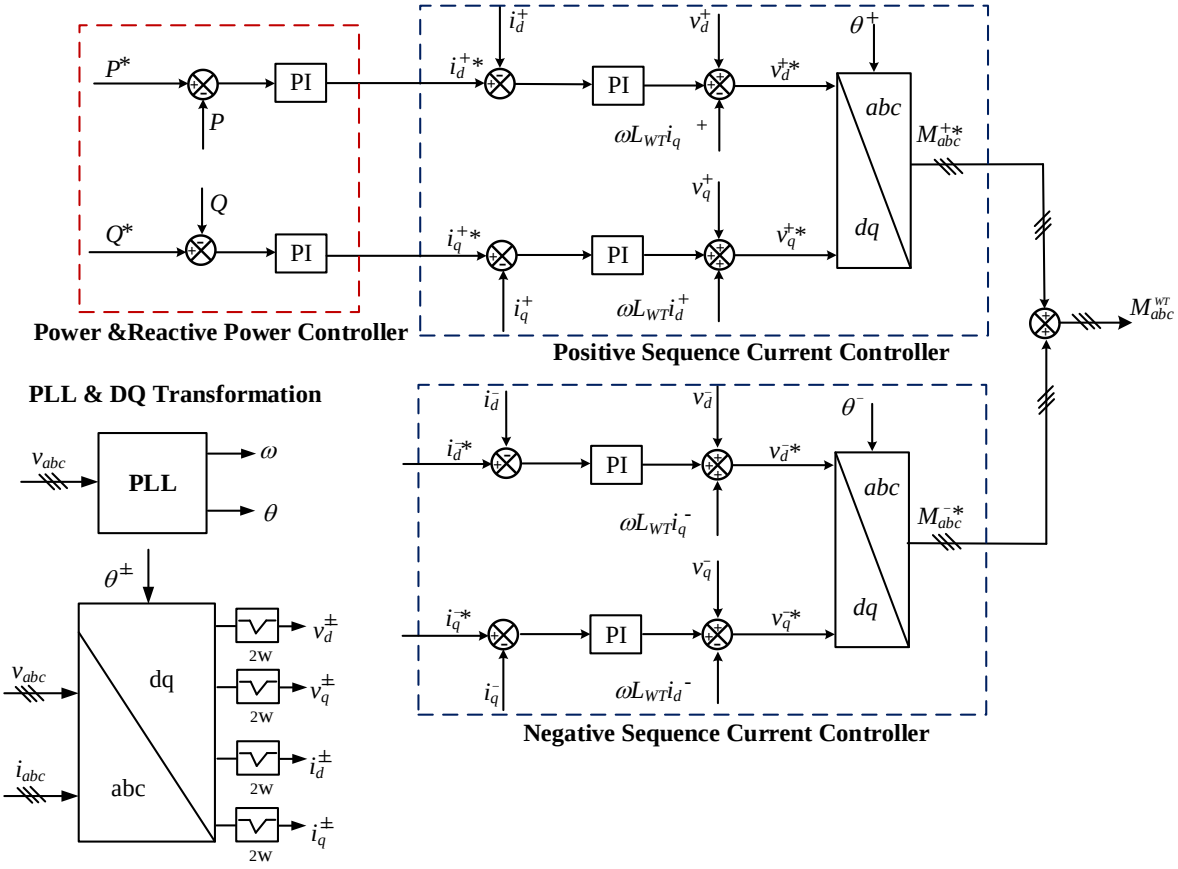

Fig. 3.13 WT LSC control diagram

3.2 Sequence network analysis during offshore asymmetrical faults

To simplify the analysis and for the purpose of illustration, the offshore AC collection grid with an AC fault applied at the 66 kV offshore cable shown in Fig. 3.1 is schematically represented in Fig. 3.14, where the offshore MMC and WT converters in Fig. 3.1 are replaced by two controllable three-phase voltage sources. As shown in Fig. 3.14, E_{MMC}^{j} and I_{MMC}^{j} (j=a, b, and c) are the phase voltage and current of the offshore MMC station, respectively; E_{WT}^{j} and I_{WT}^{j} are the respective phase voltage

and current of the WTs; V_F^j and I_F^j are the voltage and current at the fault point, respectively; Z_{MMC} and Z_{WT} are the equivalent impedances on the offshore MMC and WT sides, respectively; and the fault impedance is Z_F. The switches shown in Fig. 3.14 are used to represent different fault scenarios.

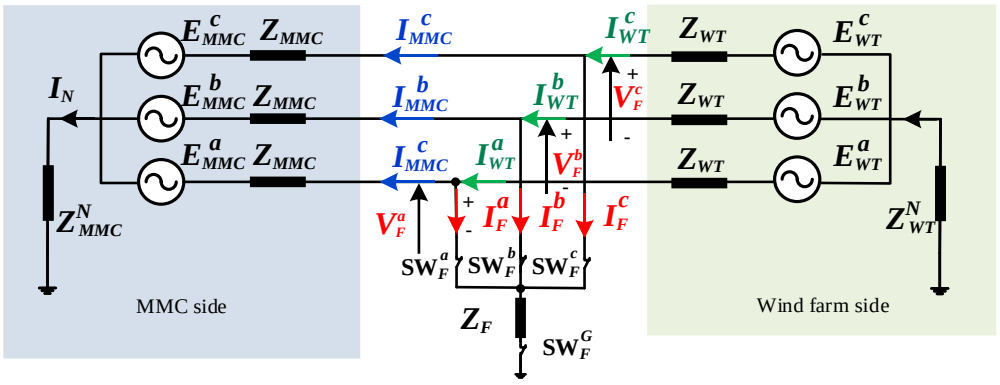

Fig. 3.14 Simplified offshore AC grid during faults.

The generic phasor expressions that describe the equivalent circuit of the offshore windfarm in Fig. 3.14 are:

$$\begin{cases} \mathbf{E}_{MMC}^{abc} + \mathbf{Z}_{MMC} \cdot \mathbf{I}_{MMC}^{abc} = \mathbf{V}_F^{abc} \\ \mathbf{E}_{WT}^{abc} - \mathbf{Z}_{WT} \cdot \mathbf{I}_{WT}^{abc} = \mathbf{V}_F^{abc} \end{cases} \tag{3.19}$$

The voltage and current vectors at potential fault point 'F' are:

$$\begin{cases} \mathbf{V}_F^{abc} = \mathbf{Z}_F \cdot \mathbf{I}_F^{abc} \\ \mathbf{I}_F^{abc} = \mathbf{I}_{WT}^{abc} - \mathbf{I}_{MMC}^{abc} \end{cases} \tag{3.20}$$

where $\mathbf{E}_{WT}^{abc}$, $\mathbf{E}_{MMC}^{abc}$ and $\mathbf{V}_F^{abc}$ are column vectors of the aggregate windfarm converter and MMC terminal voltages and the voltage at fault point, respectively; $\mathbf{I}_{WT}^{abc}$, $\mathbf{I}_{MMC}^{abc}$ and $\mathbf{I}_F^{abc}$ are column vectors of the windfarm converter and MMC currents and the fault current, respectively; and $\mathbf{Z}_{MMC}$ and $\mathbf{Z}_{WT}$ are generically defined, with 'x' referring to

'MMC' and 'WT' as:

$$\mathbf{Z}_x = \begin{bmatrix} Z_x + Z_x^N & Z_x^N & Z_x^N \\ Z_x^N & Z_x + Z_x^N & Z_x^N \\ Z_x^n & Z_x^N & Z_x + Z_x^N \end{bmatrix} \tag{3.21}$$

In (3.21), *N* denotes the corresponding grounding impedance. The three-phase *a, b, c* variables $\mathbf{F}^{abc}$ can be transformed into equivalent symmetrical component variables $\mathbf{F}^{0+-}$ in sequence frame by [126]:

$$\begin{cases} \mathbf{F}^{abc} = \mathbf{A}\mathbf{F}^{0+-} \\ \mathbf{F}^{0+-} = \mathbf{A}^{-1}\mathbf{F}^{abc} \end{cases} \tag{3.22}$$

where the transformation matrix A and A^{-1} are given as:

$$\mathbf{A} = \begin{bmatrix} 1 & 1 & 1 \\ 1 & \alpha^2 & \alpha \\ 1 & \alpha & \alpha^2 \end{bmatrix} \qquad \textit{and} \qquad \mathbf{A^{-1}} = \frac{1}{3}\begin{bmatrix} 1 & 1 & 1 \\ 1 & \alpha & \alpha^2 \\ 1 & \alpha^2 & \alpha \end{bmatrix} \tag{3.23}$$

where $\alpha = 1\angle 120°$. After transforming (3.19) to sequence frame using (3.22) and (3.23), the following expressions are obtained:

$$\begin{cases} \mathbf{E}_{MMC}^{0+-} + \mathbf{Z}_{MMC}^{0+-} \cdot \mathbf{I}_{MMC}^{0+-} = \mathbf{V}_F^{0+-} \\ \mathbf{E}_{WT}^{0+-} - \mathbf{Z}_{WT}^{0+-} \cdot \mathbf{I}_{WT}^{0+-} = \mathbf{V}_F^{0+-} \end{cases} \tag{3.24}$$

where $\mathbf{Z}_x^{0+-} = \mathbf{A}^{-1}\mathbf{Z}_x\mathbf{A}$ (subscription *x* represents MMC, WT and F) is a diagonal matrix and its components are:

$$\mathbf{Z}_x^{0+-} = \begin{bmatrix} Z_x + 3Z_x^N & 0 & 0 \\ 0 & Z_x + Z_x^N & 0 \\ 0 & 0 & Z_x + Z_x^N \end{bmatrix} \tag{3.25}$$

Expanding (3.24) leads to three pairs of decoupled equations which can be expressed graphically as three independent circuits for positive, negative and zero sequence voltages and currents. It should be noted that for converter-based networks, the negative sequence quantities can be controlled by injecting negatives sequence voltage through corresponding controllers, whilst the zero sequence is blocked by the delta-start transformer connection from converter side. Thus, compared with the traditional sequence modelling [77], the negatives sequence voltages are modelled to assess the behaviours during asymmetrical AC faults.

Similarly, the sequence voltages at the fault point are:

$$\mathbf{V}_F^{0+-} = \mathbf{Z}_F^{0+-} \cdot \mathbf{I}_F^{0+-} \tag{3.26}$$

where $\mathbf{Z}_F^{0+-}$ is a diagonal matrix of the fault impedances. From (3.24) and (3.26), considering all the four switches in Fig. 3.14 are open which represent normal operation (i.e. no fault), three independent positive, negative and zero sequence networks can be obtained as shown in Fig. 3.15.

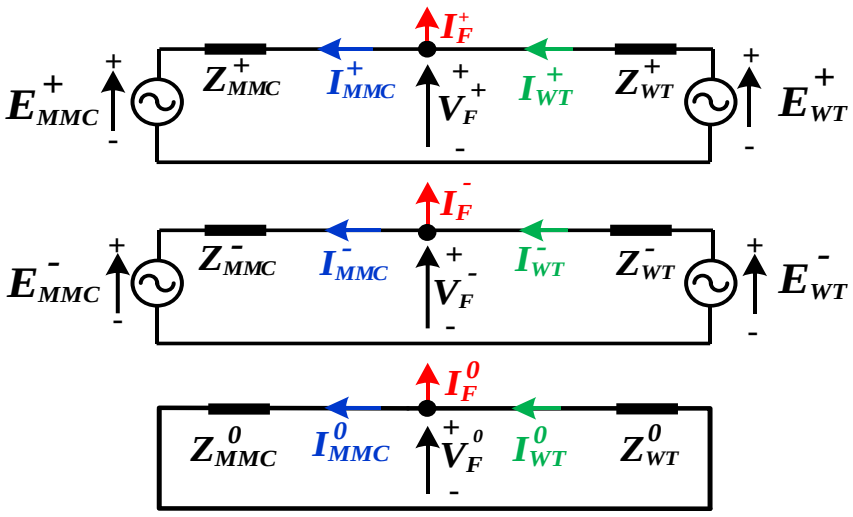

Fig. 3.15 Sequence network during normal operation.

3.2.1 Single-phase-to-ground fault

The single-phase-to-ground fault is represented by closing the switches SW_F^a and SW_F^G in Fig. 3.14. Based on circuit analysis on Fig. 3.14, the fault behaviours during a single phase to ground fault are:

- Fault current only flows on the faulty phase *a*, and the healthy phases (*b* and c) are zero.
- The voltage at the fault point in the faulty phase A is determined by the fault impedance Z_F.

These hypotheses are expressed mathematically as:

$$\begin{cases} V_F^a = Z_F^a I_F^a \\ I_F = I_F^a \;\&\; I_F^b = I_F^c = 0 \end{cases} \tag{3.27}$$

Transforming those equations to sequence networks obtain the followings:

$$\begin{cases} V_F^a = Z_F^a I_F^a \Rightarrow V_F^0 + V_F^+ + V_F^- = Z_F^a (I_F^0 + I_F^+ + I_F^-) \\ I_F = I_F^a = I_F^0 + I_F^+ + I_F^- \\ I_F^b = 0 \Rightarrow I_F^0 + \alpha^2 I_F^+ + \alpha I_F^- = 0 \\ I_F^c = 0 \Rightarrow I_F^0 + \alpha I_F^+ + \alpha^2 I_F^- = 0 \end{cases} \tag{3.28}$$

After algebraic manipulation of (3.28), it yields:

$$\begin{cases} I_F^0 = I_{WT}^0 - I_{MMC}^0 = I_F^+ = I_{WT}^+ - I_{MMC}^+ = I_F^- = I_{WT}^- - I_{MMC}^- = \frac{1}{3} I_F^a \\ V_F^0 + V_F^+ + V_F^- = I_F^a Z_F = 3 I_F^0 Z_F = 3 I_F^+ Z_F = 3 I_F^- Z_F \end{cases} \tag{3.29}$$

From the properties of series circuit exhibited in (3.29), the sequence network for a single-phase-to-ground AC fault is drawn in Fig. 3.16. Notice that the sequence network in Fig. 3.16 is similar to that of the conventional synchronous AC power system, except it includes negative sequence voltage that can be injected into the offshore AC network by offshore MMC and WT converters. From (3.29), the fault current becomes:

$$I_F^a = 3(I_{WT}^0 - I_{MMC}^0) = 3(I_{WT}^+ - I_{MMC}^+) = 3(I_{WT}^- - I_{MMC}^-). \tag{3.30}$$

From the above analysis, the following observations are drawn for single-phase faults:

- When the offshore MMC and WT control their output negative sequence currents at zero, i.e. $I_{WT}^- = I_{MMC}^- = 0$, fault current will become zero $(I_F^a = 0)$, and MMC and WT positive sequence currents must be equal $(I_{WT}^+ = I_{MMC}^+)$. Furthermore, (3.30) entails that the MMC and WT zero sequence currents will vanish regardless of their transformer ground arrangements, i.e. $I_{WT}^0 = 0$ and $I_{MMC}^0 = 0$.

- When the WT converter controls its negative sequence current at zero $(I_{WT}^{-}=0)$, while MMC does not $(I_{MMC}^{-}\neq 0)$, (3.30) indicates that the MMC alone defines the fault current level, i.e. $I_F^a = 3I_{MMC}^{-}$. Under such an operating condition, the MMC negative sequence current defines the difference between zero and positive sequence currents of the MMC and WT, i.e. $I_{WT}^{0} - I_{MMC}^{0} = I_{WT}^{+} - I_{MMC}^{+} = -I_{MMC}^{-}$.

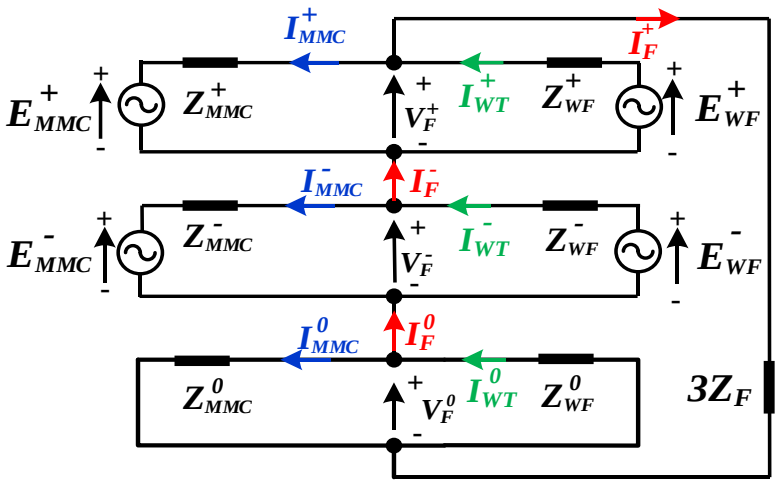

Fig. 3.16 Equivalent sequence circuits during single-phase-to-ground faults.

3.2.2 Phase-to-phase AC faults

When a phase-to-phase AC fault is considered between phases *b* and *c* as depicted by closing the switches SW_F^b and SW_F^c in Fig. 3.14 and assuming the fault impedance of Z_F, the main behaviours can be expressed as:

$$\begin{cases} V_F^c = V_F^b + Z_F I_F^b \\ I_F^a = 0 \,\&\, I_F^b + I_F^c = 0 \end{cases}. \tag{3.31}$$

From (3.31), the positive and negative sequence current and voltage relationships

are deduced as:

$$\begin{cases} V_F^+ = V_F^- - I_F^- Z_F \\ I_F^+ = -I_F^- \Rightarrow I_{WT}^+ - I_{MMC}^+ = -(I_{WT}^- - I_{MMC}^-). \\ I_F^0 = I_{WT}^0 - I_{MMC}^0 = 0 \end{cases} \tag{3.32}$$

Based on the properties exhibited by (3.32), the equivalent sequence network for a phase-to-phase AC fault is drawn in Fig. 3.17. Notice that the sequence network in Fig. 3.17 differs from the conventional synchronous AC network due to the presence of negative sequence voltages which are injected into the offshore AC grid by the WT and MMC,. Based on the above analysis of phase-to-phase AC fault, its behaviours are similar to the single-phase-to-ground AC fault established earlier. That is, no fault current will be observed if both offshore MMC and WT suppress their negative sequence currents, i.e. $I_F^+ = -I_F^- = 0$, $I_{WT}^- = I_{MMC}^- = 0$ and $I_{WT}^+ = I_{MMC}^+$.

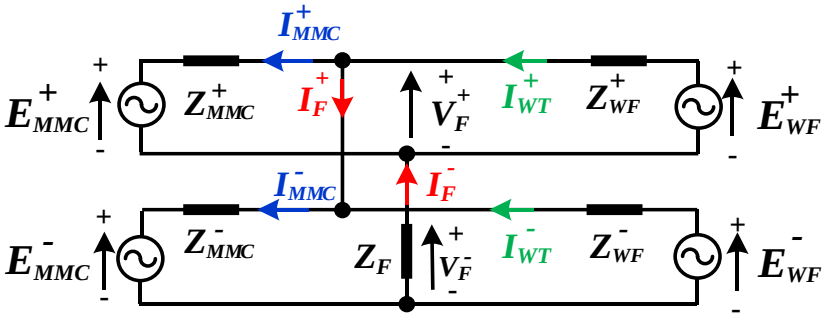

Fig. 3.17 Equivalent sequence circuit during phase-to-phase fault.

3.2.3 Phase-to-phase-to-ground AC fault

When a double phase-to-ground fault occurs in phase *b* and *c* as graphically depicted in Fig. 3.14 by closing the switches $SW_F{}^b$, $SW_F{}^c$ and $SW_F{}^G$, the fault behaviours can be described by:

$$\begin{cases} V_F^b = V_F^c = Z_F (I_F^b + I_F^c) = 3Z_F I_F^0 \\ I_F^a = 0 \end{cases} \tag{3.33}$$

From (3.33), the positive and negative sequence current and voltage relationships can be obtained as:

$$\begin{cases} V_F^+ = V_F^- = V_F^0 - 3Z_F I_F^0 \\ I_F^0 + I_F^+ + I_F^- = I_F^a = 0 \\ I_F = I_F^b + I_F^c = 3I_F^0 \end{cases} \tag{3.34}$$

Based on the circuit properties depicted by (3.34) , the sequence network for a phase-to-phase-to-ground AC fault is drawn in Fig. 3.18, where the positive, negative and zero sequence components co-exist as in the conventional synchronous AC power network. As in previous cases, the inclusion of negative sequence voltages of the offshore MMC and WTs has resulted in the following possibilities:

- Suppression of negative sequence currents at MMC and WT $(I_{WT}^- = I_{MMC}^- = 0)$ can only ensure zero negative sequence fault current $(I_F^- = 0)$ as shown in Fig. 3.18, but does not lead to zero fault current as in previous fault cases according to (3.34). This is because the network in Fig. 3.18 permits the residual positive sequence voltage at fault point to define both negative and zero sequence voltages, which indeed determines the fault current at fault point together with the effective impedance in the zero-sequence path, as depicted by (3.34). Under such conditions, positive and zero sequence currents, and the fault currents follow the relationship of $I_F^0 = -I_{WT}^0 + I_{MMC}^0 = I_{WT}^+ - I_{MMC}^+$, which entails the fault current and the net zero sequence current in the offshore AC network is determined by the net contribution from the positive sequence current. Therefore, it can deduce that lowering positive sequence voltage (and hence lower positive sequence current)

will lead to lower zero sequence current, hence fault current level.

- The equal imposition of positive, negative and zero sequence voltages dictated by the parallel nature of sequence networks during phase-to-phase-to-ground AC faults could result in overvoltage in the healthy phase as $V_F^a = V_F^+ + V_F^- + V_F^0$. Thus, due to the presence of negative sequence voltage, it is necessary to reduce the positive sequence voltage to prevent both excessive overcurrent and overvoltage in the offshore AC grid.

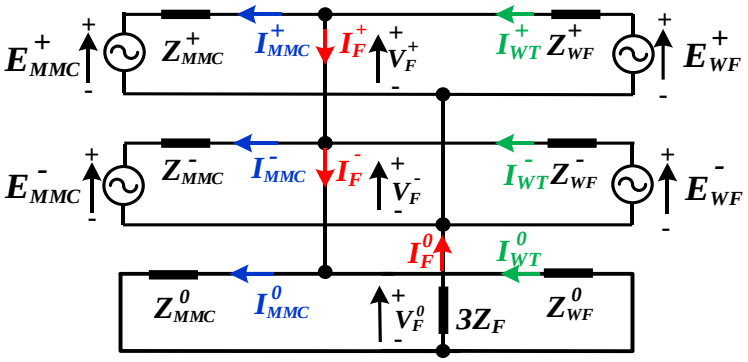

Fig. 3.18 Equivalent sequence circuit during double-phase-to-ground faults.

3.2.4 Theoretical analysis validation

To verify the theoretical analysis presented in previous sections, an offshore AC grid shown in Fig. 3.19 is built in PSCAD/EMTDC. The system consists of a 1200 MW offshore windfarm, local 66 kV offshore AC collection grid and an MMC based HVDC system rated at ±320 kV to transfer power to the onshore grid. A simple Thevenin equivalent circuit is used to represent the onshore AC grid, while offshore and onshore MMC1 and MMC2 are represented using electromagnetic Thevenin equivalent model with 350 submodules per arm available in the PSCAD library [127, 128]. MMC1 controls the offshore AC voltage while MMC2 regulates the DC voltage of the HVDC link. The offshore windfarm is composed of four 300 MW clusters and

each cluster is modelled as a lumped converter, as illustrated in Fig. 3.19. Different AC cables are used to reflect different distances of the WT clusters from offshore PCC. The detail parameters of the offshore MMC converter and WT converters are listed in Table 3.2 and Table 3.3 respectively.

The test system is subjected to a temporary asymmetric AC faults F1 at the middle of the cable C5 at t=2.5 s, with fault duration of 140 ms and fault resistance of 0.1 Ω. It is assumed that each WT converter is equipped with a DC chopper to dissipate excess energy during offshore AC faults. As discussed in previous sections, both MMC and WT suppressing their negative sequence currents to zero.

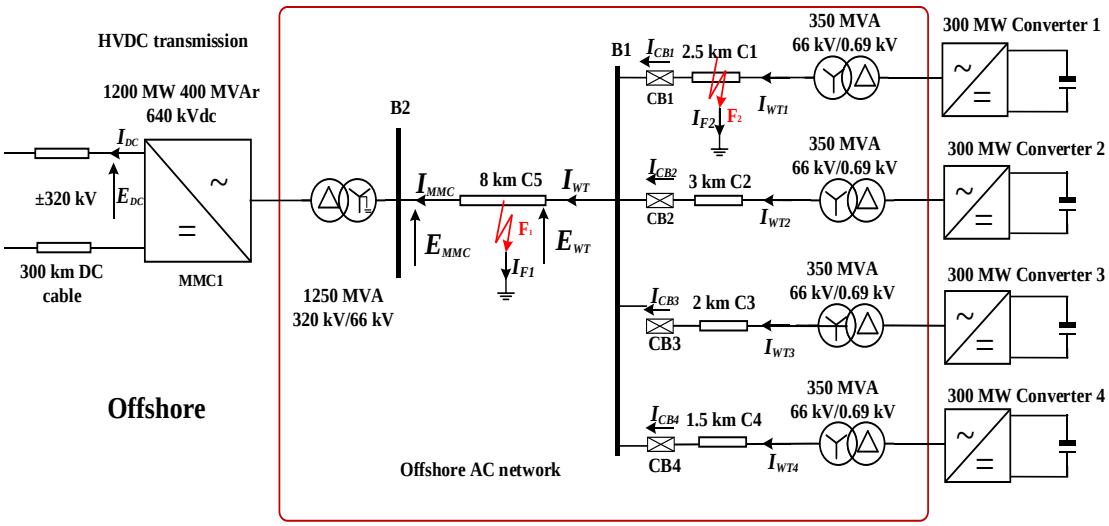

Fig. 3.19 The detailed representation of offshore network.

Table 3.2 Nominal parameter of onshore MMC.

Parameter	Nominal value
Rated power / DC voltage	1200 MW / ±320 kV
Onshore AC grid voltage	400 kV
MMC arm inductance	42 mH
No. of SMs per arm	350
Rated SM capacitor voltage / SM capacitance	1.83 kV / 8.8 mF

Table 3.3 Nominal parameters of the lumped WTs model.

Parameter	Nominal value
Rating of lumped WTs	300 MW
DC voltage	1100 V
Transformer voltage/ Leakage inductance	66/0.69 kV / 0.08 pu
Converter inductance	0.15 pu
Filter capacitance	0.1 pu

a) Single-phase-to-ground fault

Fig. 3.20 shows selected results to substantiate the analysis and observations drawn above, assuming a single-phase-to-ground AC fault occurs at 2.5 s and cleared at 2.64 s at the offshore AC cable as shown in Fig. 3.1. Observe that the WT and MMC

currents as shown in Fig. 3.20 b) and c) remain balanced during the single-phase-to-ground AC fault (after the initial transients) and consist of positive sequence components only as revealed in the above analysis. The fault current in Fig. 3.20 d) decays rapidly to zero after cables are discharged, resulting in disappearance of zero sequence currents as analysed in Section 3.2.1.

Notice that when the fault is cleared, the negative sequence voltages, which are injected by WT and MMC to suppress the negative sequence current and can be quantified by $E_{MMC}^{-} = E_{WT}^{-} = V_F^{-}$ from Fig. 3.16, remain. This is because after fault clearance, the boundary condition as depicted by (3.29) does not exist, which separates the sequence networks into the original three independent circuits, as shown in Fig. 3.15. To keep the AC currents of the offshore MMC and WTs balanced, the residual negative sequence voltages remain equal and unchanged. This behaviour prevents AC voltage recovery after fault clearance at 2.64 s as shown in Fig. 3.20 a).

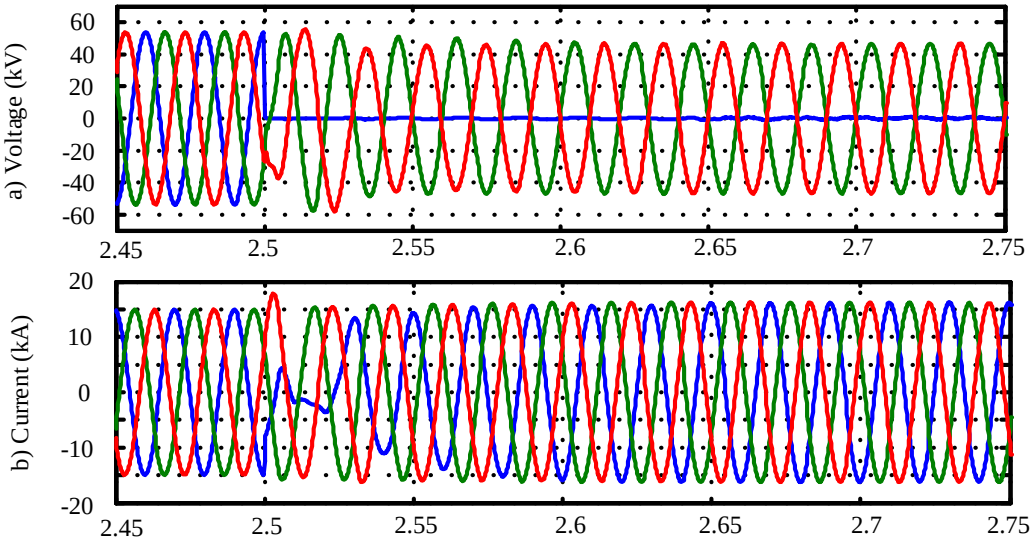

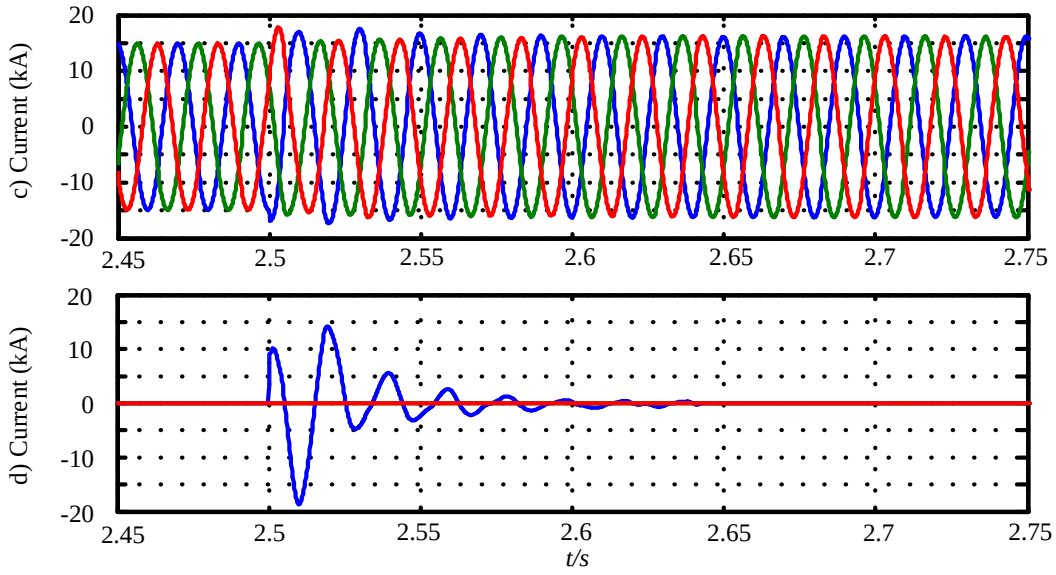

Fig. 3.20 Simulation waveforms during single-phase-to-ground fault from 2.5 s to 2.64 s when both MMC and WT suppress their negative sequence currents to zero: a) grid side voltages (E_{MMC}), b) MMC grid side three-phase currents (I_{MMC}), c) WT three-phase currents (I_{WT}), d) fault currents (I_F).

b) Phase-to-phase fault

A solid phase *b* to *c* fault is applied at 2.5s and cleared at 2.64s, and the simulation results are shown in Fig. 3.21. The system behaviours during phase-to-phase faults are similar to that during the single-phase-to-ground AC fault established earlier, i.e. no fault current will be observed when both offshore MMC and WT suppress their negative sequence currents to zero (i.e. $I_F^+ = -I_F^- = 0$, $I_{WT}^- = I_{MMC}^- = 0$ and $I_{WT}^+ = I_{MMC}^+$) as illustrated in Fig. 3.21. Also, operation under such condition leads to residual negative sequence voltage, which prevents AC voltage from recovering after fault clearance as discussed in the previous section.

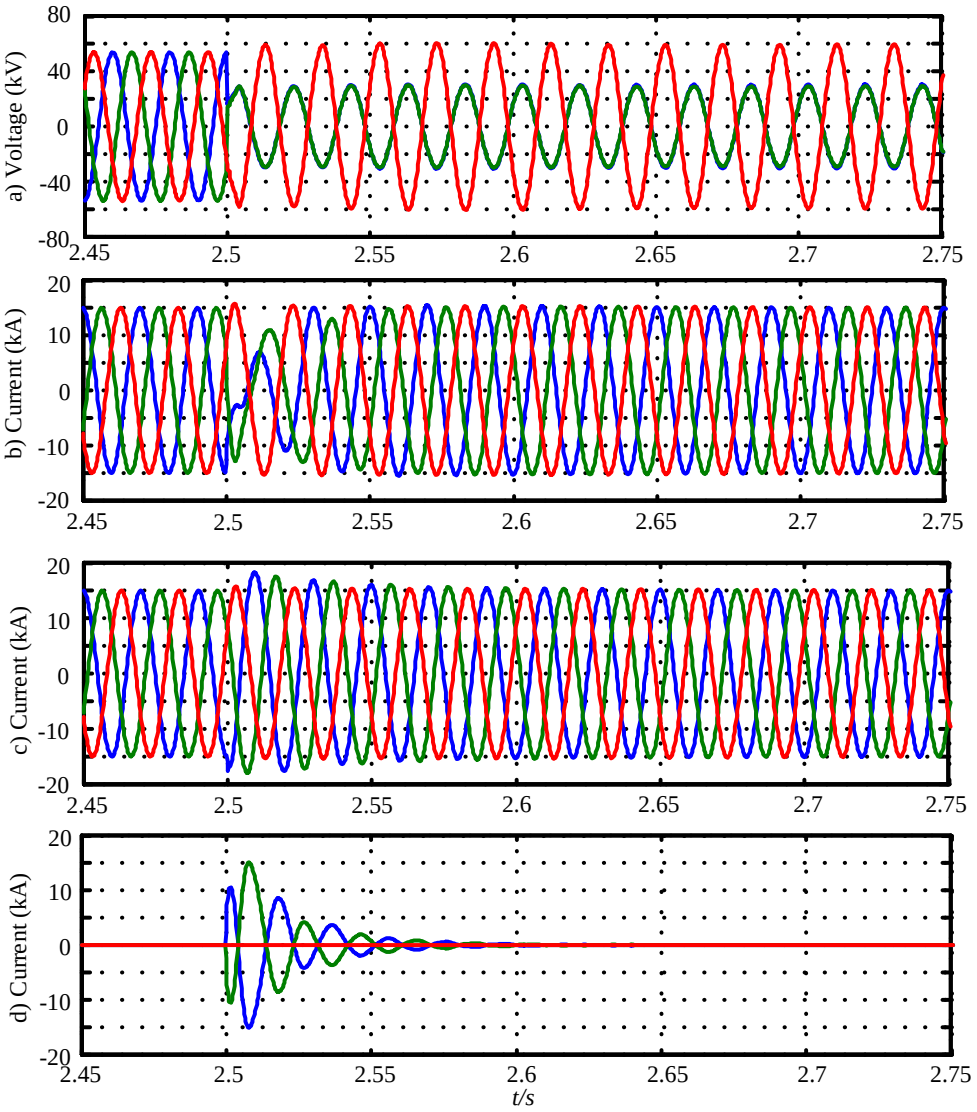

Fig. 3.21 Simulation waveforms during phase-to-phase fault from 2.5 s to 2.64 s when both MMC and WT suppress their negative sequence currents to zero: a) grid side voltages (E_{MMC}), b) MMC grid side three-phase currents (I_{MMC}), c) WT three-phase currents (I_{WT}), d) fault currents (I_F).

c) Phase-to-phase-to-ground fault

Fig. 3.22 shows selected simulation waveforms during an offshore phase-to-phase-to-ground fault from 2.5 s and to 2.64 s to validate the above analysis. Fig. 3.22 c) shows that the MMC currents measured at the converter side remain balanced with

reduced magnitude and contain no zero-sequence component, while that measured at grid side in Fig. 3.22 b) exhibit sustained unbalance due to zero sequence component. The three-phase fault currents as shown in Fig. 3.22 d) are no longer zero. Notice that the significant overvoltage in the healthy phase is observed during the fault as shown in Fig. 3.22 a), which is due to the induced zero and negative sequence voltages as aforementioned. After fault clearance, the negative sequence voltage remains unchanged and the currents are balanced as shown in Fig. 3.22 b) whereas the zero-sequence voltage disappears. These residual negative sequence voltages prevent the recovery of the offshore network as shown in Fig. 3.22 a), which is similar to the previously discussed cases.

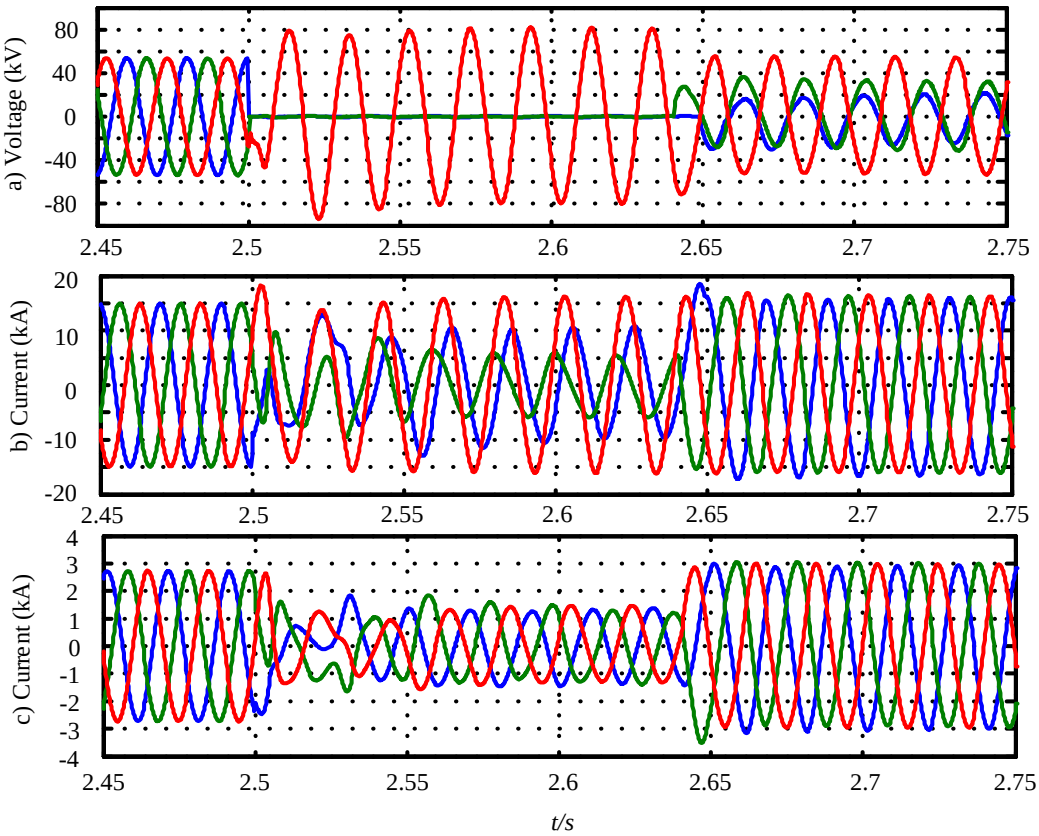

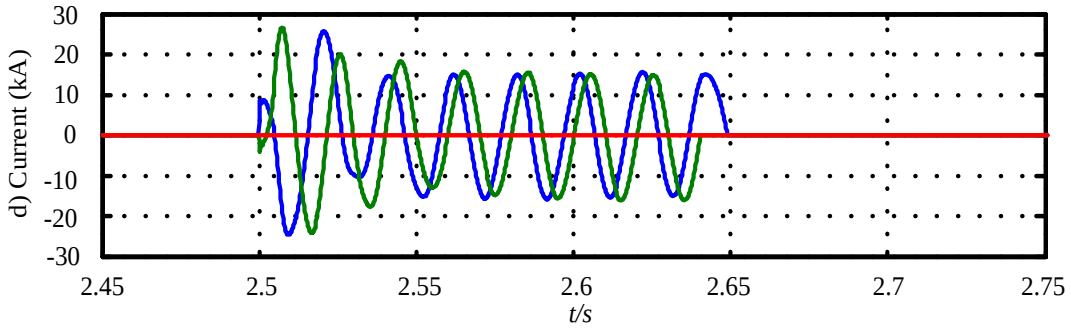

Fig. 3.22 Simulation waveforms for phase-to-phase-to-ground fault occurring at 2.5 s and cleared at 2.64 s when both MMC and WT suppress their negative sequence currents to zero: a) grid side voltages (E_{MMC}), b) MMC grid side currents (I_{MMC}), c) MMC converter side currents (I_{CMMC}), d) fault currents (I_F).

3.3 Proposed Scheme for Offshore AC Fault Management

From the anomalies revealed in the above discussions, the previous negative sequence suppression control, which regulates the negative sequence current from both the MMC and WTs to zero, is inadequate. Thus, a modified approach that exploits the inherent characteristics imposed by the sequence network analysis to control fault currents in offshore AC network is proposed to achieve the following objectives:

- Enable fault detection and discrimination by defining safe converter fault current level.
- Prevent excessive overvoltage in the offshore AC network.
- Accelerate offshore AC voltage recovery following clearance of asymmetric AC faults.

3.3.1 Proposed fault current management scheme

Fig. 3.23 shows the overall structure of the proposed MMC grid forming control. Compared with the conventional grid control, an additional outer negative sequence AC voltage control is equipped for the offshore MMC, which regulates both d^- and q^- axis components of the negative sequence voltage to zero during normal operation and actively injects negative sequence currents into offshore AC network during offshore asymmetrical AC faults.

As established in previous discussions, the magnitude of the fault current is determined by the negative sequence current that is injected by the offshore MMC and WT during asymmetrical faults. Therefore, WTs suppress their negative sequence currents during these asymmetric AC faults and the offshore MMC exclusively defines the fault current level for protection purpose by controlling the injected negative sequence currents. According to the theoretical analysis in Section 3.2 and control scenario stated above, the fault currents during single-phase-to-ground and phase-to-phase AC faults are respectively linked to MMC negative sequence currents, i.e., $I_F^a = 3I_{MMC}^-$ and $I_F^a = -I_F^b = j\sqrt{3}I_F^- = j\sqrt{3}I_{MMC}^-$, as demonstrated quantitatively by Fig. 3.24 a) and b).

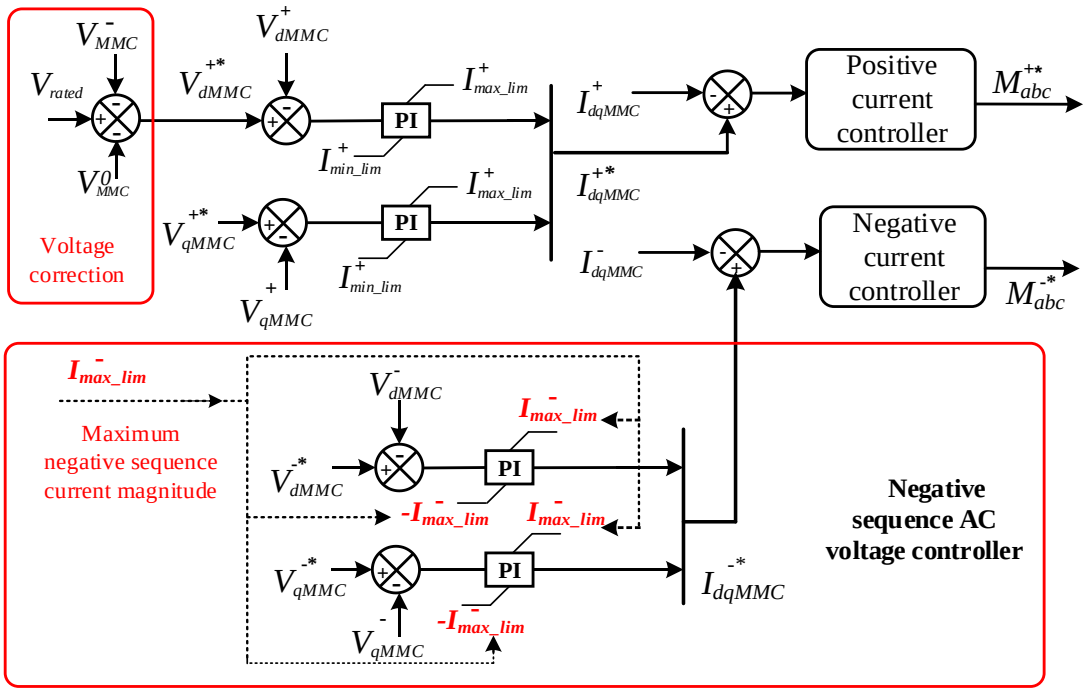

Fig. 3.23 Modified control strategy for offshore MMC stations.

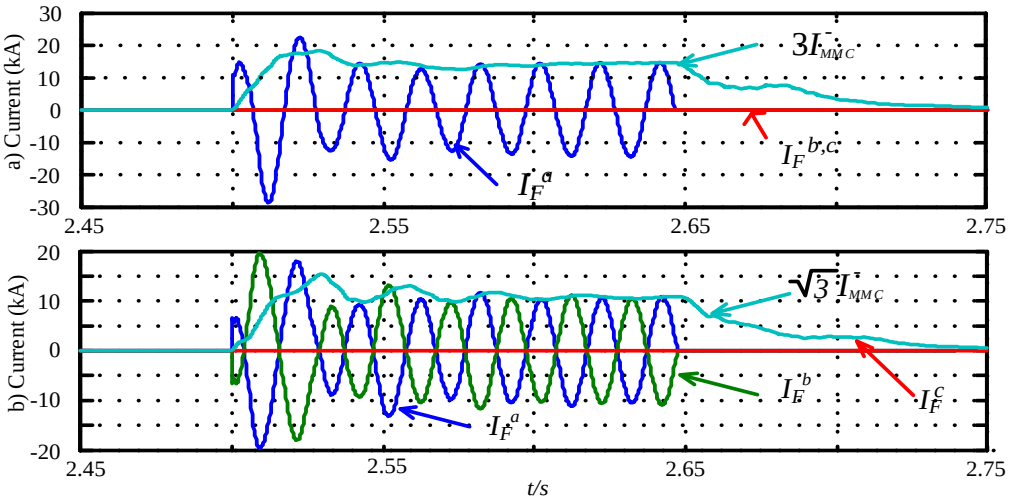

Fig. 3.24 Simulation waveforms for illustrating the relationship between fault current magnitude and corresponding injected negative sequence current: a) single-phase-to-ground fault, b) phase-to-phase fault.

Generally, during asymmetrical AC faults, the negative sequence current injected by MMCs is insufficient to correct the unbalanced grid voltage. Therefore, the outer

negative sequence AC voltage controller shown in Fig. 3.23 should not pursue the objective of suppression of negative sequence voltage to zero. Instead, it defines a safe level of negative sequence current set by the maximum negative sequence current magnitude $I^{-}_{\max\_lim}$. The injected negative sequence current should also be compatible with protection system requirements. Thus, $I^{-}_{\max\_lim}$ must account for circuit breaker settings and ratings of individual lines.

After fault clearance, the offshore MMC will facilitate controlled injection of negative sequence current in an effort to nullify the residual negative sequence voltages created by the fault to accelerate AC voltage recovery, while the WT converters keep negative sequence current at zero. It must be emphasized that the magnitude and characteristics of the injected negative sequence current impact the AC voltage recovery speed. Injection of small negative sequence current leads to slow nullification of residual negative sequence voltage after fault clearance, as demonstrated in Fig. 3.25.

Based on the principles articulated above, cascaded d-q negative sequence voltage and current loops are designed to facilitate controlled injection of negative sequence current by the offshore MMC, with d-q negative sequence current orders given equal priorities as determined by $I^{-}_{\max\_lim}$ shown in Fig. 3.23.

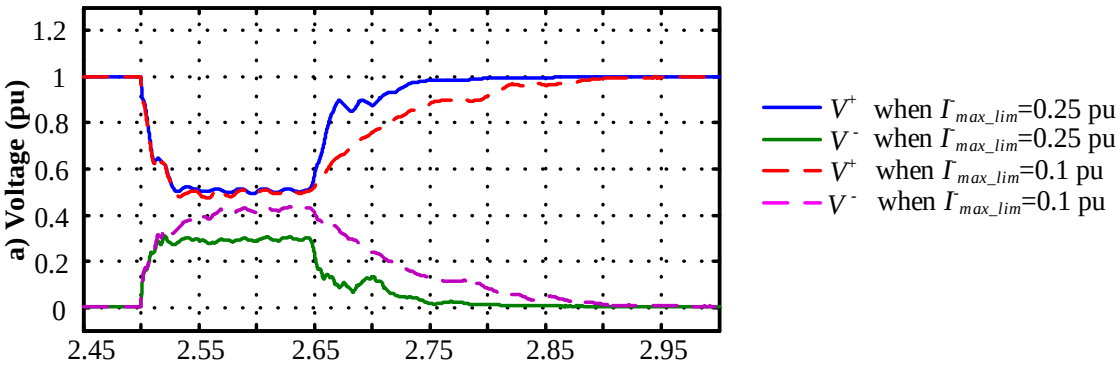

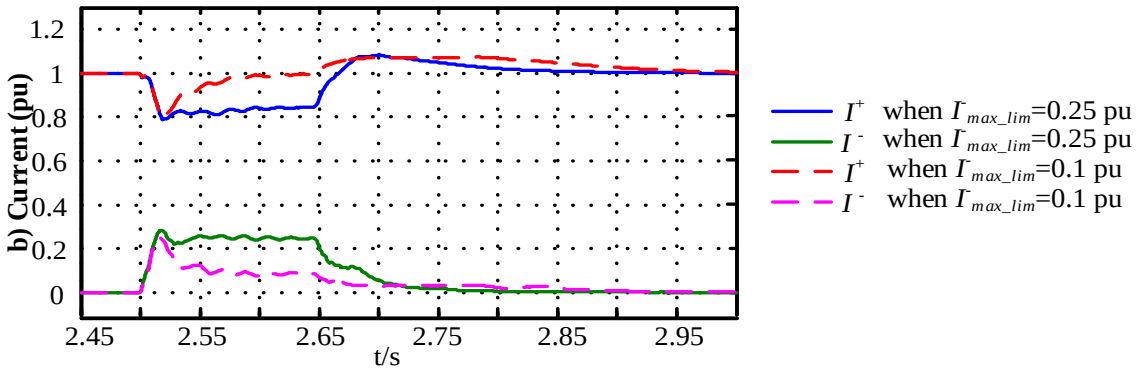

Fig. 3.25 Influence of injected negative sequence current amplitude on system recovery speed: a) positive and negative sequence voltages, b) positive and negative sequence currents.

3.3.2 Over-modulation and overvoltage consideration for offshore MMC

During phase-to-phase-to-ground AC faults, the magnitudes of zero sequence current and voltage depend on the residual positive sequence voltage, and the simultaneous co-existence of positive, negative and zero sequence voltages could potentially create significant overvoltage in the healthy phase on the grid side. Also, when negative sequence currents are no longer controlled at zero during single-phase-to-ground AC faults, zero sequence voltage is induced, which will also exacerbate the overvoltage problem in the healthy phases.

In addition, the required converter output voltage is the sum of negative and positive sequence components generated by their corresponding inner current controllers. Trying to maintain the positive sequence voltage at nominal value in the presence of negative sequence voltage during asymmetrical AC faults will lead to the total required voltage over the converter voltage limitation [129] and the saturation of both positive and negative control loops. This over-modulation behaviour degrades the controllability of the system and thus should be avoided.

Therefore, to prevent overvoltage in the offshore AC network and converter over-modulation, this thesis introduces an adjustment to the positive sequence voltage set-point of the offshore MMC that takes into account both induced negative and zero sequence voltages as shown in the top left of Fig. 3.23. Thus, a further modification that describes the positive sequence voltage set-point is given as:

$$V_{dMMC}^{+*} = V_{rated} - V_{MMC}^{-} - V_{MMC}^{0} \tag{3.35}$$

By applying (3.35), reduction of the positive sequence voltage magnitude in the offshore AC network will be initiated by the MMC to prevent overvoltage in the AC grid during asymmetric AC faults. In the meantime, the reduction of positive sequence voltage also prevents the saturation of the voltage and current controllers and the over-modulation of the converter to ensure controllability of the system.

3.4 Simulation results

To validate the analysis and effectiveness of the proposed method, the test system as detailed in Section 3.24 is subjected to a temporary asymmetric AC faults F1 at the middle of the cable C5 at t=2.5 s, with fault duration of 140 ms and fault resistance of 0.1 Ω. During asymmetric AC faults, the WT LSC control their negative sequence currents at zero, whereas the maximum negative sequence current contribution from the offshore MMC is limited to 0.25 pu, considering the need for fault detection and post-fault recovery though it can be set to different values based on system control and protection requirements.

3.4.1 Single-phase-to-ground fault

Fig. 3.26 displays the simulation waveforms during a single-phase-to-ground fault (F1, Fig. 3.19) at cable C5. Unlike the illustrative case presented in Fig. 3.20, Fig. 3.26 a) shows that the AC voltage in the offshore AC network has recovered to pre-fault level 60 ms after fault clearance. During the fault period, Fig. 3.26 b) shows that the currents injected to the 66 kV offshore network by the MMC contain negative sequence currents, which feed the fault currents shown in Fig. 3.26 e). Due to the use of star-delta interfacing transformer, the zero sequence currents are absent on the converter side and thus the converter side currents exhibit different waveforms to the grid side currents, as shown in Fig. 3.26 d). The WT side AC currents shown in Fig. 3.26 c) remain balanced. The results show no significant overvoltage on the healthy phases nor excessive overcurrent. Fig. 3.26 f) and g) show that the MMC DC side does not exhibit second-order oscillation during faults with the proposed control. As the positive sequence voltage and current are both reduced due to the fault, the power transferred to the onshore grid is also decreased as shown in Fig. 3.26 f). The offshore MMC arm currents shown in Fig. 3.26 h) do not increase significantly and remain well below the safe limit of 1.2 pu [51]. Similarly, the MMC SM capacitor voltages exhibit some disturbances during the fault but the maximum over-voltage is limited to 20% during the transients [130].

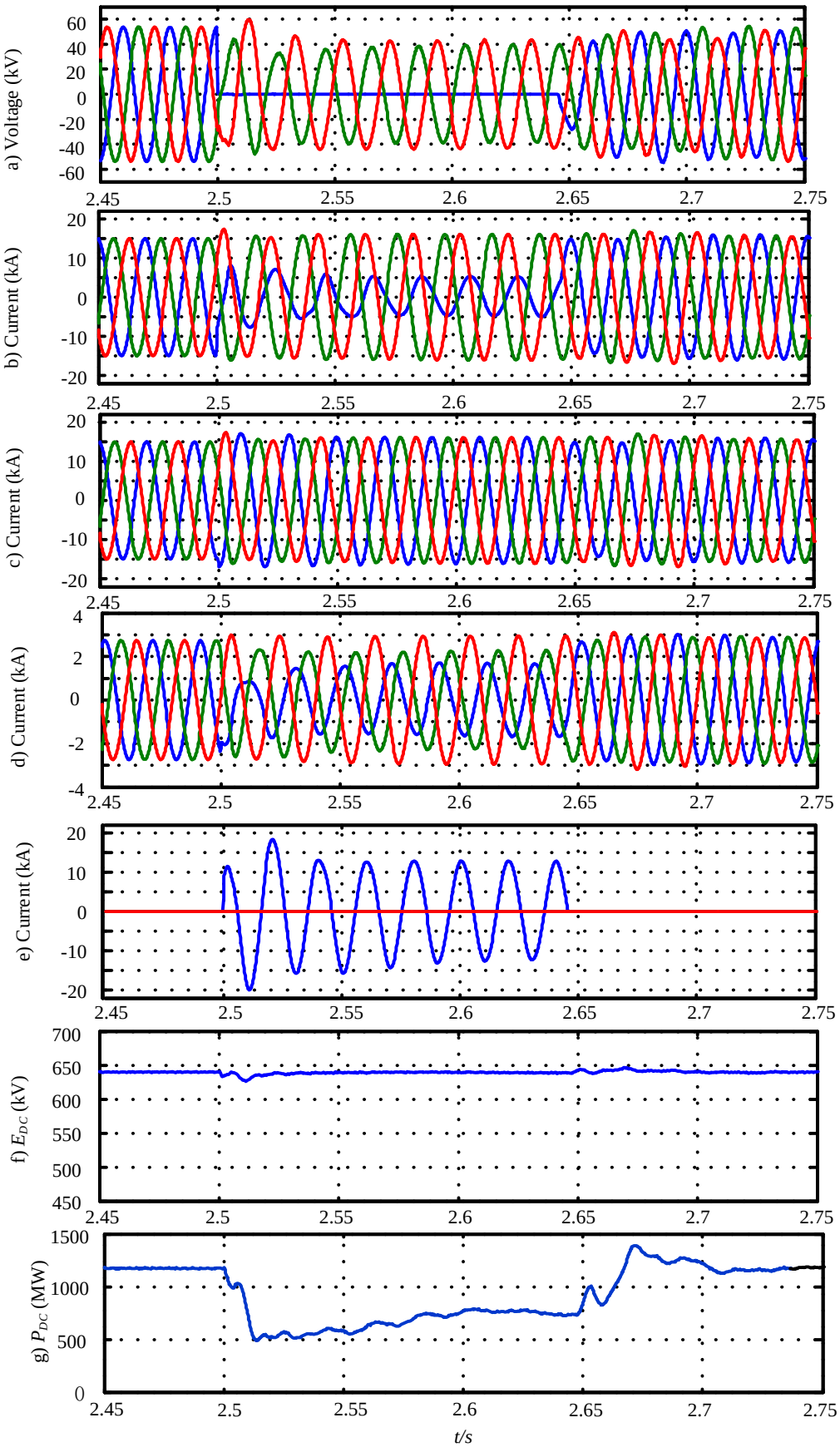
a) Voltage (kV)
60
40
20
0
-20
-40
-60
2.45
2.5
2.55
2.6
2.65
2.7
2.75
b) Current (kA)
20
10
0
-10
-20
c) Current (kA)
d) Current (kA)
4
2
0
-2
-4
e) Current (kA)
f) E_{DC} (kV)
700
650
600
550
500
450
g) P_{DC} (MW)
1500
1000
500
0
t/s

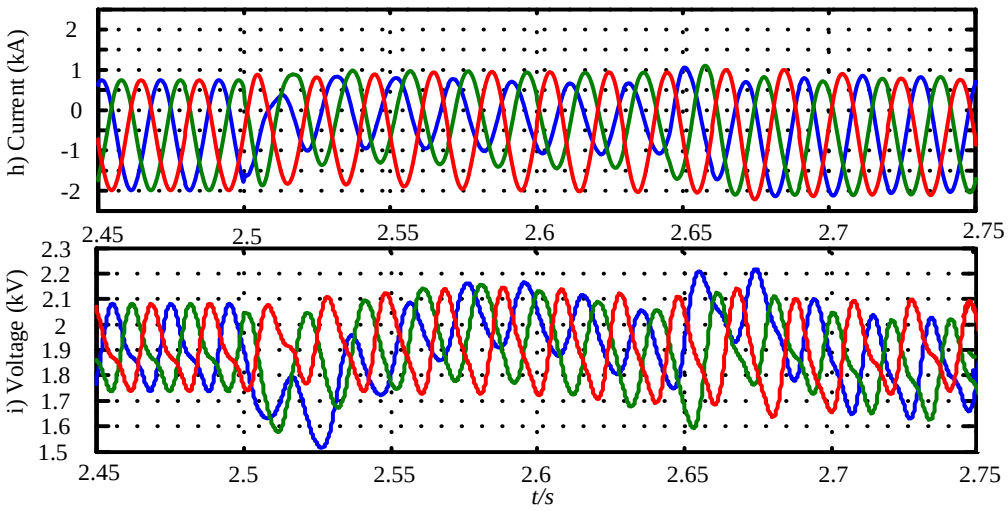

Fig. 3.26 Simulation waveforms during single-phase-to-ground fault: a) offshore MMC AC voltages (E_{MMC}), b) and c) are AC currents injected into offshore network by the offshore MMC (I_{MMC}) and WTs (I_{WT}), respectively, d) MMC converter side currents (I_{CMMC}), e) fault current (I_F), f) DC side voltage (E_{DC}), g) DC side power (P_{DC}), h) MMC upper arm currents, i) MMC average capacitor voltages

3.4.2 Phase-to-phase AC faults

Fig. 3.27 summarizes the simulation waveforms for a phase-to-phase AC fault when offshore MMC injects controlled negative sequence currents to accelerate AC voltage recovery, while the WT converters control their negative sequence currents at zero. As illustrated in Fig. 3.27 a), the offshore AC voltage quickly recovers in after fault clearance (around 60 ms). Fig. 3.27 b) and c) confirm that the offshore grid AC currents are followed its order as the WTs suppress the negative sequence to zero while the offshore MMC injects the certain negative sequence current to help the offshore AC voltage recovery. Fig. 3.27 d) indicates that the MMC converter side currents remain tightly controlled without significant over-current. Also, the supplied fault currents remain well-regulated as demonstrated in Fig. 3.27 and can be adjusted accordingly to facilitate fault detection and prevent overcurrent and overvoltage.

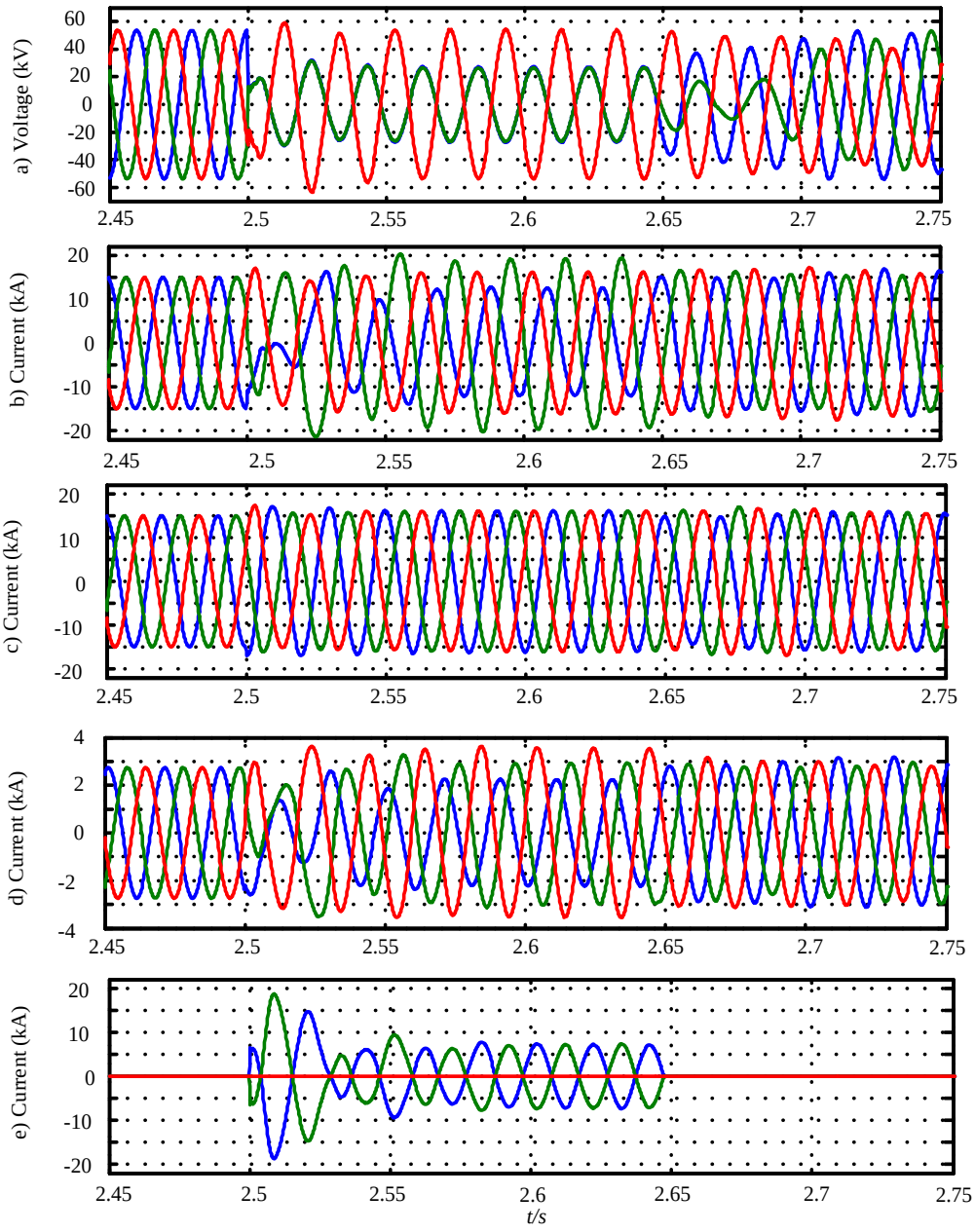

Fig. 3.27 Simulation waveforms for the scenario during phase-to-phase (a-b) fault: a) offshore MMC AC voltages (E_{MMC}), b) and c) are AC currents for the offshore MMC (I_{MMC}) and WTs (I_{WT}) injected into offshore network, respectively, d) MMC converter side currents(Ic_{MMC}), e) fault current (I_F).

3.4.3 Phase-to-phase-to-ground faults

Fig. 3.28 summarizes the simulation waveforms for a phase-to-phase-to-ground AC fault. As shown in Fig. 3.28 a), the overvoltage of the healthy phase during the fault is effectively suppressed by actively reducing the positive sequence voltage according to (3.35), which considers both the negative and zero sequence voltages. In addition, the offshore AC voltage starts to recover to pre-fault condition as soon as the fault is cleared. If desired, the magnitude of the fault current in Fig. 3.28 e) can be further reduced by instructing the MMC to reduce the magnitude of the positive sequence voltage, as aforementioned in Section 3.2.3.

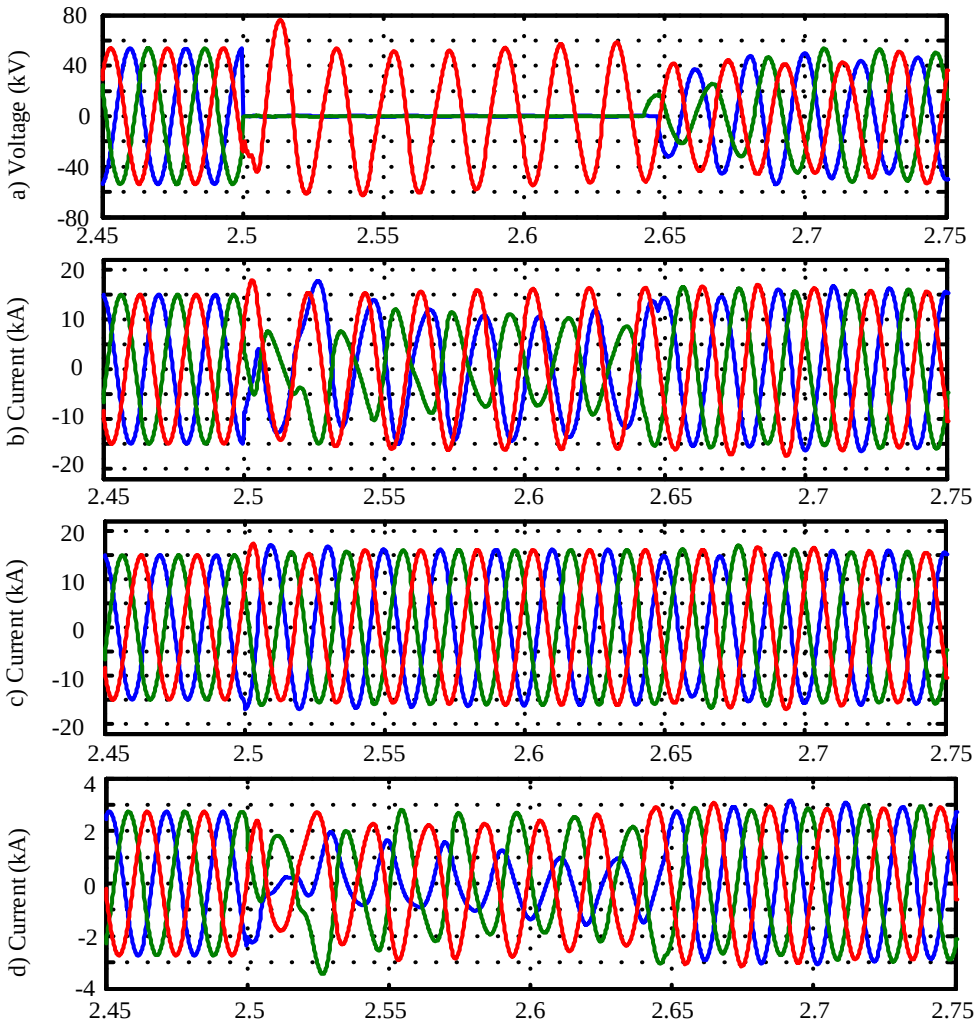

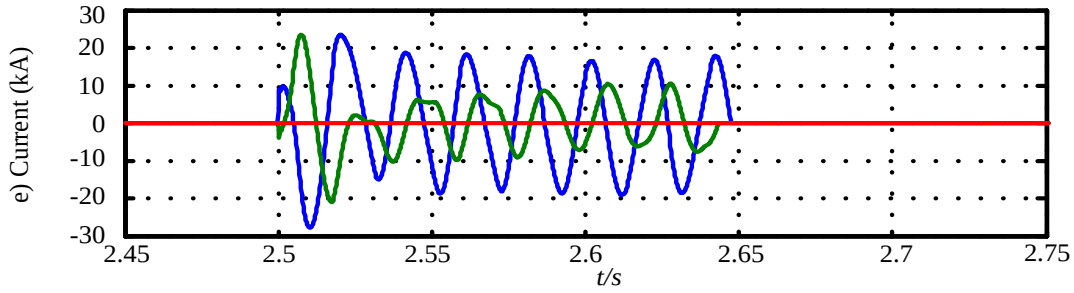

Fig. 3.28 Simulation waveforms during phase-to-phase-to-ground AC fault: a) offshore MMC AC voltages (E_{MMC}), b) and c) are AC currents for the offshore MMC (I_{MMC}) and WTs (I_{WT}) injected into offshore network, respectively, d) MMC converter side currents (Ic_{MMC}), e) fault current I_F).

3.5 Example illustration of potential application

The proposed control strategy can help the fault detection for protection system during offshore asymmetric AC faults. For example, when an asymmetric AC fault F2 occurs on the cable C1 as shown in Fig. 3.19, according to the discussions and analysis presented earlier, the current distribution in the offshore AC network can be summarized as follows:

- As WT converters do not inject negative sequence current, no overcurrent will be observed in WT converters and the cables associated with healthy clusters and their respective ACCBs (CB2, CB3 and CB4, Fig. 3.19).

- Only the AC cable and circuit breaker CB1 in the faulty cluster will experience overcurrent, dominantly due to additional negative sequence current provided by the offshore MMC, i.e., AC cable C5 and part of cable C1 in the fault current path. No extra current stress will be exerted on the part of C1 associated with the WTs. Thus, the current in CB1 is $I_{CB1}^{abc} = I_{WT1}^{abc} - I_{F2}^{abc}$ and consists of positive

sequence current from WT converters which is limited to 1.1 pu, and negative sequence current from the offshore MMC.

To substantiate the above discussion, the permanent single-phase-to-ground fault F2 is simulated. The ACCBs are opened with a fixed delay of 7 cycles. As articulated throughout the chapter, the injected negative sequence current by the MMC is set at 0.25 pu, which determines the fault current level. In practical system, the setting of the negative sequence current threshold will be decided by the protection system requirements.

The simulation results as shown in Fig. 3.29 support the above analysis. No overcurrent is observed from the healthy clusters as depicted in Fig. 3.29 d), f) and h), with their peaks limited to 1.1 pu as stated earlier. In contrast, Fig. 3.29 b) shows that the currents flowing through CB1 of the fault cluster has well exceeded 2.0 pu and has led to its tripping. Following the fault isolation, the faulty cluster is shut down and the remaining parts of the offshore grid regain their steady-state conditions, see Fig. 3.29 a) and c).

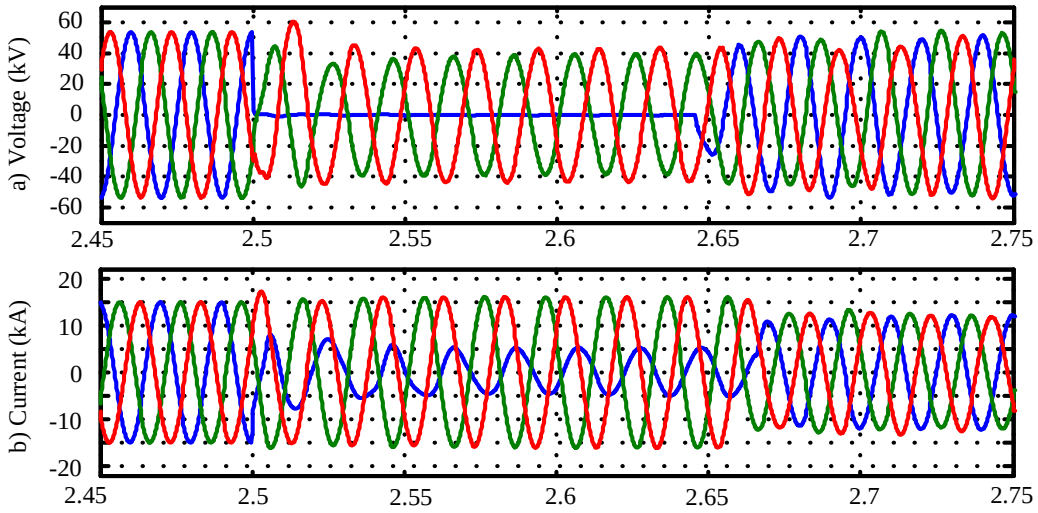

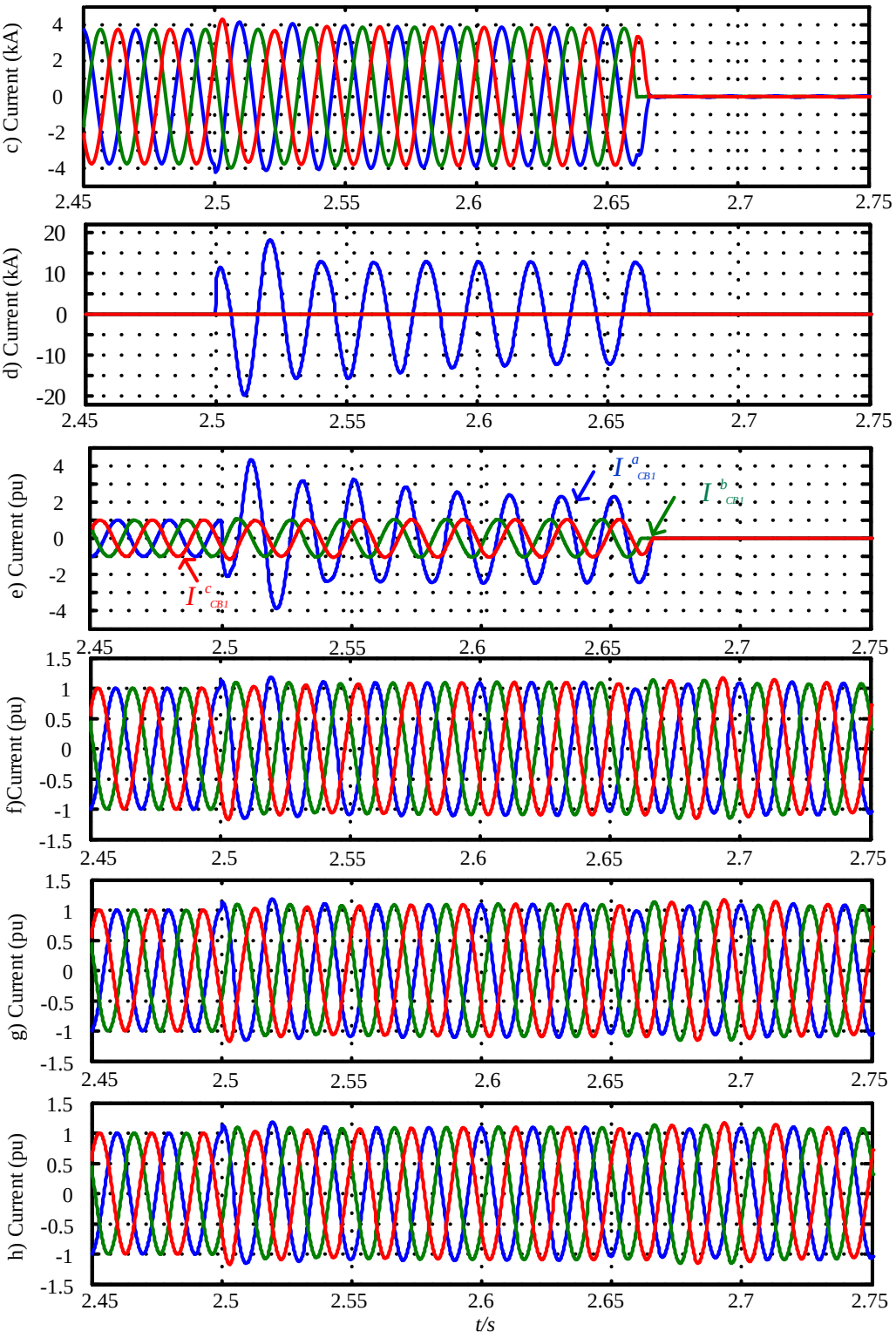

Fig. 3.29 Overcurrent protection waveforms during cluster fault: a) grid side voltage (E_{MMC}), b) MMC grid side currents (I_{MMC}), c) WT currents of the faulty cluster (I_{WT1}), d) fault currents (I_F) e), f), g) and h) are currents for CB1-4 (I_{CB1}, I_{CB2}, I_{CB3}, I_{CB4}) in pu,.

3.6 Summary

This chapter has conducted a comprehensive study on the ways to regulate the positive, negative and zero sequence currents and voltages during asymmetrical offshore faults for MMC-HVDC connected offshore wind farm systems. Detailed analysis and simulation validation reveal that, when negative sequence currents are completely suppressed to zero during asymmetrical faults, the induced negative sequence voltage does not allow the automatic recovery of the AC voltage to the pre-fault condition after fault clearance. Such behaviour could make protection system unable to distinguish between the fault and post-fault conditions as the voltages and currents remain the unchanged after fault is cleared.

To address the aforementioned issues, this chapter proposes a new modified control scheme that employs negative sequence voltage controller to facilitate controlled injection of negative sequence currents to not only define a safe level of fault current but also enable quick recovery of the AC voltage following clearance of AC faults. The excessive overvoltage in the healthy phases during asymmetrical AC faults is prevented by modifying the setting of the positive sequence voltage reference for the offshore MMC converter, which takes the induced negative and zero sequence voltages into consideration. The impact of proposed control method impact on overcurrent protection of cluster cables is also presented and discussed. The viability of the proposed control has been tested and confirmed using simulation performed in PSCAD.

Chapter 4
Enhanced Control of Offshore Windfarm Connected to Meshed DC Grid during DC Fault

In Chapter 3, enhanced system control and operation during offshore asymmetrical AC faults are discussed and analysed. Many studies and projects have confirmed the benefits of using MTDC networks for increased power transmission reliability by reducing the overall downtime of loss of infeed resulting in lower overall investment and operation cost [24-26]. Thus, it is very likely in the future that the onshore terminals will be combined with offshore windfarm connections, transforming those infrastructures into a MTDC system to provide a cost-effective and secure energy supply. However, system protection and control during DC fault is a challenge for the development of MTDC connected offshore windfarms.

Thus, this chapter investigates the DC fault handling strategies for MMC based minimal meshed DC grid which is used for the benchmark model in the PROMOTioN project [29]. To save the investment cost, a partially selective DC fault protection scheme is proposed where the expensive and bulky DCCBs are avoided in offshore platforms. However, such protection scheme may cause problems when the offshore MMC station is suddenly blocked during DC faults or the ACCBs in offshore AC grid suddenly open for fault clearance operation. In such a situation, the offshore AC grid loses its voltage regulation, and the offshore WT GSCs commonly equipped with grid following control lose their voltage reference, leading to over-voltage and frequency deviation in the AC offshore grid. Such behaviours may result in the shutdown of the offshore windfarm which would prevent a speedy recovery of the system even after

fault isolation.

To address such issues, an enhanced control for WT LSCs is proposed to enable the retention of AC voltage and frequency control when the offshore converter is lost, in which seamless transition of the WT control between grid following and forming modes is facilitated. The viability and application of the proposed control is demonstrated in proposed partially selective DC fault protection in the studied meshed DC grid, which includes detailed implementations of DC fault clearance, system restart and power transfer resumption. The effectiveness of the proposed control and the partially selective DC fault protection are validated in PSCAD/EMTDC.

4.1 Meshed DC grid and DC fault protection solutions

4.1.1 Meshed four-terminal DC network

The studied system is illustrated in Fig. 4.1. All the four HVDC stations in the DC grid are modelled as HB-MMCs with detailed description in Chapter 3 and equipped with the following controllers: DC voltage/active power, AC voltage and frequency (for the offshore MMCs), inner currents controller, circulating current suppression, and vertical and horizontal energy balancing. The DC grid control adopted in this thesis is the master-slave control and the control functions allocated to each converter station in are:

- MMC 1 regulates the DC voltage of the DC network at 640 kV and reactive power exchange at PCC 1 at zero.
- MMC 2 exports 1000 MW to PCC 2 at unity power factor.
- Both MMC 3 and MMC 4 operate as grid forming and control the AC voltage

and frequency at 155 kV and 50 Hz for the offshore networks of the offshore windfarms 1 and 2.

Each of the 1200 MW offshore windfarms 1 and 2 shown in Fig. 4.1 is modelled as four lumped converters as presented in Chapter 3 with detailed parameters listed in Table 3.2 and Table 3.3.

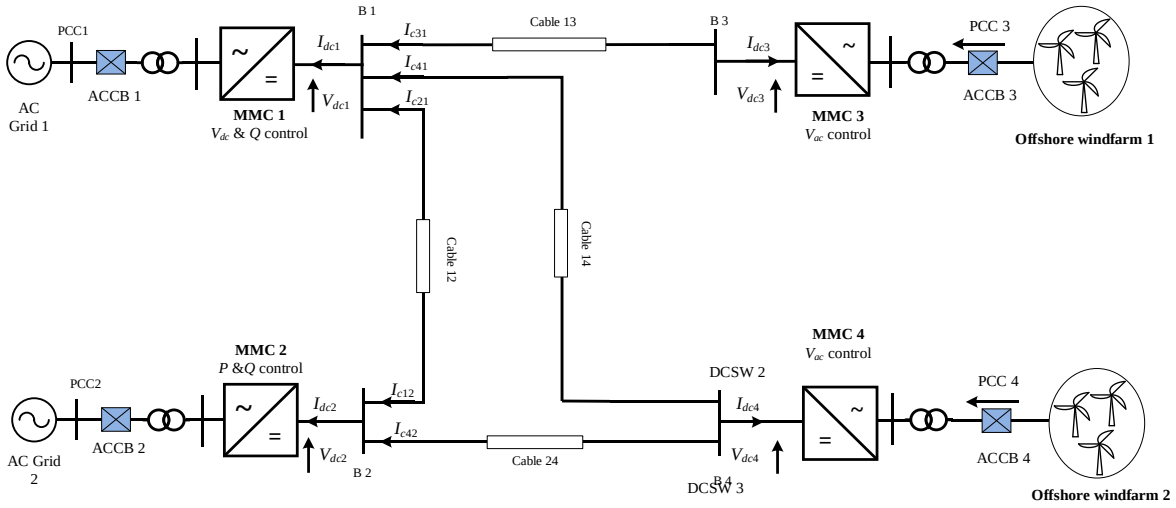

Fig. 4.1 The meshed four-terminal DC network for offshore wind power transmission.

4.1.2 DC grid protection solutions

a) Selective fault clearing strategy with DC circuit breakers

The general fault handling scheme with selective fault clearing strategy is to use DCCBs with large current limiting inductance at each DC line as shown in Fig. 4.1. After fault occurrence, the fault propagates through the DC system very quickly due to the low DC impedance and results in high fault current. The common detection and localization criteria for DC fault are based on the voltage breakdown and current rise [101]. To avoid damage to the HVDC converter hardware (mainly IGBT due to the limited overcurrent capability), DCCBs need to take reaction in a few milliseconds to

break the large DC fault current. After successful fault clearance, the DC voltage in the system needs to be restored so power flow can be restarted and adjusted to the new system configuration.

However, the high costs and large footprints of DCCBs and their associated current limiting inductors will enlarge the total investment cost for offshore platforms and reduce the viability of offshore DC grid.

b) No-selective Fault Clearing Strategy with AC circuit breakers

Another fault handling scheme with non-selective fault clearing strategy is to use ACCBs at each converter terminal and replace the expensive DCCBs with fast DCSWs to isolate DC fault as shown in Fig. 4.1. After DC fault occurrence, all the MMCs are blocked after the arm current exceeds the pre-set threshold. As the DC side contains DCSWs which can only be opened when their currents become zero, fault isolation is done by using ACCBs. In such a scheme, the DC grid needs to be totally shut down until the fault current die out and DCSWs open. After fault clearance, the fault can be located by the "hand shaking" method as detailed in [27].

However, the non-selective method is extremely slow and may not be adequate for critical power corridors because of the use of slow ACCBs and DCSWs for DC fault clearance.

c) Partially selective fault clearing strategy

To minimize power interruption through prevention of total shut down of the DC grid and reduce the total investment cost for protection, the partially selective fault clearing strategy is used here. The cost reduction is achieved by restricting the use of expensive DCCBs only at the onshore converter DC terminals, while the offshore end of each DC cable is connected to offshore converter via fast DCSWs to enable DC

fault clearance using ACCBs offshore as illustrated in Fig. 4.2. Such arrangement also avoids the use of the expensive offshore platforms for the installation of bulky DCCBs. After the DC fault occurrence, the onshore DCCBs will split the offshore grid into two segments which refers as healthy and fault segments. Consider the fault happens on cable 24, DCCB 5 will be the first one to detect the fault and trip. DCCB 2 will then detect the fault and activate to isolate the fault. Thus, windfarm 1 is unaffected and the power transmission continues, while power generation and transmission from windfarm 2 are interrupted. When the fault is detected by MMC 4, the internal MMC protection blocks the converter and trips the offshore ACCB 4 to de-energise cable 24. The faulty cable 24 is then isolated by DCSW 3 and power generated from offshore windfarm 2 can then be export through cable 14 after the reclosing of DCCB 2. During the blocking of MMC4 and opening of ACCB 4 the offshore AC voltage regulation at windfarm 2 is lost which may result in the shutdown of the windfarm and prevent quick system recovery after fault isolation. Therefore, ensuring continuous control of the offshore AC grid during the fault clearance to provide speedy system recovery is a big challenge for the proposed partially selective protection scheme.

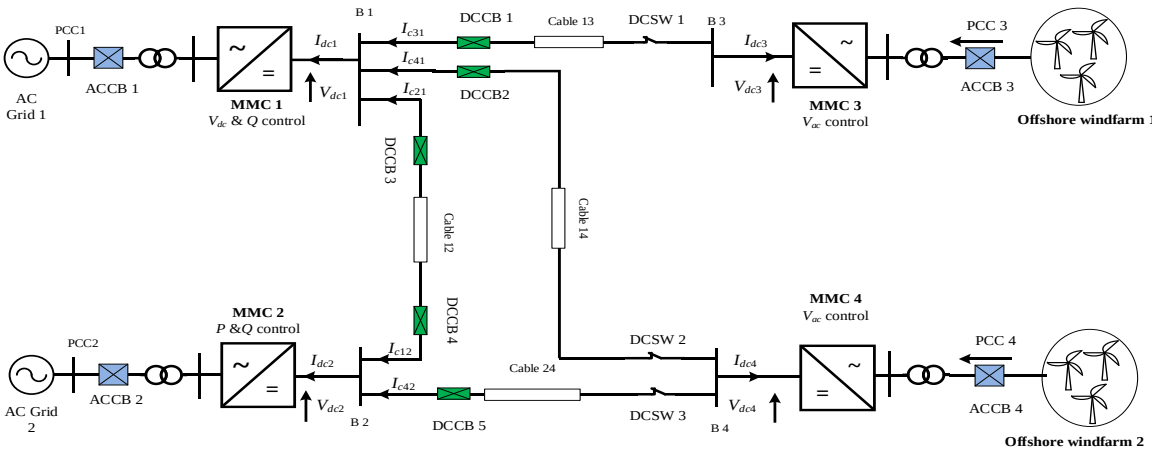

Fig. 4.2 Proposed partially selective protection scheme

4.2 Offshore WT behaviour during DC fault and functional requirement for post fault recovery

4.2.1 Offshore WT behaviours during the DC fault

Fig. 4.3 shows a simplified diagram of the HVDC connected offshore windfarm, which consists of HB SM based offshore MMC and WT clusters represented by an aggregated WT.

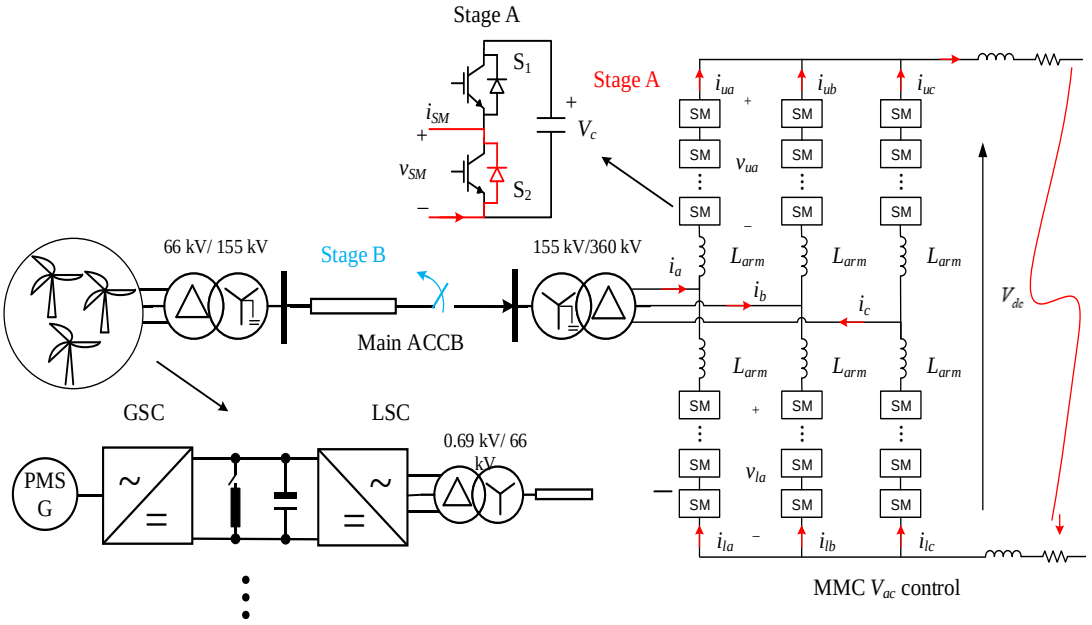

Fig. 4.3 Simplified equivalent circuit during DC faults for offshore windfarm systems

During a DC short circuit fault, the offshore MMC that sets AC voltage and frequency of the offshore AC grid is blocked and the offshore AC voltage will experience significant reduction due to the conduction of the MMC freewheeling diodes[87]. The scenario for the WTs is similar to a severe offshore three-phase AC fault, which forces WTs to operate at their current limits. The fault currents will feed to the DC side through MMC's freewheeling diodes as illustrated in Fig. 4.3.

When the main ACCB is opened to isolate the DC fault as previously described, the offshore WTs will be isolated from the MMC. This indicates the control over the offshore AC frequency and voltage is completely lost. If the WTs continue export power/current, the current injection into the offshore AC grid which is disconnected to the MMC and appears as having an open circuit will charge the offshore AC array cable and filter capacitors, potentially leading to an uncontrolled rise of offshore AC voltage.

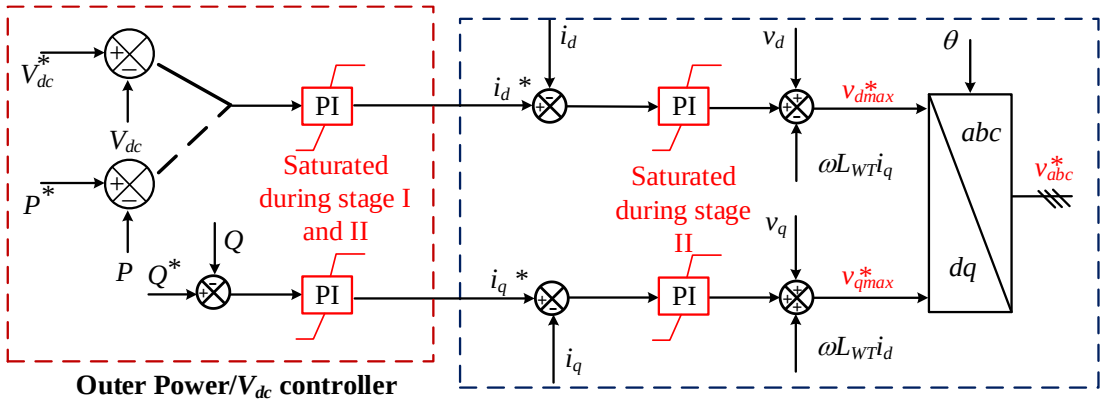

Fig. 4.4 Saturated controllers for conventional grid following control

With a typical WT controller as illustrated in Fig. 4.4, under open circuit condition, the inner current controllers in the WTs cannot follow their current reference orders generated by the outer controllers, and thus, inner PI controllers saturate, leading to the saturation of modulation index to its maximum value, e.g. 1, as demonstrated in Fig. 4.5 a). To avoid the over-voltage on WT converter DC capacitor, the DC choppers installed at are activated to dissipate the generated wind power, and the DC voltage of the WT is limited to 1.1 pu (½V_{dc}=725 to 797.5 V) as shown in Fig. 4.5 b). Thus, the saturated modulation index combined with DC overvoltage could lead to offshore AC overvoltages, as observed in Fig. 4.5 b). Similarly, the offshore frequency previously regulated by the offshore MMC will diverge after the blocking of the MMC, potentially leading to circulating power among WT converters and resonance issues as

presented in [131]. Such behaviours could lead to the shutdown of the offshore windfarm to avoid catastrophic failures.

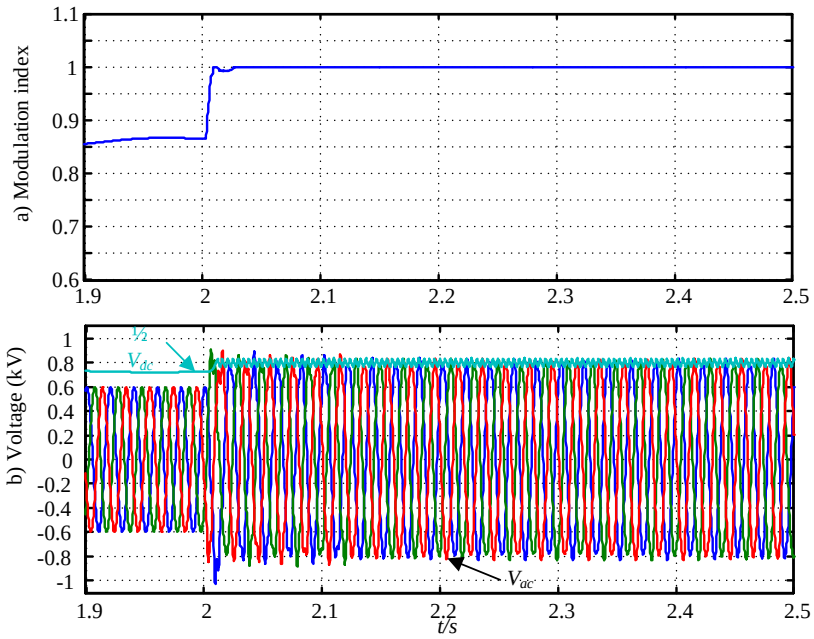

Fig. 4.5 Overvoltage phenomena with conventional control method when offshore ACCB opens at t=2 s: a) WT LSC modulation index, b) offshore AC voltage and half of WT DC capacitor voltage.

4.2.2 WT post fault recovery requirement in MTDC network

In a MTDC grid that connects multiple offshore windfarms, continued operation to retain large proportion of pre-fault power transfer to the consumption centres during a DC fault is critically important to onshore AC systems. The proposed partially selective DC fault protection strategy in which DCCBs can quickly isolate faulty DC lines (e.g. less than 5 ms) without the need for converter blocking (onshore) while the offshore windfarms use the ACCBs and DSCWs to isolate the DC fault provides a cost-effective solution for handling DC faults in offshore MTDC grids. Nonetheless, the partially selective DC fault protection strategy requires significant modifications to WT control, particularly to maintain offshore AC voltage and frequency for

extended period to maintain the offshore AC grid and enable a fast power restoration.

Some of the desirable control requirements of WTs to facilitate partially selective DC fault ride-through strategies in MTDC grids are:

1) Each WT autonomously treats AC and DC faults in the same manner by controlling its fault current contribution to the fault. The freewheeling diodes of the blocked offshore MMC can sustain limited fault currents from the WTs until opening of the main ACCB.
2) WTs must rely on local measurements for detection of abnormal offshore grid conditions, and initiation of automatic transition from grid following to grid forming control mode to maintain AC voltage and frequency of the isolated offshore AC grid after opening of the main ACCB.
3) Shutdown of the islanded offshore AC grid must be prevented to avoid time-consuming individual WTs restart.
4) When the faulty DC line is isolated and offshore MMC reconnected, WTs must automatically detect the fault clearance, initiate orderly transition back to the grid following control mode and resume power generation.

4.3 Enhanced DC fault ride-through control of WT LSCs

To facilitate partially selective DC fault ride-through control in line with the requirements outlined in Section 4.2.2, a new enhanced WT control shown in Fig. 4.6 is proposed. As shown, the proposed control method uses a passive V_{ac} controller to facilitate seamless transition of the WTs between grid following (during normal operation) and grid forming (during MMC blocking) modes based on the local measurements, and to provide fast resumption of power transfer after fault clearance.

The enhanced WT control method shown in Fig. 4.6 consists of active power or DC voltage (P/V_{dc}) and reactive power (Q) controllers in the outer loops and passive V_{ac} controller that manipulates the output dynamic limiters of the P/V_{dc} controllers to facilitate smooth transition of the WT control modes. For ease of illustration, four operating modes are considered as detailed in the following subsection.

4.3.1 Normal operation

As the set-point of the passive V_{ac} controller is fixed at 1.05 pu, its output will saturate at maximum current I_{dmax_v} (1.1 pu in this study) during normal operation (when the offshore MMC that operates in grid forming mode tightly controls the AC voltage and frequency in the offshore AC network). As the dynamic current limit I_{dmax_v} imposed at the output of the P/V_{dc} controller by the passive V_{ac} controller is greater than the nominal d-axis current (1.0 pu in this study), the normal operation of the P/V_{dc} control is not affected. In addition, saturation of the passive V_{ac} controller will force the output of the auxiliary q-axis voltage controller in the passive V_{ac} control, which is incorporated into the Q controller to act on q-axis, to zero. This allows Q controller to define the entire q-axis current order I_q^*. Also, saturation of the passive V_{ac} controller during the above-mentioned scenarios is designed to ensure that the output of the PI controller of the phase-locked loop (PLL) is unaffected as the dynamic frequency limit $\pm\Delta\omega_{max}$ is set at the maximum by the proposed V_{ac} controller ($\Delta\omega_{max}=K_f I_{dmax\_v,}$). Thus, individual WT follows the PLL detected AC frequency (around ω_0 set by the offshore MMC).

4.3.2 Fault mode

This mode represents the period after DC fault inception, during which the main ACCB in Fig. 4.3 remains closed and offshore grid AC voltage collapses similarly to

that typically occurring during offshore symmetrical three-phase AC faults. As a result, the WT DC choppers will be activated to dissipate excessive active power in WTs. When the offshore AC voltage V_{ac} becomes lower than the pre-set threshold, e.g. 0.5 pu as illustrated in Fig. 4.6, the fault current control will be activated to provide maximum reactive current to support offshore AC voltage [132]. Thus, the WTs will operate at their maximum current limitation with reactive current as priority (denoted as $I_{d\max} = \sqrt{1^2 - I_q^{*2}}$ in Fig. 4.6 while the proposed passive V_{ac} controller remains inactive.

4.3.3 Open circuit mode

When the offshore MMC station that sets the offshore AC voltage and frequency is disconnected from the offshore network due to the opening of the main ACCB, the offshore AC voltage will rise, and frequency will drift as described earlier. The passive V_{ac} controller is thus out of saturation and its output is reduced from the upper limit of 1.1 pu to a lower value (close to zero) which is substantially less than the output from the P/V_{dc} controller. This forces the d-axis current order I_d^* to follow that from the passive AC voltage controller, and thus V_{ac} is maintained at 1.05 pu. As the output of the passive AC voltage controller I_{dmax_v} will be approaching zero when it limits the AC voltage at 1.05 pu after its activation, the output of the PLL $\Delta\omega$ will be forced toward zero ($\Delta\omega=\Delta\omega_{max}=K_f I_{dmax\_v}\approx 0$, Fig. 4.6). This locks the individual WT to nominal pre-fault frequency ω_0. The activation of the passive V_{ac} controller also enables the auxiliary q-axis voltage controller (as its limit is no longer set at zero, i.e. $I_{qmax\_v} > 0$). Thus, the q-axis voltage controller forces the q-axis voltage V_q of each WT to zero to maintain the synchronization of the offshore grid. In this manner, seamless, autonomous and controlled transition of the WTs between grid following and forming modes based on local measurements is achieved. Thus, compared with

the conventional grid following control method [131, 133, 134] as in Fig. 4.5, the passive AC voltage controller avoids the saturation of the WT controller, and thus, maintains the offshore AC voltage as demonstrated in Fig. 4.7.

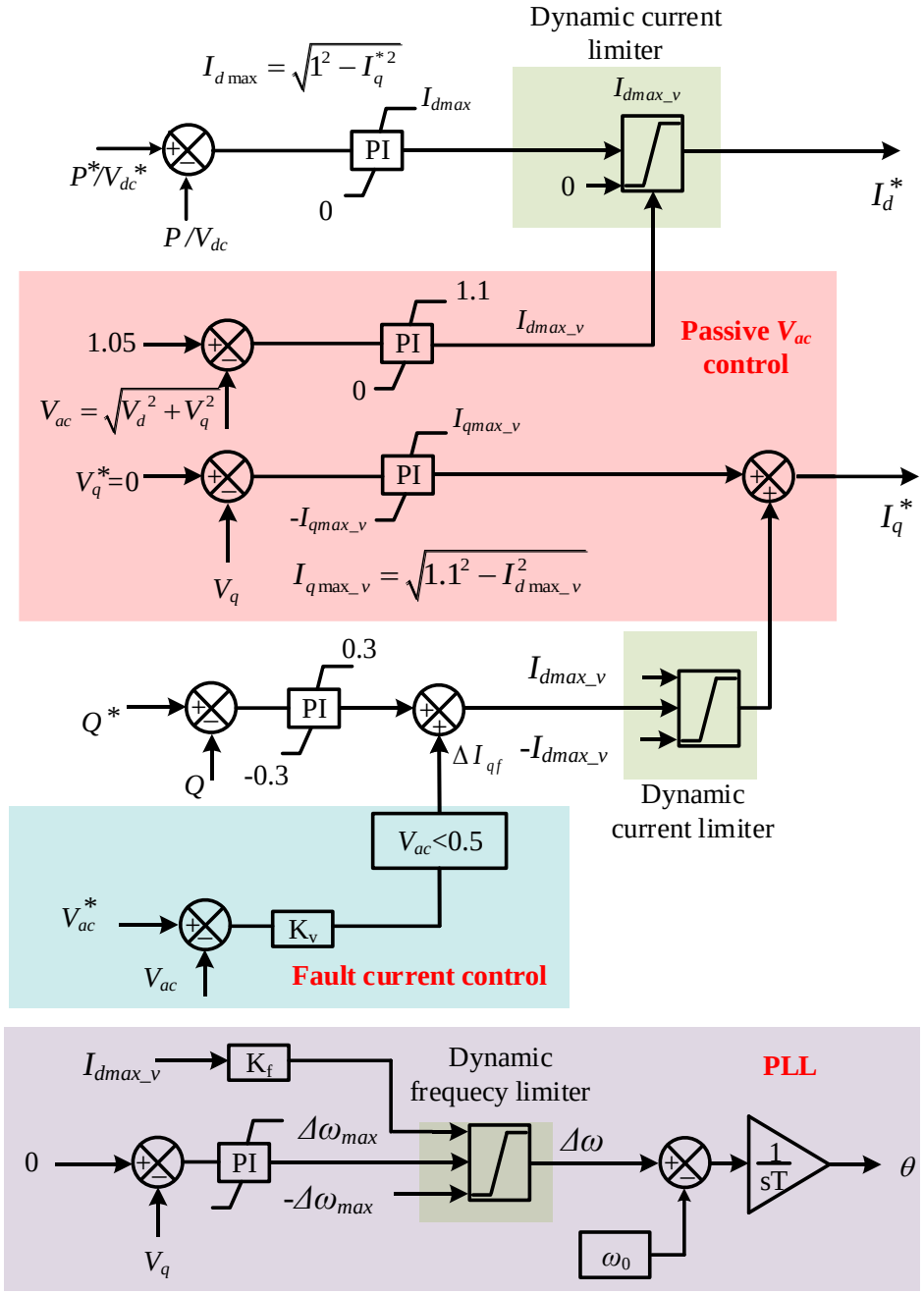

Fig. 4.6 Proposed control strategy of WT LSC.

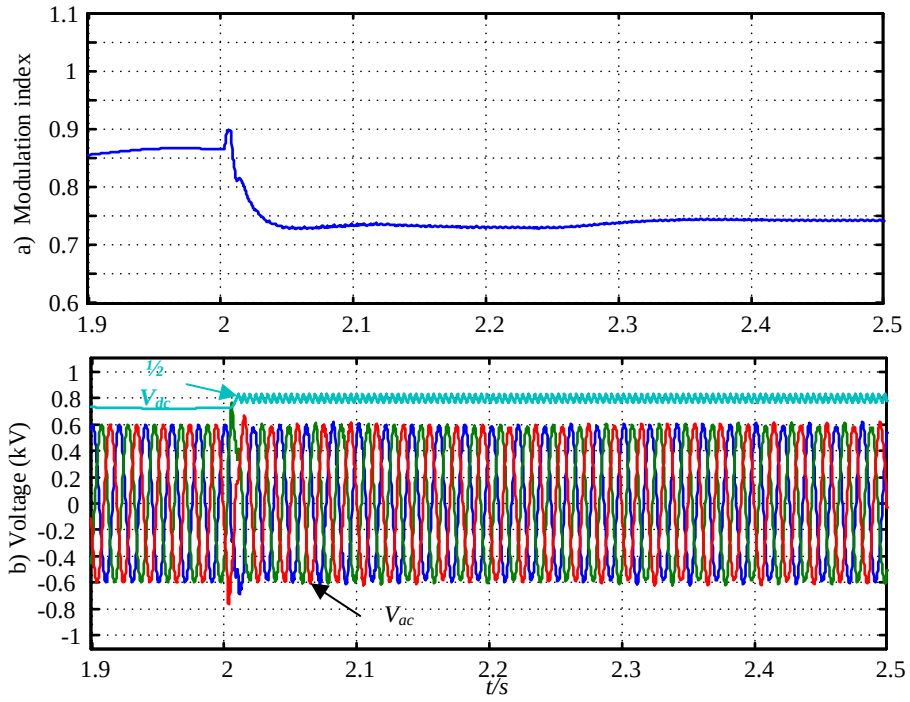

Fig. 4.7 Waveforms with the proposed control when offshore ACCB opens at t=2 s: a) total modulation index, b) converter side AC voltages and half of DC voltage.

4.3.4 DC fault recovery consideration for offshore MMC

If the fault is in other part of the MTDC network and after the fault is isolated, the ACCB closes while the WTs continue controlling the offshore AC network voltage and frequency with the proposed control. The offshore MMC station is thus re-energized by the offshore windfarm. After re-energization, the offshore MMC is activated and operates on DC voltage control mode with PLL activated. Fig. 4.8 illustrates the PLL operation mode switches during system restart. As shown in Fig. 4.8, when the DC fault happens, the converter is blocked due to converter overcurrent protection. Under such scenario, the PLL will switch to DC voltage control mode (Mode=1) which locks the PCC voltage frequency. When the DC voltage of the offshore MMC station is close to that of the DC grid, the offshore MMC can be connected to the DC grid. Then, the offshore MMC station switches back to offshore AC voltage control mode and

regulates the offshore AC grid voltage at the nominal value (i.e. 1 pu) with fixed frequency (Mode =0). This forces the passive V_{ac} controllers of the WTs to saturate again and move back to idle state. The WTs thus return to grid following mode automatically.

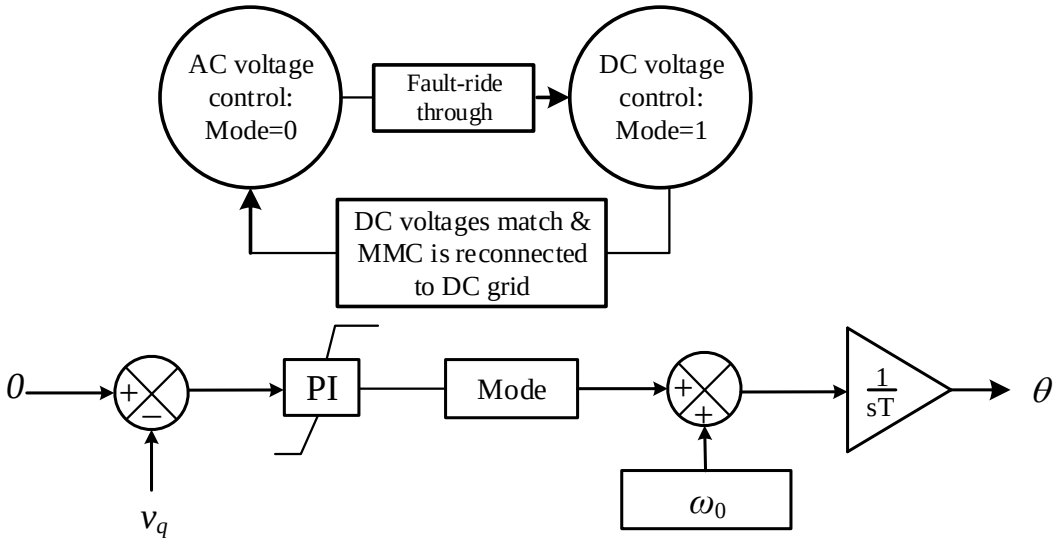

Fig. 4.8 Criterion of mode switching for the offshore MMC station.

4.4 Proposed partially selective DC fault ride through scheme

This section details the implementation for the proposed partially selective DC fault ride-through using the four-terminal DC grid shown in Fig. 4.2. As an example, considering the fault happens at cable 24, the offshore station MMC 4 needs to go through fault clearance and post-fault recovery. To better discuss the overall sequences, including fault isolation and fault recovery as well as WT control behaviours, the fault isolation and fault recovery are discussed separately as follows.

4.4.1 Fault clearance

When a DC fault occurs at a particular line in DC grids using partially selective DC fault protection, dedicated DCCBs must be triggered to split the system into healthy and faulty parts. The DC fault detection and localization used in this case is based on the DC reactor voltage change rate as detailed in [101] to enable a fast and accurate selection for the corresponding DCCBs. Considering the DC fault at Cable 24 connecting DC nodes B2 and B4 in Fig. 4.2, DCCB 2 and 5 will be opened. In this way, the system will be separated into the healthy and faulty parts, with MMC 1, 2 and 3 constituting the healthy section in which the power exchange continues. Thus, the loss-of-infeed from offshore windfarms to onshore AC Grid 1 and 2 is minimized to around 50%.

MMC 4 in the faulty part is blocked upon overcurrent / undervoltage detection and offshore windfarm 2 will contribute limited fault currents to the DC fault through the antiparallel diodes of MMC 4. The fault current contribution from the offshore windfarm 2 will continue until ACCB 4 opens to isolate MMC 4 and the faulty DC side from the offshore AC network. After ACCB 4 opens, the offshore AC voltage will increase as analysed in Section 4.2.1, leading to the activation of the WT passive V_{ac} controller to maintain the offshore AC voltage and frequency as illustrated in Fig. 4.9. Operational logics of the ACCBs of the offshore MMCs are designed as follows:

- As shown in Fig. 4.9, in the first 20 ms from the fault detection, the ACCB of the affected MMC remains closed so as not to act in case the fault is not at cables directly connected to the offshore MMC.
- After 20 ms from the fault detection, if the MMC DC voltage remains below 50% of the rated value, the ACCBs are opened. Otherwise, if the MMC DC voltage recovers, the ACCBs remain closed.

When the installed DC inductors at the DC terminals of the MMCs are unable to prevent the blocking of MMC following remote DC fault due to brief period of overcurrent, the station will recover quickly as long as its ACCB remains closed and DC voltage recovers as stated in the operational logics described above.

After the opening of DCCB 2 and 5, the current in DCSW 2 drops to zero, while the fault current contribution from the offshore windfarm 2 continues to flow through DCSW 3. The fault is thus detected on the cable connected with DCSW 3, which needs to be opened to isolate the fault. Before the opening of DCSW 3, ACCB 4 must be opened to force the fault current that flows through DCSW 3 to decay. Once the DC fault current approaches zero (less than 10 A), DCSW 3 is safely opened to isolate the faulty Cable 24 from MMC 4.

4.4.2 System recovery

After the isolation of the faulty cable as described above, MMC 4 and parts of DC network need to be restarted to enable power transmission of offshore windfarm 2 through the remaining DC Cable 14. MMC 4 can be re-energized from DC side with the aid of DCCB 2 and DC side pre-charging current limiting resistor. However, the DC side pre-charging resistor needs to be rated at higher voltage to limit possible disturbances to the healthy parts of the DC network and with fast communication systems to initiate the restart sequence from onshore when the fault is cleared by the offshore protection system. As the proposed enhanced control allows the WTs of the offshore windfarm 2 to remain operational after opening of ACCB 4 (with the offshore AC network voltage controlled at 1.05 pu), the AC side PIR will be rated for relatively low AC voltage compared with DC equivalent. Thus, the WTs are used to re-energize offshore MMC 4 and Cable 14. The detailed restoration sequence is as follows:

- Offshore ACCB 4 recloses and the offshore windfarm 2 charges MMC 4 and DC Cable 14 through AC PIR. After the DC voltage at faulted terminal recovers, the PLL of MMC 4 is enabled to track the frequency and angle of the offshore AC grid (now controlled by the WTs) for synchronization and MMC 4 is then de-blocked and subsequently operated in DC voltage control mode to regulate the DC voltage to the rated value, as illustrated in Fig. 4.8. When the DC voltage across DCCB 2 closes to zero, it can be reclosed.
- Following the closure of DCCB 2, MMC 4 switches back to AC voltage control mode and regulates the offshore AC voltage to the nominal value. This will force the passive V_{ac} controller of the WTs to saturate, increasing the current limit I_{dmax_v} imposed at the output of the active power controller to the maximum value. Consequently, the WTs reverse back to power control mode and power transmission of offshore windfarm 2 resumes.

It is worth emphasizing that, during the proposed DC fault ride-through, the offshore WTs automatically change operation mode without any communications.

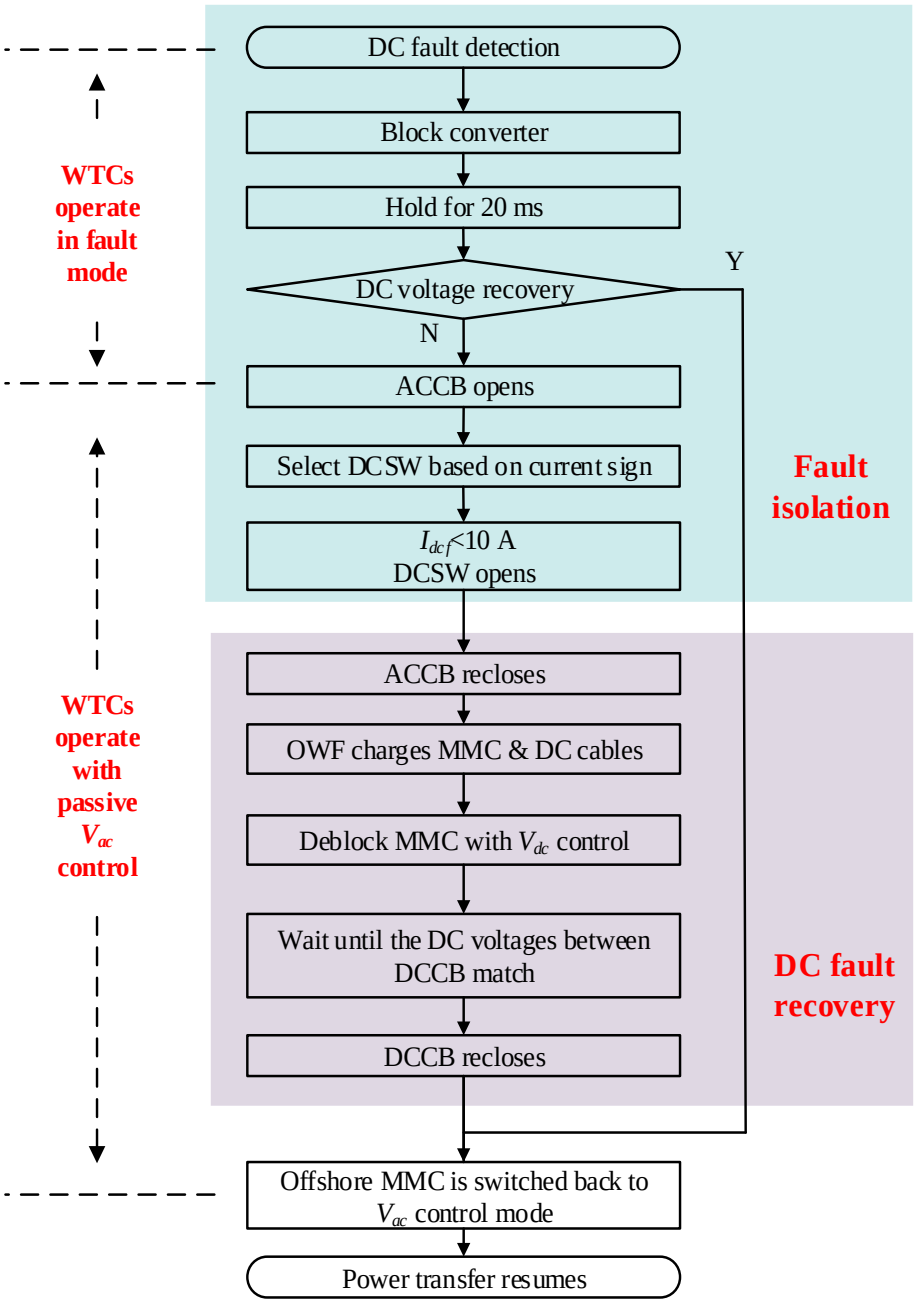

Fig. 4.9 Sequence of the proposed DC fault protection scheme for the faulty offshore MMC station.

4.5 Simulation results

To assess the effectiveness of the proposed enhanced WT control that facilitates

cost-effective DC fault ride-through in offshore DC grids, a permanent pole-to-pole DC short circuit fault is applied at the middle of Cable 24 at t=2 s, as illustrated in Fig. 4.2. The faulty DC line is isolated using a combination of ACCB 4, DCCB 2 and DCCB 5. After isolation of the faulty DC line, the remaining healthy part of the DC grid, which is disconnected from the faulty DC line, is reconnected and re-energized from offshore windfarm 2 via the MMC 4. The system performances during fault clearance and recovery are addressed in subsections 4.5.1 and 4.5.2 respectively.

4.5.1 Fault clearance

After DC fault occurrence at t=2 s, DCCB 2 and 5 open at t=2.006 s (fault detection and the DCCBs operation time) to isolate the fault from the healthy part, i.e. MMC 1, 2 and 3 and offshore windfarm 1. It is worth underscoring that the onshore stations MMC 1 and 2 are protected by DCCBs plus DC inductors, so that the arm currents of MMC 1 and 2 are below 2 pu (1 pu current is 2 kA) during the fault and thus, both remain operational without blocking [23, 89] as shown in Fig. 4.10 a).

Observe that the DC voltages of the healthy part experience brief disturbances but quickly recover as shown in Fig. 4.11 a) and b). After system separation into healthy and faulty parts, the majority of the power that offshore windfarm 1 injects into the healthy DC network via MMC 3 is transferred to MMC 2 through Cable 13 and 12 as shown in Fig. 4.11 e), f), g) and h).

As the offshore MMC 4 uses DCSWs with no DC inductors, its DC voltage quickly collapses, as seen in Fig. 4.12 a). This leads to the rapid rise of the fault currents. Once the arm current exceeds 2 pu [23, 89], MMC 4 is blocked at 2.0015 s and the offshore AC network voltage is also collapsed, as shown in Fig. 4.12 b), c) and Fig. 4.11 b). With the proposed control, WTs inject reactive currents to support the

offshore AC voltage, which flow through the antiparallel diodes of MMC 4 and feed the fault, as shown in Fig. 4.12 b), d) and e) and Fig. 4.11 b).

Considering 20ms delay time and the ACCB operation time, the ACCB 4 opens at t=2.078 s, leading to isolation of MMC 4 from the offshore windfarm 2. Opening of ACCB 4 causes the offshore AC voltage to rise as the WTs inject currents into the offshore AC network with no power transmission path. Once the offshore AC voltage increases to 1.05 pu at t=2.12s, the passive V_{ac} controllers incorporated in WTs are activated to maintain the AC voltage by limiting the active current from the WTs around 0, as depicted in Fig. 4.12c) and d). As displayed in Fig. 4.12 c), the offshore AC voltage only experiences slight over-voltage for around 23 ms at the initial stage after the main ACCB opens and the offshore overvoltage is then effectively suppressed. At the same time, the dynamic frequency limiter of the PLL loosely locks the offshore frequency at 50 Hz while the q-axis voltage control loop maintains the synchronization for WTs as in Fig. 4.12 f). In this way, both AC voltage and frequency in the offshore network of the offshore windfarm 2 are controlled by WTs.

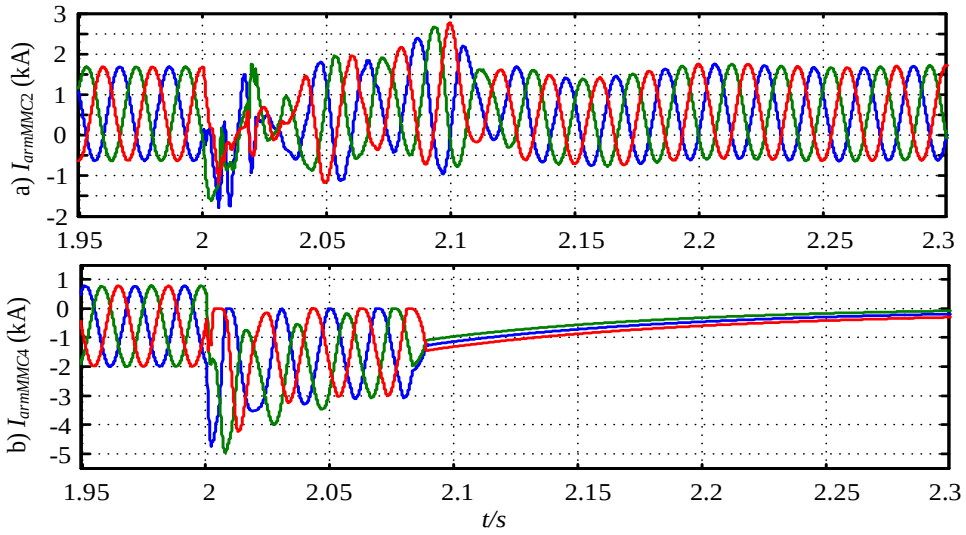

Fig. 4.10 Upper arm currents of MMC 2 and 4 during the DC fault: a) onshore MMC 2, b) offshore MMC 4.

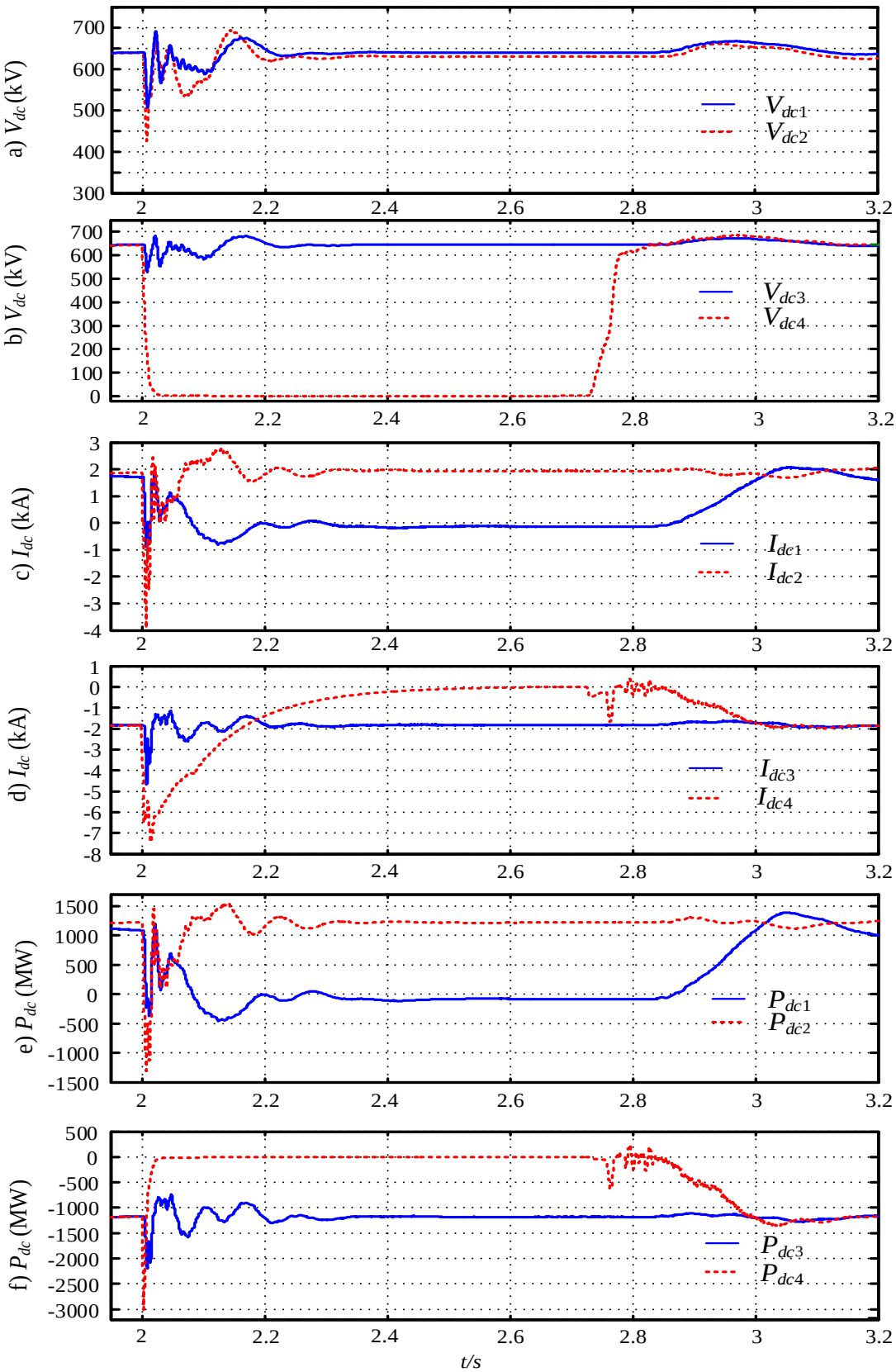
a) V_{dc} (kV)
700
600
500
400
300
V_{dc1}
V_{dc2}
b) V_{dc} (kV)
700
600
500
400
300
200
100
0
V_{dc3}
V_{dc4}
c) I_{dc} (kA)
3
2
1
0
-1
-2
-3
-4
I_{dc1}
I_{dc2}
d) I_{dc} (kA)
1
0
-1
-2
-3
-4
-5
-6
-7
-8
I_{dc3}
I_{dc4}
e) P_{dc} (MW)
1500
1000
500
0
-500
-1000
-1500
P_{dc1}
P_{dc2}
f) P_{dc} (MW)
500
0
-500
-1000
-1500
-2000
-2500
-3000
P_{dc3}
P_{dc4}
2
2.2
2.4
2.6
2.8
3
3.2
t/s

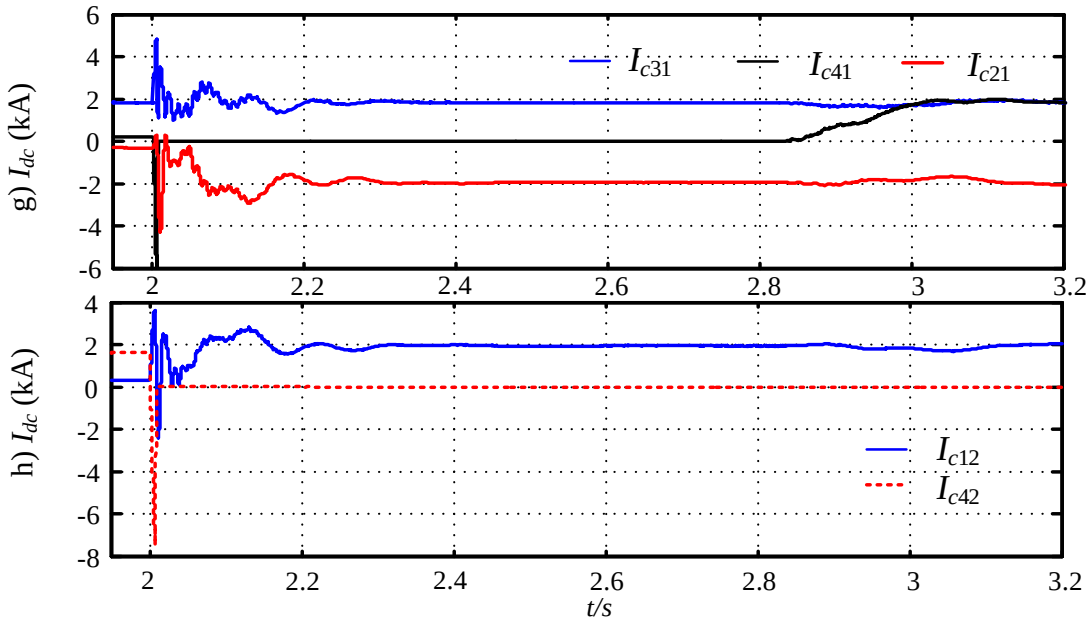

Fig. 4.11 DC side dynamics during offshore DC fault at Cable 24: a) onshore DC voltages, b) offshore DC voltages, c) onshore DC currents, d) offshore DC currents, e) onshore DC power, f) offshore DC power, g) DC cable currents flowing to MMC 1, h) DC cable

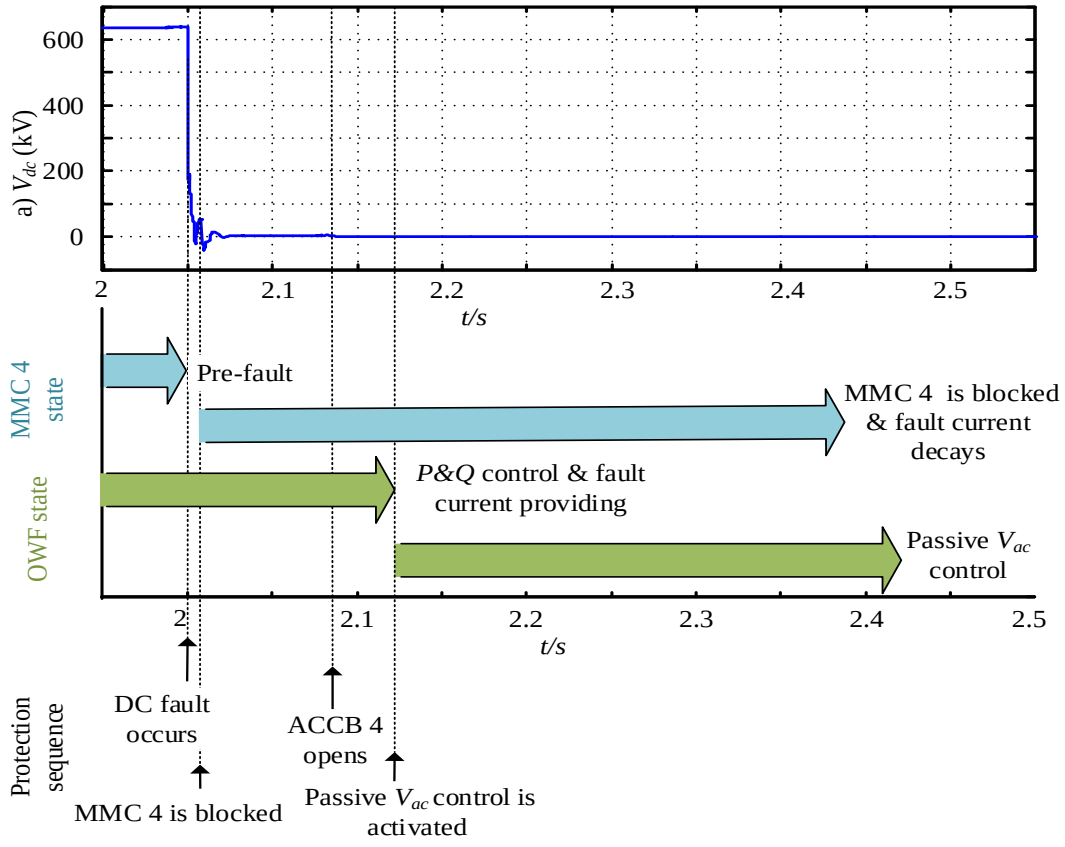

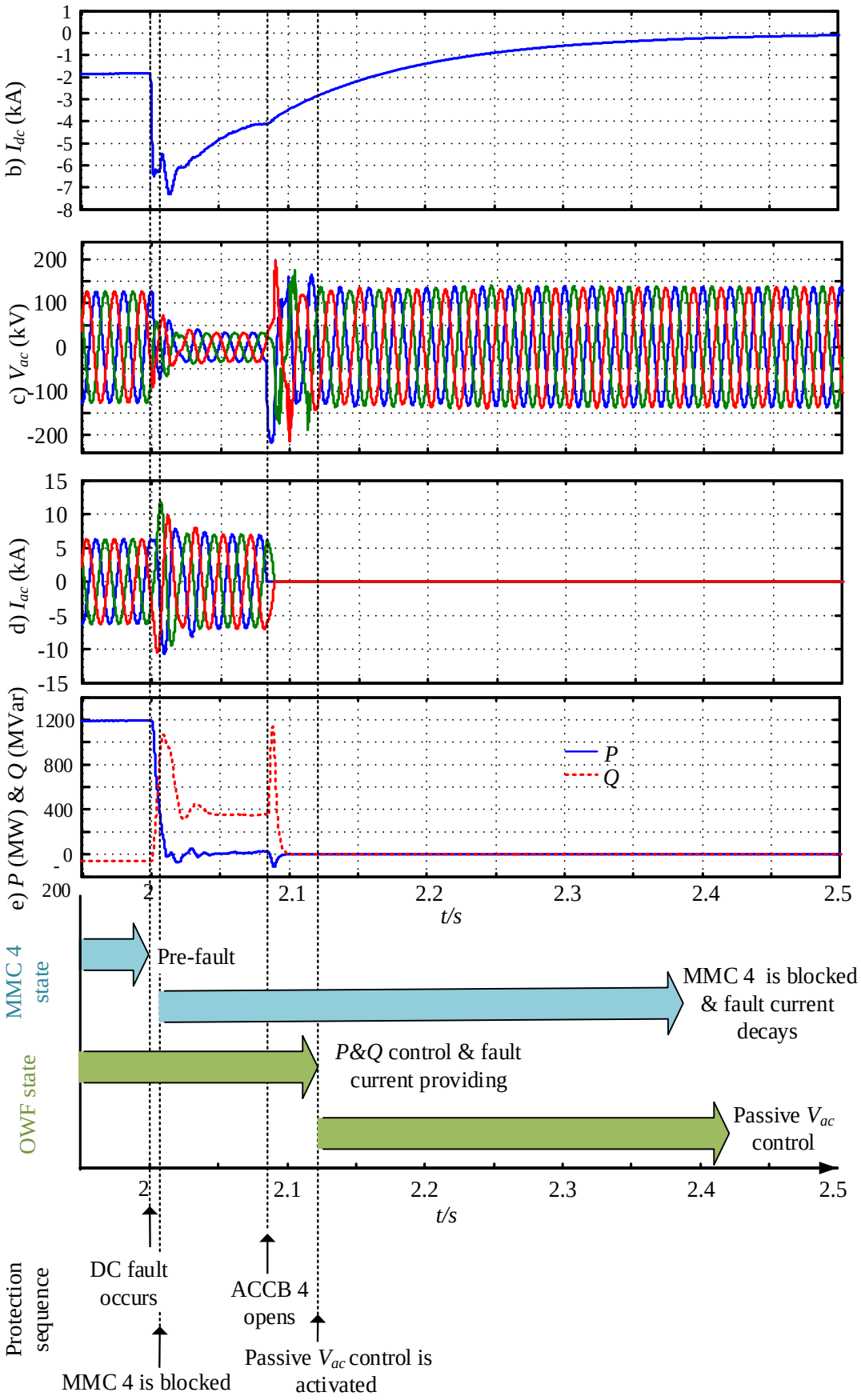
b) I_{dc} (kA)
c) V_{ac} (kV)
d) I_{ac} (kA)
e) P (MW) & Q (MVar)
P
Q
t/s
MMC 4 state
Pre-fault
MMC 4 is blocked & fault current decays
OWF state
P&Q control & fault current providing
Passive V_{ac} control
t/s
Protection sequence
DC fault occurs
ACCB 4 opens
MMC 4 is blocked
Passive V_{ac} control is activated

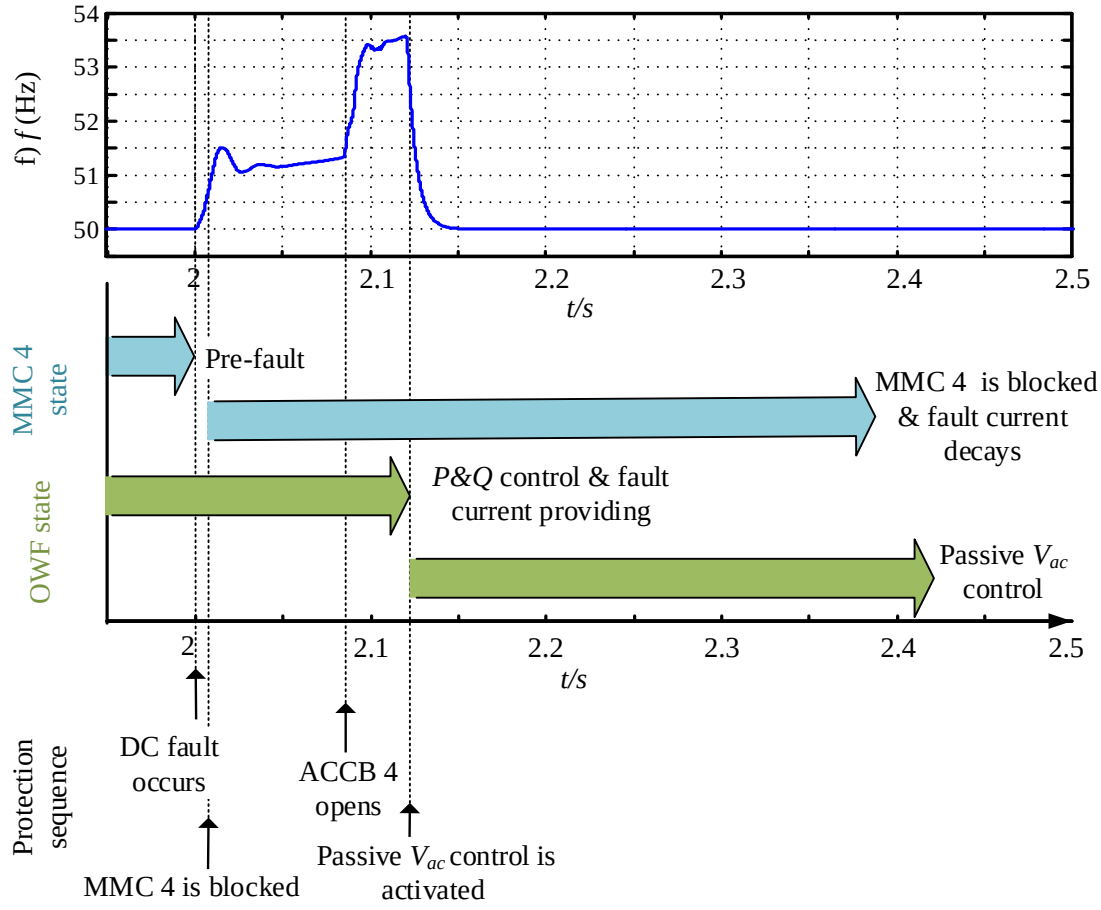

Fig. 4.12 Waveforms of offshore station MMC 4 and offshore windfarm 2 during fault clearance: a) MMC 4 DC voltage, b) MMC 4 DC current, c) WT AC voltages, d) WT AC currents, e) MMC 4 active and reactive power, f) WT frequency.

4.5.2 System recovery

After isolation of the faulty line from offshore windfarm 2 by opening ACCB 4, the DC current in the faulty DC line decays to zero as displayed in Fig. 4.12 b). DCSW 3 is opened once its current approaches zero at t=2.7 s to isolate the faulty Cable 24, and offshore MMC 4 can now be restarted.

To avoid DC side disturbance, the DC voltages of MMC 4 and Cable 14 are recovered using offshore windfarm 2. Following ACCB 4 reclosing through current

limiting PIR at t=2.73 s, offshore windfarm 2 charges the DC link of the blocked MMC 4 and DC Cable 14 through MMC 4 antiparallel diodes. After bypassing the PIR, the MMC 4 DC link voltage rises to around 580 kV (±290kV) as shown in Fig. 4.13 a) and d). MMC 4 is then de-blocked at t=2.77 s and is operated in DC voltage control mode to boost the DC voltage to 640 kV (±320 kV), as in Fig. 4.13 a). Subsequently, onshore DCCB 2 is reclosed at t=2.82 s when the DC voltages across DCCB 2 match, reconnecting MMC 4 to the DC grid. During the DCCB 2 reclosing process, the DC grid voltages and currents do not exhibit large disturbances as shown in Fig. 4.13 a) and b). MMC 4 subsequently switches back to grid forming mode in which the offshore AC voltage and frequency are restored to 1 pu and 50 Hz, respectively. At this stage, MMC 4 takes control of the AC voltage and frequency, and WTs of the offshore windfarm 2 will transit back from passive V_{ac} control to power control mode as the active current upper limit I_{dmax_v} imposed by the passive AC voltage controller is restored to the maximum value of 1 pu.

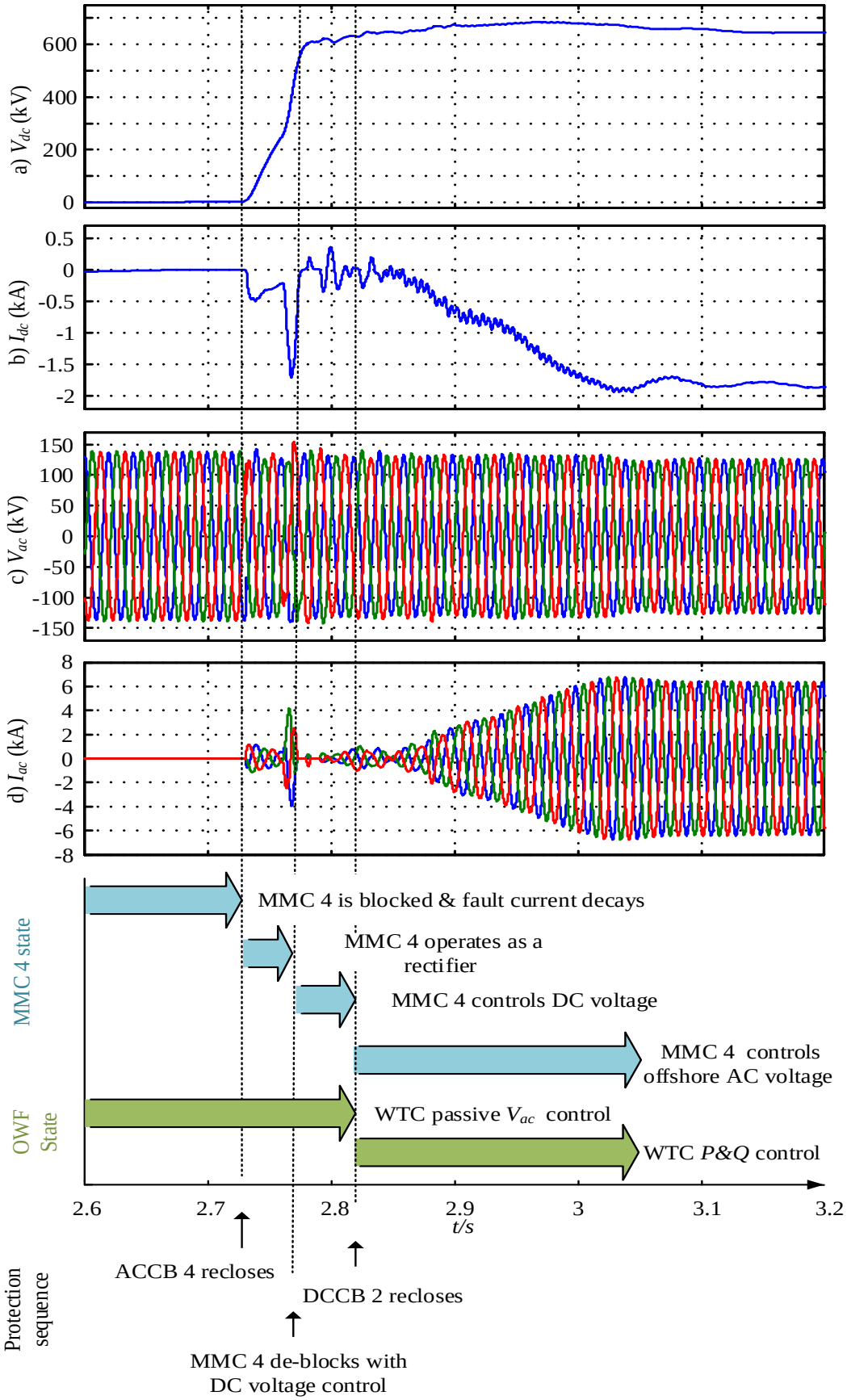
a) V_{dc} (kV)
600
400
200
0
b) I_{dc} (kA)
0.5
0
-0.5
-1
-1.5
-2
c) V_{ac} (kV)
150
100
50
0
-50
-100
-150
d) I_{ac} (kA)
8
6
4
2
0
-2
-4
-6
-8
MMC 4 state
MMC 4 is blocked & fault current decays
MMC 4 operates as a rectifier
MMC 4 controls DC voltage
MMC 4 controls offshore AC voltage
OWF State
WTC passive V_{ac} control
WTC P&Q control
2.6
2.7
2.8
2.9
3
3.1
3.2
t/s
Protection sequence
ACCB 4 recloses
DCCB 2 recloses
MMC 4 de-blocks with DC voltage control

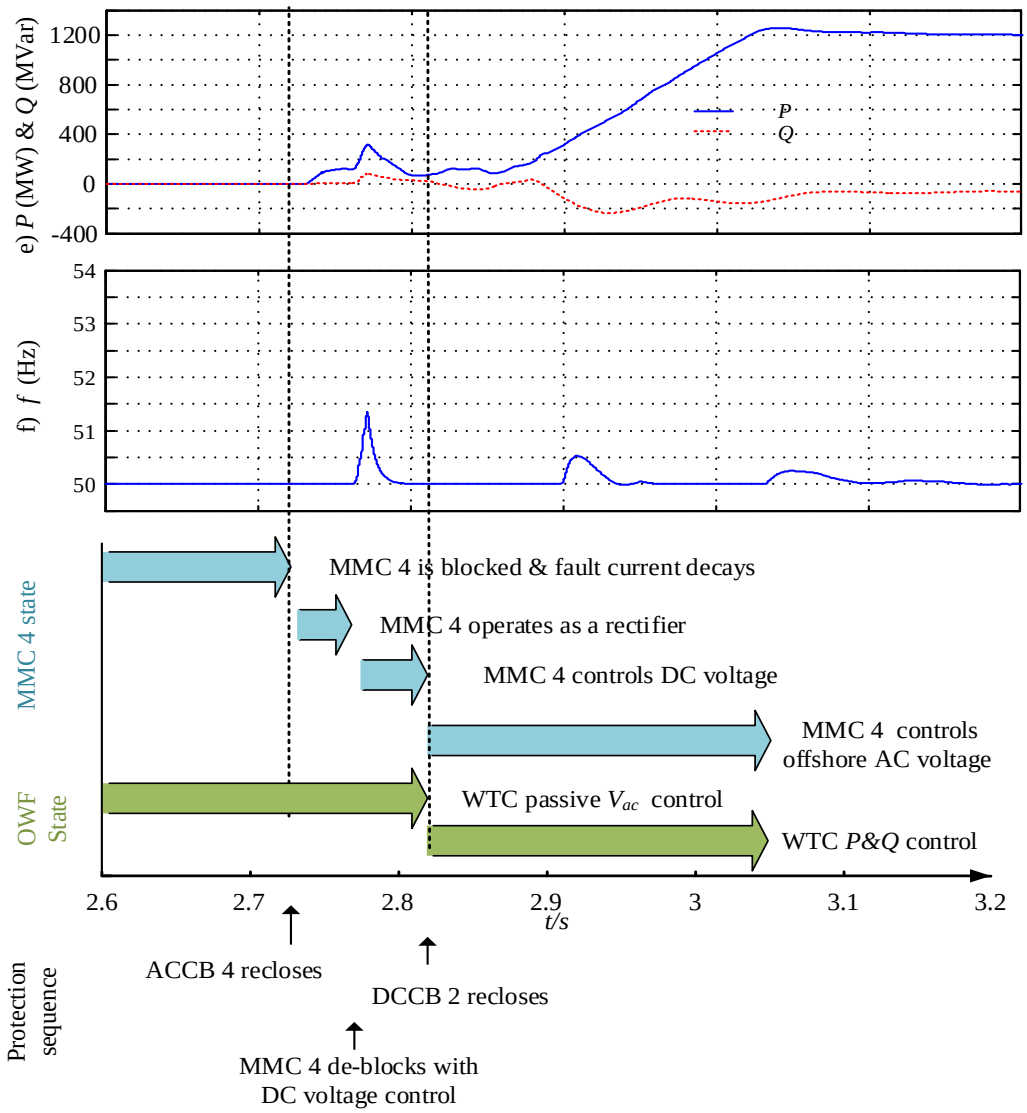

Fig. 4.13 Waveforms of offshore station MMC 4 and offshore windfarm 2 during system recovery: a) MMC 4 DC voltage, b) MMC 4 DC current, c) WT AC voltages, d) WT AC currents, e) MMC 4 active and reactive power, f) WT frequency.

4.6 Summary

This chapter proposes an enhanced WT control method that facilitates partially selective DC fault clearance and ride-through using reduced number of fast acting DCCBs. To avoid the collapse of offshore AC voltage due to sudden loss of offshore

MMCs, the proposed passive AC voltage control of wind turbine converters detects the abnormal condition based on local measurements and seamlessly transits between grid following and forming modes. The offshore grid voltage is thus maintained stable during faults and the offshore restoration after fault clearance is enabled by the proposed control. Detailed simulation studies confirm that the proposed WT control can facilitate clearance of DC faults in multi-terminal offshore DC grid with low cost partially selective DC fault ride-through scheme, while significant proportion of pre-fault power transfer is retained during fault clearance process. After fault clearance, system recovery can be initiated with the aid of survival offshore windfarm. Thus, the power transfer can resume if there is another energy path available, as demonstrated in this Chapter.

Chapter 5
Black Start Operation of DR-HVDC Connected Offshore Windfarms

The rapid increases of RES in power system introduces new challenges to maintain reliability, stability, and security of power supplies [34]. In the event of system blackout, the ability of RES to black start part of a large network could bring significant economic and technical benefits to system operators. Thus, black start and islanding capabilities of RES have been proposed in ENTSO-E's network connection requirement as an optional requirement by TSOs to support power system restorations [33]. The use of HVDC connected offshore wind farms for onshore black start operation provided has also been studied in several works [34, 110, 111]. DR-HVDC systems have recently been proposed for integrating large offshore windfarms [42, 44] due to its potential lower transmission losses and total investment cost. Due to the uncontrollability of the passive DR station, the offshore AC network is controlled by the WTs which has been addressed in [56, 58]. However, if DR-HVDC connected offshore wind farm is used for black start of onshore AC networks, system power balancing control and DC link voltage regulations during black start are significantly different to MMC connected systems and have not been addressed.

Thus, a frequency-AC voltage droop control is proposed to the offshore WT to maintain the DC voltage of the DR-HVDC link and keep the power balance between onshore and offshore grid during black start operation. The detailed energization process of the DR-HVDC link, onshore AC network load pick-up and fault ride through operation studies are carried out to validate the proposed scheme. Moreover, the power redistribution among WTs due to unpredictable wind condition is considered.

5.1 DR-HVDC connected offshore windfarm system and general control

Fig. 5.1 shows a general structure of the DR connected offshore windfarm system, which consists of an offshore diode rectifier station and an onshore MMC. The DR station is made of a 12-pulse bridge rectifier and the onshore MMC controls the DC voltage of DR-HVDC link during normal power transmission.

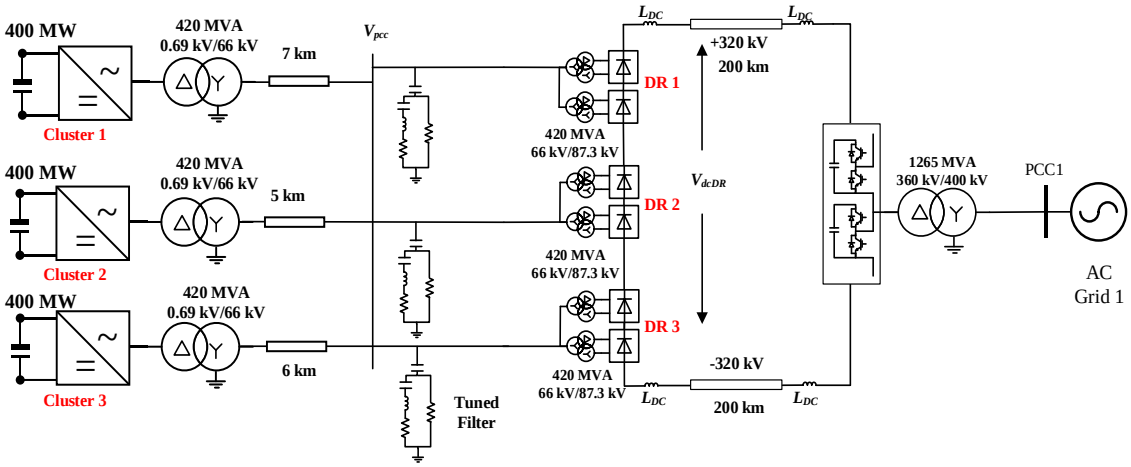

Fig. 5.1 DR-HVDC connected offshore windfarm

The control of DR connected offshore windfarm differs from MMC connection described earlier. This is due to the fact that the uncontrollability of the DR necessitates the WT LSCs to operate in grid-forming to define offshore AC voltage and frequency and control the power dispatch to onshore. In addition, the inherent active and reactive power coupling characteristic of DR requires the control of reactive power sharing among individual WTs. Thus, to address the general control requirement, the *P-V, Q-f* with distributed PLL frequency regulation control method developed in [58] is adopted in this thesis and is briefly described in the following subsections. Fig. 5.2 shows the overall WTs control structure of the distributed PLL-based *P-V* and *Q-f* control.

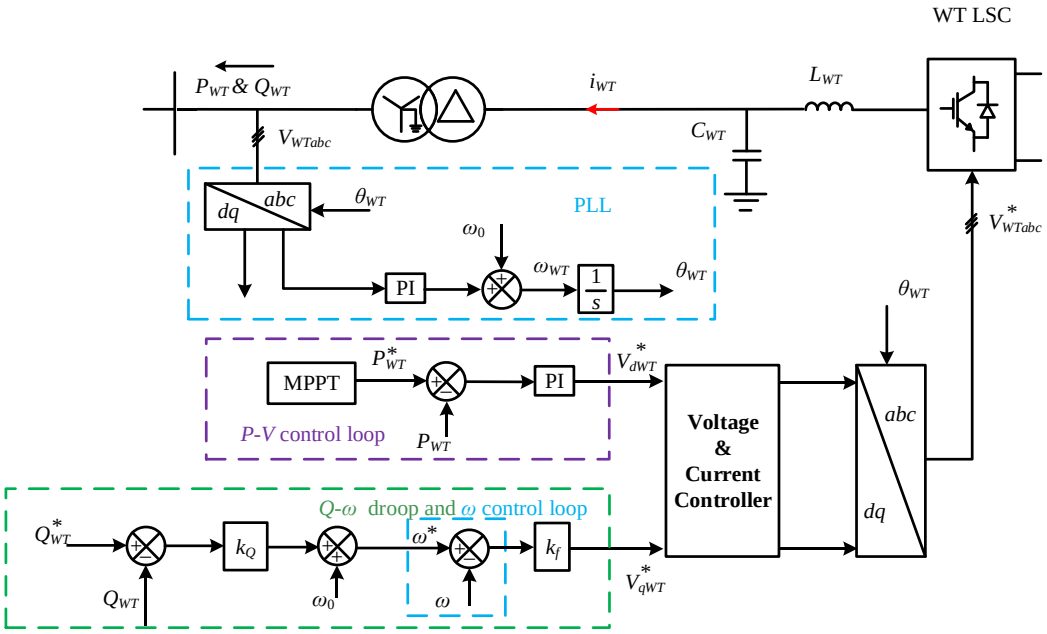

Fig. 5.2 DR- HVDC connected WT control [58]

5.1.1 Distributed PLL-based frequency regulation

Due to uncontrollability of diode rectifiers, the offshore WT control system needs to ensure autonomous frequency regulation by the large number of WTs and to provide synchronization for offline WTs. To tackle this problem, the distributed PLL based frequency control is proposed in [58] as illustrated in Fig. 5.2.

In the existing voltage control for converter-based islanding network, the *q*-axis reference is normally set at zero while the voltage magnitude of islanding network normally controlled by the *d*-axis voltage. When a PLL is used, it normally takes *q*-axis voltage reference as an input to adjust the frequency output to ensure the *q*-axis always locates at synchronise rotation frame and is kept at zero. Therefore, for each WT system, the *q*-axis voltage V_{qWT} can be used to control the offshore AC frequency. Thus, an additional PLL-based frequency loop is utilized to generate the desired V^*_{qWT} as:

$$V_{qWT}^{*} = k_f(\omega_{WT}^{*} - \omega_{WT}) \tag{5.1}$$

When the frequency measured by WT meets $\omega_{WT} < \omega_{WT}^{*}$ (i.e. $V_{qWT}^{*} > 0$), the PLL-based frequency control produces a positive V_{qWT}^{*} feeding to the AC voltage controller. The voltage and current loops ensure the converter to generate the required V_{qWT} according to its reference value produced by the frequency loop. Consequently, the frequency measured by the PLL is increased (due to $V_{qWT} > 0$) until it becomes identical to the reference ($\omega_{WT} = \omega_{WT}^{*}$). Similarly, when $\omega_{WT} > \omega_{WT}^{*}$ (i.e. $V_{qWT}^{*} < 0$), the proposed frequency control produces a negative V_{qWT}, so the frequency is reduced accordingly. Such frequency control enables individual WTs operating autonomously to contribute to the overall frequency regulation of the offshore AC network.

5.1.2 Active power control

As the DC voltage of the DC grid is controlled at the rated value by the onshore MMC station, the transmitted active power is largely determined by the DC voltage produced by the DR, which is given by [56] considering 3 DR units in series:

$$V_{dcDR} = \frac{18}{\pi}(\sqrt{2}nV_{pcc} - X_T I_{dcDR}) = \frac{18}{\pi}(\sqrt{2}nV_{pcc} - X_T \frac{P_{DR}}{V_{dcDR}}) \tag{5.2}$$

where n is the rectifier transformer turns ratio, X_T is the leakage reactance of the DR transformer, and I_{dcDR} and P_{DR} are the DC current and power at the rectifier DC terminal, respectively.

Thus, the active power exported to DC grid can be controlled by adjusting the offshore PCC voltage magnitude, as illustrated in the left top active power control block in Fig. 5.2.

5.1.3 *Q-f* reactive power sharing control

As AC voltage magnitude is selected as the control variable to regulate the WT active power, the reactive-power/frequency droop shown in Fig. 5.2 is adopted here. Such droop control ensures steady-state reactive power to be shared among WT converters due to the same steady-state frequency across the offshore network. The adopted reactive power sharing control is expressed as:

$$\omega^* = \omega_0 + k_Q Q_{WT} \tag{5.3}$$

where ω_0 is the rated frequency of the offshore AC network, k_Q is the droop gain, and Q_{WT} represents the reactive power of individual WT. The error between the frequency reference ω^* and the frequency ω measured by the PLL is fed to the frequency controller, which sets the converter q-axis voltage reference to ensure WT reactive power sharing.

5.2 Black start requirements and characteristics of DR-HVDC connected offshore windfarm systems

5.2.1 System layout

The layout of the DR-HVDC connected offshore windfarm system for black start study is shown in Fig. 5.3. The DR station consists of three 12-pulse DR units connected in series, each rated at 400 MW and 213.3 kV DC to enable operation at 640 kV DC voltage. Pre-insertion resistors are equipped at each of ACCB 1-3 to limit inrush current into the transformer and DC link. The tuned AC filters are installed at DR station to improve the power quality while compensating the reactive power for

DR station. The detailed parameters for DR-system are listed in Table 5.1.

Table 5.1 Nominal parameter of the DR station

Components	Parameters	Values
DR-HVDC link	Power	1200 MW
	DC voltage	± 320 kV
12-pulse diode rectifier	Transformer (Y/Y/Δ)	66/87.3 kV
	Leakage inductance	0.18 pu
	Tuned filters	0.3 pu

Moreover, the onshore MMC operates in V_{ac} control mode as detailed in Chapter 3, and the system parameters are listed in Table 3.2.

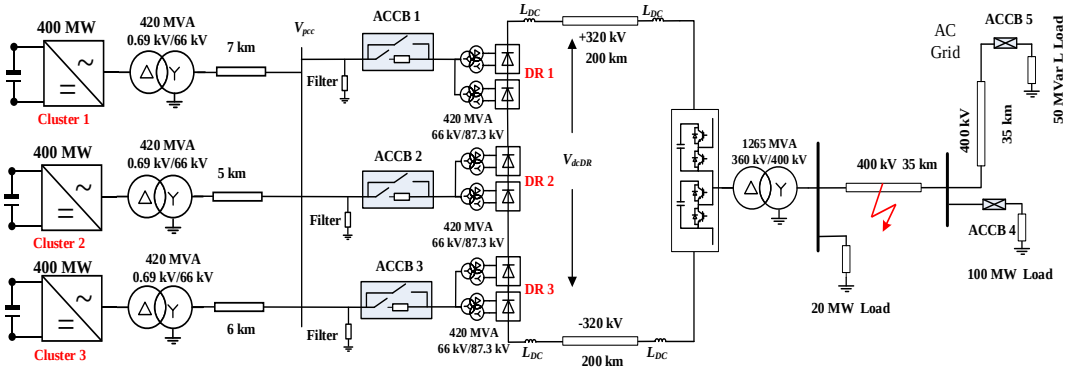

Fig. 5.3 Layout of studied offshore windfarm system with DR-HVDC

5.2.2 Main requirements of WTs for black start

During normal operation, the onshore MMC station regulates the DC voltage at the rated value of ±320 kV. The offshore WT LSCs establish the offshore AC network and control the generated wind power, while the GSCs regulate the DC voltage of WT converters [75]. However, during black start of the onshore AC system, the onshore MMC station needs to operate in grid-forming mode to build up the onshore AC grid

and supply the energy required to the onshore loads. Thus, the control of the DC voltage of the DR-HVDC link needs to be shifted from the onshore MMC station (as in normal operation) to offshore WTs. Furthermore, the transmitted power from offshore WTs during black start needs to match the onshore load, so the WTs need to maintain power balance between offshore and onshore. Thus, the main requirements for the offshore WTs connected to DR-HVDC during black start are:

- Offshore AC grid voltage and frequency control;
- DC voltage control of the DR-HVDC link;
- Onshore and offshore power balancing.

5.2.3 System characteristics during black start

To ensure the DC voltage V_{dcDR} remains largely constant as required in practical systems during black start, the relationship between the transmitted power P_{DR} and V_{pcc} derived from (5.2) is plotted in Fig. 5.4 and given as:

$$P_{DR} = \frac{3\sqrt{2}nV_{dcDR}}{X_T}V_{pcc} - \frac{V_{dcDR}^2\pi}{18X_T} \tag{5.4}$$

It shows that if the offshore V_{pcc} regulated by WTs during black start follows the curve defined in Fig. 5.4 when the transmitted/generated active power varies, V_{dcDR} can be largely maintained at the rated value. However, the offshore DR power P_{DR} is not a local measurement for WTs and the individual WT power capability is small compared with the whole DR transmitted power. Therefore, it is difficult to directly modify the WTs AC voltage magnitude (which determines V_{pcc} and V_{dcDR}) based on local WT active power measurement.

During black start, the power provided by the DR-HVDC link is typically low and mainly used to restart large thermal power plants. Thus, the maximum power $P_{bs\max}$ required for black start is considered to be 400 WM in this thesis. In addition, it is assumed that the power consumed by onshore loads is less than the available wind power during black start, and pitch control and WT speed control are used to reduce the captured wind energy when required [81, 82].

The reactive power Q_{DR} consumed by the DR is:

$$Q_{DR} = P_{DR}\left(\frac{2\mu - \sin 2\mu}{1 - \cos 2\mu}\right) \tag{5.5}$$

where

$$\mu = \arccos\left(1 - \frac{2X_T I_{dcDR}}{nV_{pcc}}\right) = \arccos\left(1 - \frac{2X_T P_{DR}}{nV_{pcc}V_{dcDR}}\right) \tag{5.6}$$

As depicted by (5.5) (5.6) and illustrated in Fig. 5.4, the reactive power consumption of the DR varies with the transmitted active power. Due to the relatively small active power required during black start, the switching of the AC filters of the DR station is not considered and the reactive power Q_{DR} consumed by the DR is compensated by the WTs and a fixed 150 MVAr AC filter, which remains connected to the DR AC terminal during black start.

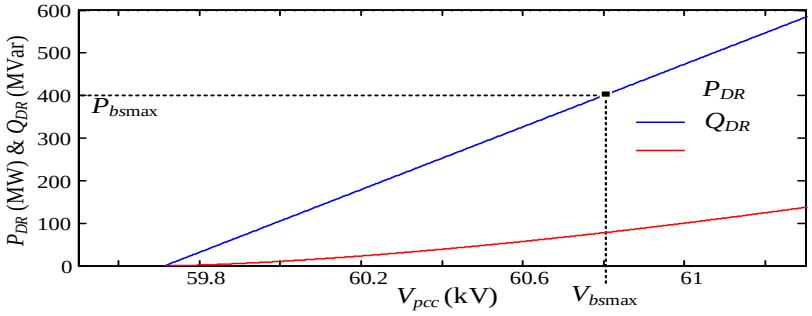

Fig. 5.4 P_{DR}-V_{pcc} and Q_{DR}-V_{pcc} characteristics of the DR-HVDC system assuming constant DC voltage of the DR-HVDC link.

5.3 Black start control and fault consideration

5.3.1 Enhanced *f-V* droop control

To ensure the regulation of the DC voltage of the DR-HVDC link and power balance between offshore and onshore grids during black start, a frequency-AC voltage (*f-V*) droop control is proposed for the WT LSCs.

As discussed in previous sections, the reactive power Q_{DR} consumed by DR stations varies with the active power P_{DR}. Thus, by coordinating with the reactive power sharing control as detailed in previous sections and in [58], the offshore frequency can be utilized to reflect the transmitted DR active power P_{DR} without communication. As the AC voltage variation is relatively small across the full power range, the reactive power variations across the DR filters and offshore AC cables are negligible compared with DR consumptions. Thus, the offshore frequency will mainly vary with the changes of the transmitted active power of the DR-HVDC link and all the WTs will share the same offshore frequency, which is locally measurable by PLL. Thus, the offshore frequency is given as:

$$f^* = f_0 + k_Q\left(\frac{Q_{DR} + Q_{passive}}{N_{WT}}\right) \tag{5.7}$$

where N_{WT} is the number of WTs and $Q_{passive}$ represents the largely fixed reactive power provided by the offshore passive elements such as DR filters and AC cables.

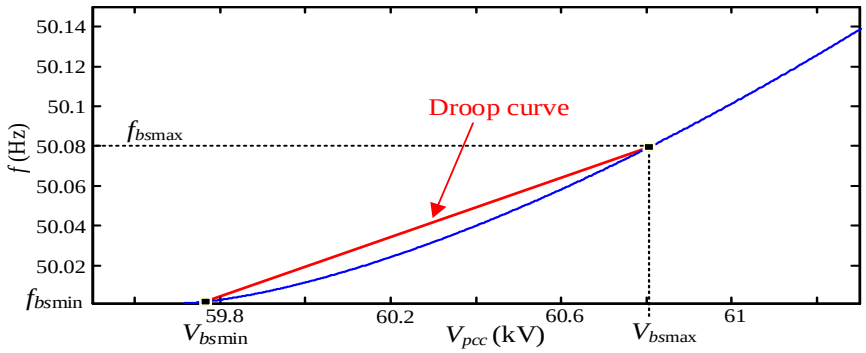

Fig. 5.5 f-V_{pcc} characteristics of the DR-HVDC system.

From (5.4)-(5.7) , the offshore AC frequency with variation of PCC voltage is shown in Fig. 5.5. As observed in (5.7) and Fig. 5.5, the offshore frequency is not a linear function of V_{pcc} but considering limited V_{pcc} variation, a simple linear f-V relationship can be approximated, as depicted in (5.8) and also illustrated in Fig. 5.5 as:

$$k_{f-V} = \frac{V_{bs\max} - V_{bs\min}}{f_{bs\max} - f_{bs\min}} \tag{5.8}$$

where $V_{bs\max}$ and $f_{bs\max}$ are the maximum offshore voltage and frequency when transmitting the maximum power $P_{bs\max}$, as depicted in Fig. 5.4 and Fig. 5.5. $V_{bs\min}$ is the minimum AC voltage set for WTs under the zero-power transmission when the DC terminal voltage V_{dcDR} is at the rated value V_{dcDR0}, and can be derived from (5.2) as:

$$V_{bs\min} = \frac{\pi V_{dcDR0}}{18\sqrt{2}n} \tag{5.9}$$

As described earlier, it is assumed that the power consumed by onshore loads is less than the available wind power during black start. Therefore, the active power-AC voltage (P-V) controller in the WT grid-side converter [58] will saturate, and the offshore AC voltage is thus determined by the limit of the WT d-axis voltage. Consequently, the proposed f-V droop control imposes the dynamic limit of the WT d-axis voltage $V_{d\max}$ to mimic the PCC voltage V_{pcc} during black start as:

$$V_{d\max}=\begin{cases}V_{bs\min}, & f^{*}\le f_{bs\min}\\ k_{f-V}f^{*}, & f_{bs\min}<f^{*}\le f_{bs\max}\end{cases} \tag{5.10}$$

Fig. 5.6 shows the control block diagram for WT converters including the proposed controller and the *Q-f*, *P-V* droop control and frequency control loops which have been introduced in Section 5.1. Since the output of the *P-V* control loop saturates during black start, the *d*-axis voltage reference V_d^* is only determined by the limit $V_{d\max}$. Thus, by dynamically limiting V_{dmax} according to the output of the *f-V* droop controller during black start, the offshore V_{pcc} is controlled according to the relationship shown in Fig. 5.5 and (5.10). Therefore, V_{dcDR} can be maintained in a small range when the transmitted power varies.

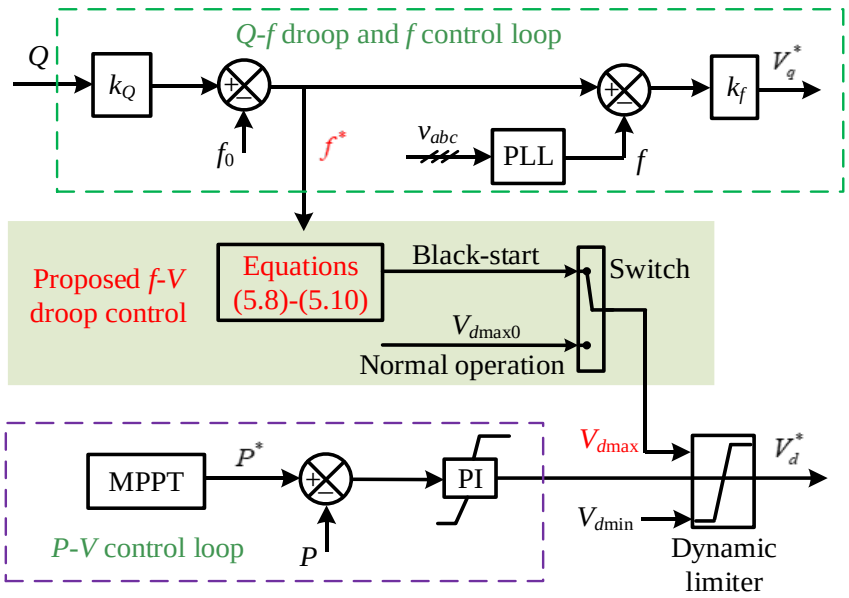

Fig. 5.6 Proposed *f-V* droop control for WTs.

During normal operation, the dynamic limit $V_{d\max}$ of the proposed *f-V* droop control is set at the minimal value $V_{d\max 0}$ (typically 1.05pu [46, 75]) as shown in Fig. 5.6, which is the upper limit of the active power controller output. Thus, the embedded *f-V* droop control has no impact on normal operation of the system.

To better understand the operation mechanism of the proposed control method, the system dynamics during onshore power change are graphically shown in Fig. 5.7. Assuming the onshore power demand $P_{onshore}$ increases, the offshore exported power P_{DR} will increase accordingly, leading to the rise of the reactive power Q_{DR} consumed by the DR and the drop of the DC link voltage V_{dcDR}. Consequently, WTs reactive power Q_{WT} increases and so does the offshore frequency f due to the effect of the Q-f droop. As a result, the proposed f-V droop increases the dynamic voltage limit according to (5.10) such that V_{PCC} is increased and the DC link voltage V_{dcDR} restored. Therefore, the DC voltage of the DR-HVDC link is controlled within the safe operation region, without communication.

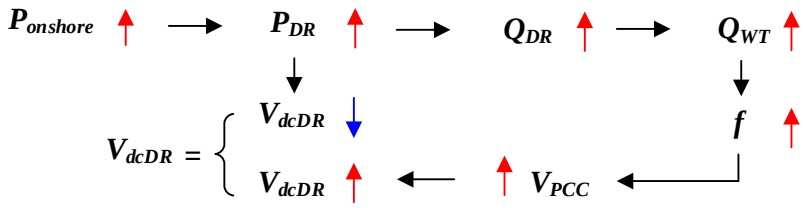

Fig. 5.7 Graphically illustration of transients during the onshore demand change.

5.3.2 Onshore fault consideration during black start

In the event of onshore AC faults during black start, the onshore MMC operates in current limiting mode due to the sudden drop of the AC voltage, and the active power demands both onshore and offshore significantly decrease. Due to the coupling between the active and reactive power (P-Q) as depicted by (5.5) and (5.6), the reactive power consumed by the DR station is also reduced, leading to the decrease of the offshore frequency. Thus, the proposed f-V droop control automatically reduces the dynamic limit $V_{d\max}$ according to (5.10), forcing the offshore AC voltage to decrease. This accelerates the decrease of the power transmitted to the DR-HVDC link and overvoltage of the HVDC link is thus avoided. The surplus power generated by

WTs will need to be dissipated by the internal DC choppers at each WT.

In this way, the WTs automatically track the required operation droop curve and handle onshore AC grid faults during black start with the proposed control.

5.4 Energization of HVDC link and onshore MMC

Since offshore AC grid energization has been studied in [58], this thesis will mainly focus on the DR-DC link energization and MMC station soft energization. Thus, the offshore AC network is assumed already built up by WTs by adopting the method presented in [58].

The DR-DC link will be energized through the different ACCBs (ACCB 1-3) as illustrated in Fig. 5.3. To avoid large inrush current to the MMC SM capacitors and DC cable, the DR-DC link is energized softly by closing the ACCB 1-3 one by one. Thus, the DC voltage is built in three steps. When one DR unit reaches the rated DC voltage of 213.3 kV, the ACCB for the next DR unit will be closed.

The energization of the onshore MMC station is split into two stages, i.e. the passive charging stage and the active charging stage, as in following subsections.

5.4.1 Passive charging stage

When the DC link energization is initiated, all the SMs in the onshore MMC are blocked. As shown in Fig. 5.8 a) the blocked MMC will automatically be charged through its free-wheeling diodes. As there are $2N$ blocked SMs in each phase in total, the voltage the SM capacitors can be charged to at passive charging stage is:

$$V_{SM\_ave} = \frac{18\sqrt{2}nV_{bs\min}}{2\pi N} = \frac{V_{dcDR}}{2N} \tag{5.11}$$

This likely leads to the SM capacitors to be charged to around half of their rated voltages. It should be noted that, as the AC side already has the PIR to limit the inrush current, DC side PIR is not required in this study.

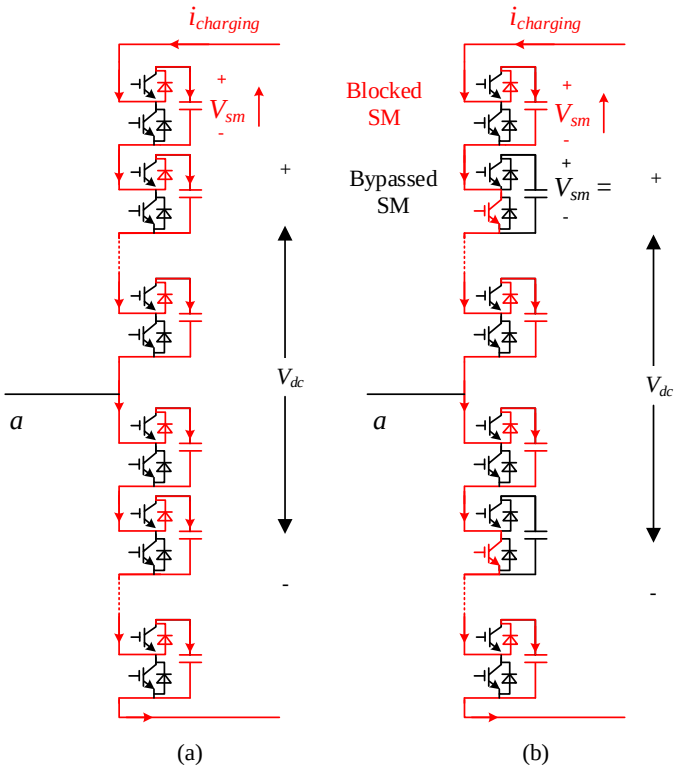

Fig. 5.8 HB-MMC charging from DC side a) Passive charging state and b) Active charging state

5.4.2 Active charging stage

Following the passive charging stage, the active charging stage is initiated, where the number of bypassed SMs in each arm is gradually increased (up to *N/2*, where *N* is the SM number per arm), as shown in Fig. 5.8 b) and Fig. 5.9 a). This would increase the SM capacitor voltages to the rated value while preventing potential large transients

when the SM capacitors are charged from the HVDC link without DC-side PIRs.

As shown in Fig. 5.9 b), at the i^{th} (i=1, 2, …, and N/2) charging step, all the N SMs in each arm are sorted according to their capacitor voltages and the i SMs with the highest capacitor voltage are bypassed while the rest of (N-i) SMs with the lower voltage are connected in the circuit to be charged. This ensures all SM capacitors are equally charged. At the final step, i=N/2, half of the SMs in each arm are bypassed and there are N SMs connected in the charging circuit in each phase. The number of SMs connected in the charging circuit in each arm remains at N/2 for a period, and with the aid of voltage sorting algorithm, the SMs with the lowest voltages are charged to ensure all the SM capacitors can be charged to around the rated value. Then, the MMC can be de-blocked to initiate gradual build-up of the onshore AC grid voltage and provide power to onshore loads.

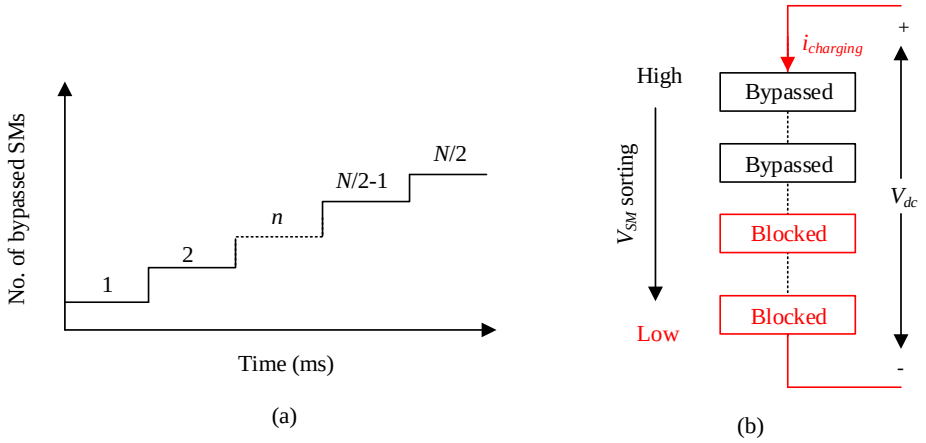

Fig. 5.9 Sequential charging strategy in onshore MMC active charging stage: a) illustration of sequentially bypassing SMs and b) MMC SM states.

5.5 Simulation results

The proposed black start scheme and energization sequence are demonstrated using PSCAD based on the system model as detailed in Section 5.2.1 and illustrated in Fig. 5.3. As shown, a resistive load rated at 20 MW is initially connected with the MMC. Another two loads, i.e. an100 MW resistive load and a 50 MVar inductive load, are connected to the network at different locations and different times.

5.5.1 Energization of DR-HVDC link

The energization of the offshore AC network using the offshore WTs has been studied in [58], so it is not included here. Thus, the study assumes that the offshore AC network is already built up by WTs before energizing the HVDC link and is connected with some small local loads e.g. auxiliary supplies, offshore protection systems and the losses in the filters and cables). The simulation results are shown in Fig. 5.10. The observed small power differences between the clusters as shown in Fig. 5.10 a) are due to different impedances between WTs and DR terminal (as the results of different cable lengths considered for the three wind turbine clusters).

At t=0.9 s, ACCB 1 is closed with its PIR to connect the offshore AC grid to DR 1. As seen in Fig. 5.10 b), the offshore frequency exhibits small disturbance with the variation of active and reactive power demands from DR side. The offshore AC voltage follows the frequency variation, as observed in Fig. 5.10 c), which is in line with the theoretical basis that underpins the operation of the proposed *f-V* droop control. The WTs charge the DR 1 system and DC link to 213 kV, as can be seen from Fig. 5.10 e). At t=1 s, ACCB 2 is closed through its PIR to further build up the DC voltage and is followed by DR 3 energization by closing ACCB 3 at t=1.1 s. At t=1.31 s the DC voltage increases to nearly the rated value of 640 kV and the offshore AC-side PIRs

are bypassed. During the passive charging stage, the onshore MMC SM capacitors are passively charged to 0.91 kV (0.5 pu), without noticeable overcurrent, as shown in Fig. 5.10e)- h).

After the capacitor voltage reaches 0.91 kV, the onshore MMC active charging method is automatically activated at t=1.32 s. As seen in Fig. 5.10 g) and h), all six arms are equally charged during this start-up period with the aid of the SM capacitor voltage balancing algorithm. At t=2.36 s, the SM capacitors are charged to 1.83 kV as illustrated in Fig. 5.10 g) and h). After the completion of the onshore MMC energization, the onshore MMC can be de-blocked with AC voltage control and is ready to start the onshore grid.

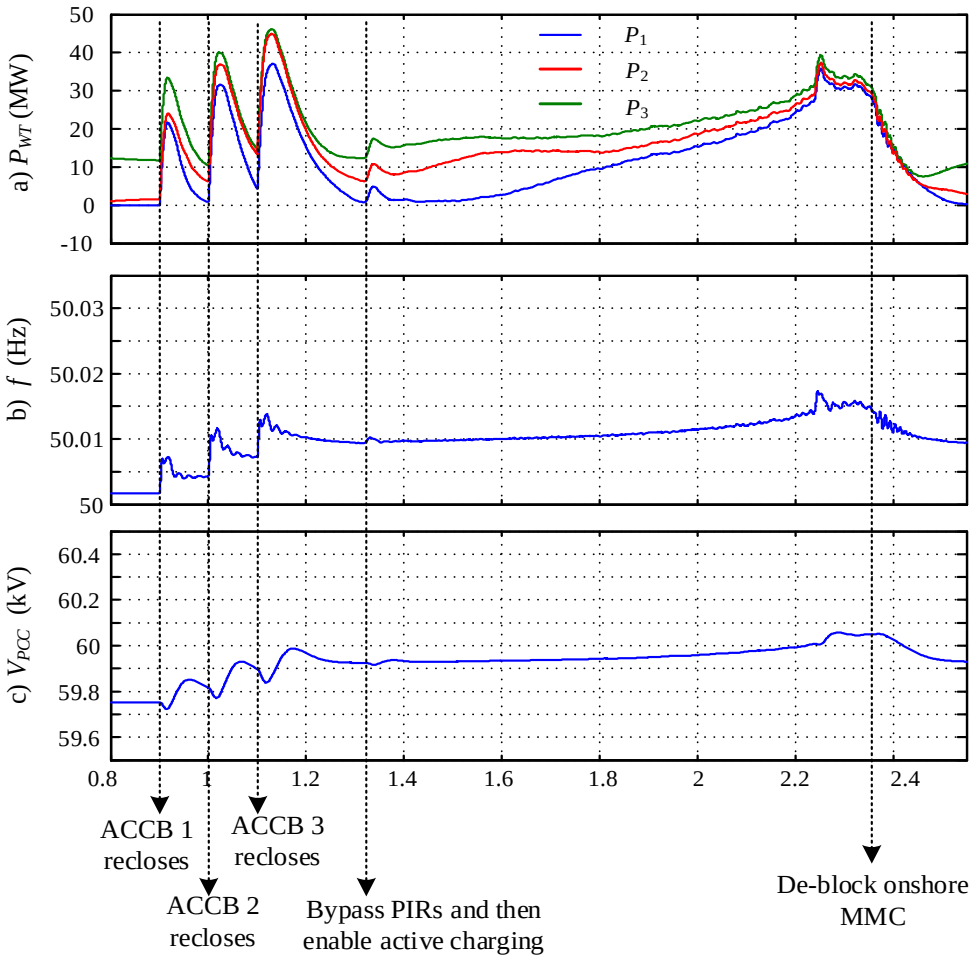

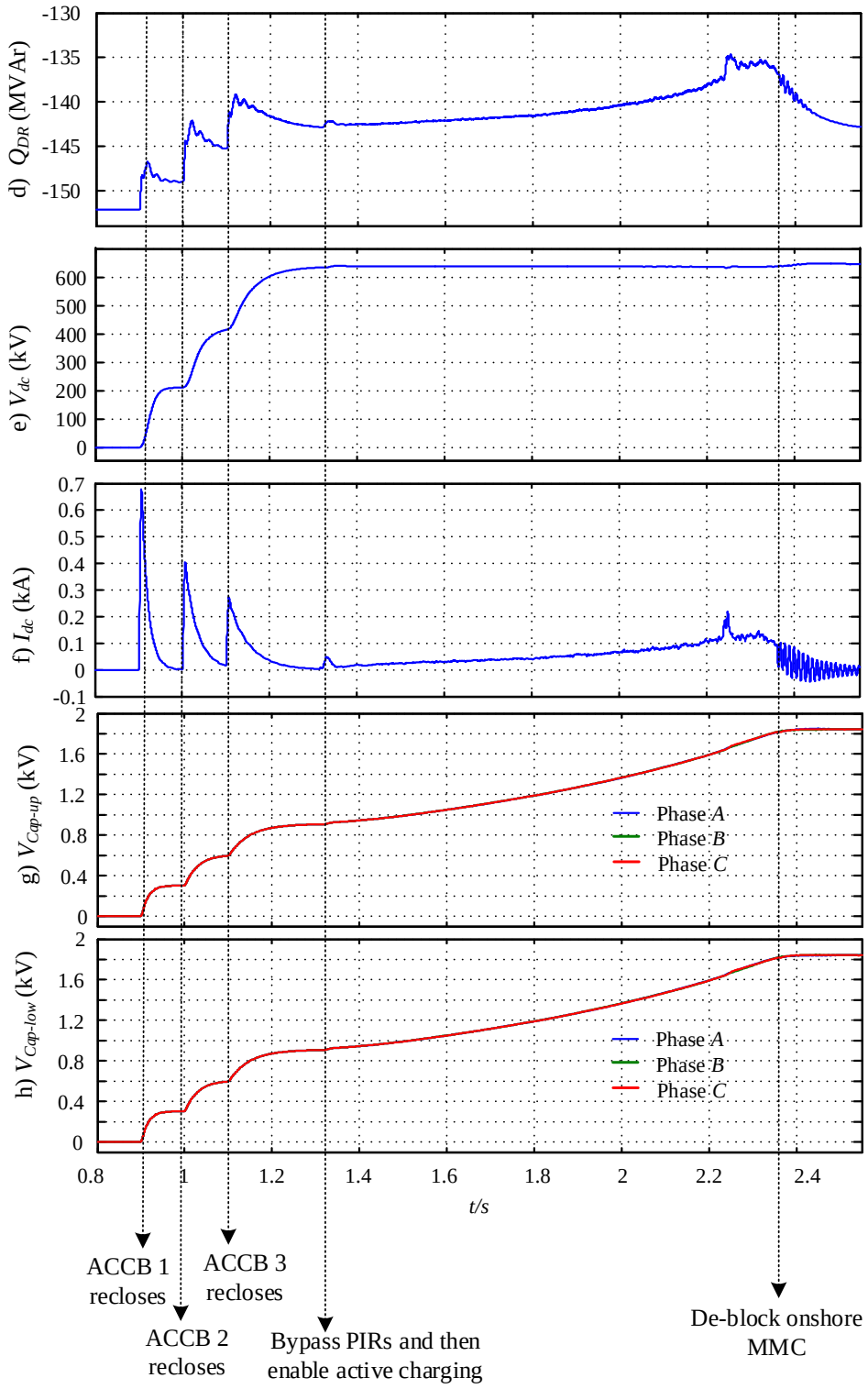

Fig. 5.10 Performance of start-up of DR-HVDC system: a) offshore WT power, b) offshore frequency, c) offshore PCC voltage, d) DR reactive power, e) DC voltage of DR-HVDC link, f) DC current of DR-HVDC link g) MMC upper arm average capacitor voltages, and h) MMC lower arm average capacitor voltages.

5.5.2 Onshore AC grid energization and load pick up

Fig. 5.12 displays the system behaviour during onshore grid energization and load pick up for the proposed black start scheme. At t=2.6 s, the onshore MMC starts to ramp up the AC voltage to energize the converter transformer and the onshore AC cables and supply a 20 MW load. The onshore AC grid voltage reaches the rated value of 400 kV at t=3 s. With the increase of the onshore AC voltage, the reactive power consumption of the onshore AC grid increases from zero to -310 MVAr (capacitive) during 2.6~3.0 s, predominantly to feed the transformer and onshore AC cables, as shown in Fig. 5.12 c) and d). At t=3.1 s, an additional 100 MW load is suddenly connected to the onshore AC grid, leading to an increase of the onshore power demand $P_{onshore}$. The offshore WT generated power P_{WT} increases accordingly, which in turn leads to the increase of reactive power demand of DR station, as illustrated in Fig. 5.12 e) and h), respectively. The WTs, which are equipped with the frequency-reactive power (*f*-*Q*) sharing droop control, increase their reactive power outputs and offshore frequency, as shown in Fig. 5.12 f). As a result, the proposed droop control is activated and increases the offshore PCC voltage according to the droop curve in Fig. 5.5, as shown in Fig. 5.12 g). In this way, the DC voltage of the DR-HVDC link remains largely at 640 kV as illustrated in Fig. 5.12 a).

Another 50 MVar (inductive) load is connected to the onshore AC grid at t=3.5 s. As demonstrated in Fig. 5.12, the whole system behaves exactly the same as described in section III B and graphically shown in Fig. 5.7. The final DC voltage stabilizes at 637.45 kV.

Across the entire process of the voltage ramping up and load pick up, the onshore and offshore AC grids remain stable while the DC voltage of the DR-HVDC link is maintained within the safe range due to the proposed *f*-*V* droop control, as

demonstrated in Fig. 5.12.

To further highlight the superior behaviour of proposed scheme, another loading ramping case is carried out, in which the onshore power demand is ramping up from 0 to 400 MW within 3.5-4 s.

Fig. 5.11 compares the DC voltages between the proposed f-V droop control and the scheme with fixed voltage reference (denoted as fixed V_{dmax} in Fig. 5.11). As can be seen, when $V_{d\max}$ is fixed to its upper limit $V_{bs\min}$ during black start, the DC voltage varies over 40 kV, while with the proposed droop control, the DC voltage variation is limited to a mere 10 kV.

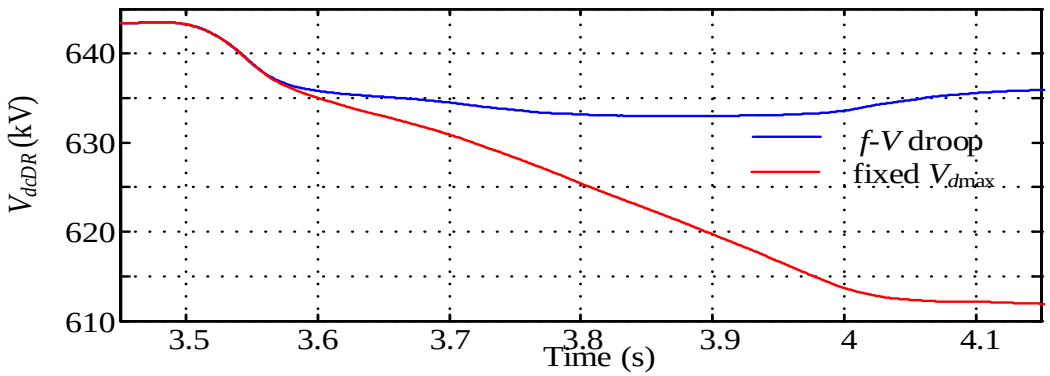

Fig. 5.11 Comparison of DC voltages between the proposed control and conventional control, when the onshore power demand ramping up from 0 to 400 MW.

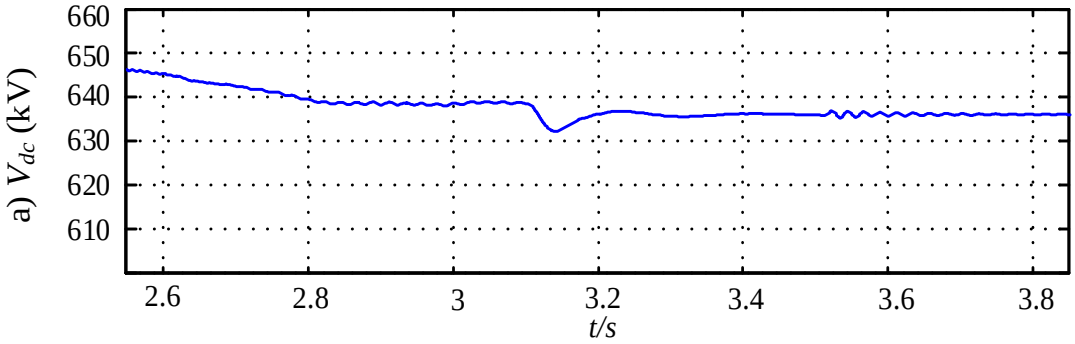

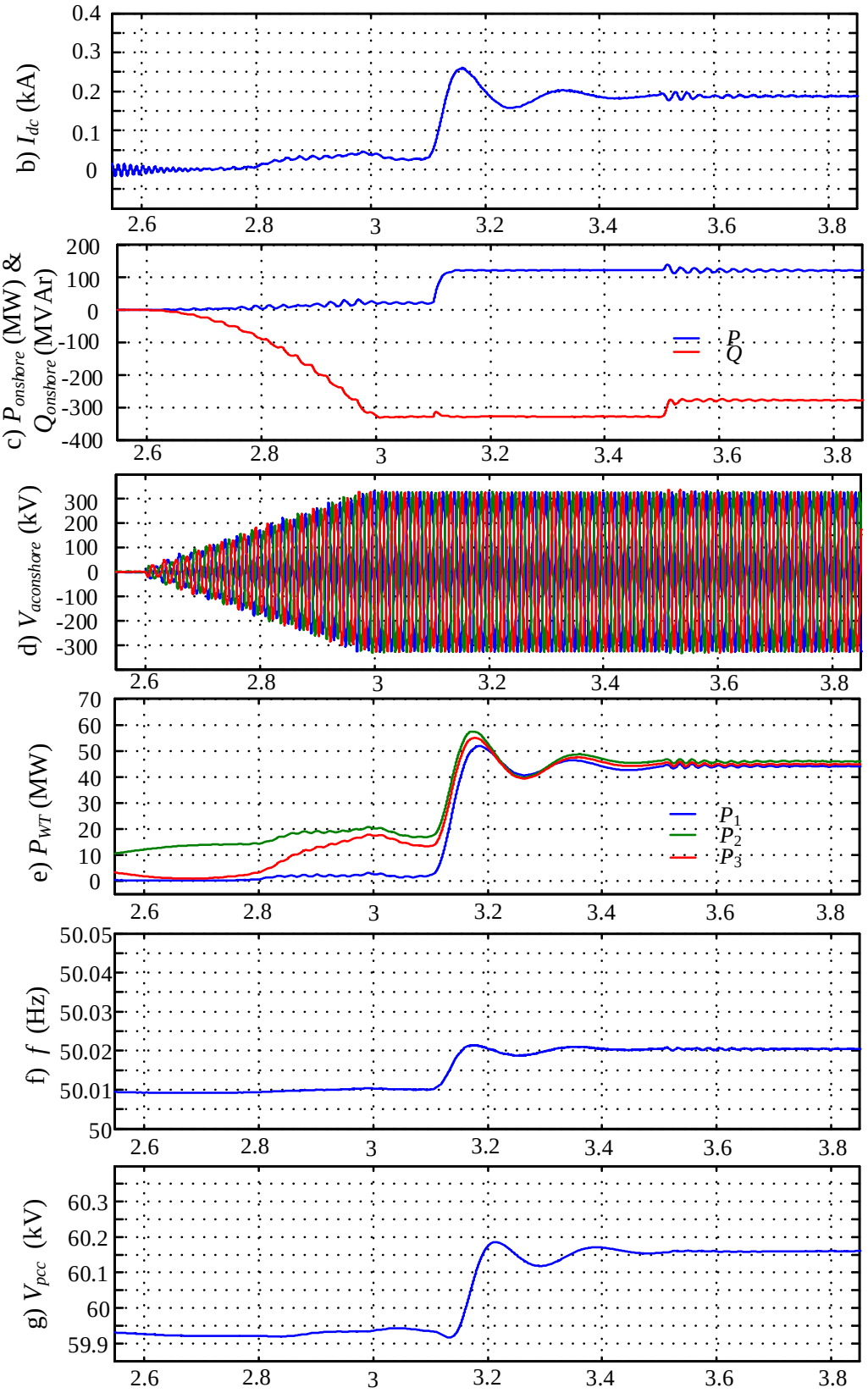
b) I_{dc} (kA)
0.4
0.3
0.2
0.1
0
2.6
2.8
3
3.2
3.4
3.6
3.8
c) $P_{onshore}$ (MW) & $Q_{onshore}$ (MVAr)
200
100
0
-100
-200
-300
-400
P
Q
d) $V_{aconshore}$ (kV)
300
200
100
0
-100
-200
-300
e) P_{WT} (MW)
70
60
50
40
30
20
10
0
P_1
P_2
P_3
f) f (Hz)
50.05
50.04
50.03
50.02
50.01
50
g) V_{pcc} (kV)
60.3
60.2
60.1
60
59.9

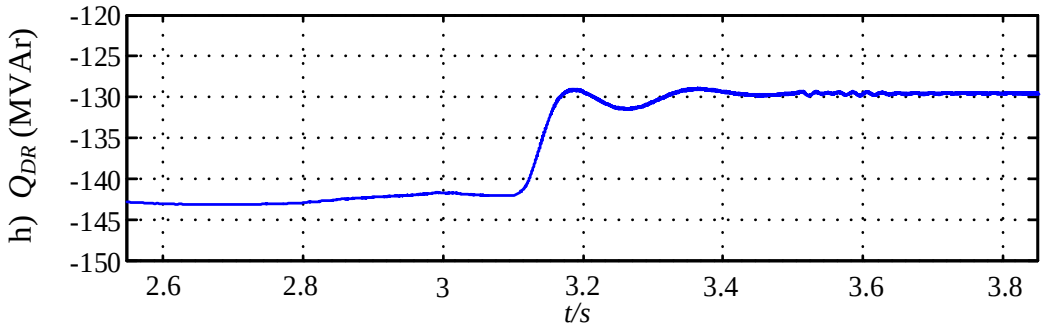

Fig. 5.12 Performance of the onshore AC grid energization and load pick up for the proposed black start scheme: a) DC voltage of DR-HVDC link, b) DC current of DR-HVDC link, c) onshore active and reactive power, d) onshore AC voltages, e) offshore WT power, f) offshore frequency, g) offshore PCC voltage and h) DR reactive power.

5.5.3 Onshore fault ride through

The performance of the proposed control scheme during onshore AC fault is tested and the onshore and offshore dynamics are shown in Fig. 5.13. Before the fault occurrence, the onshore AC grid has been built up using the proposed black start scheme as aforementioned and feeds a 200 MW load.

At t=4.0 s, a solid three-phase fault occurs at the onshore MMC AC terminal and is cleared at t=4.14 s. After fault occurrence, the onshore AC voltage, and active and reactive power rapidly decrease to zero, as shown in Fig. 5.13 c) and d). The offshore WTs still try to transmit the generated active power to onshore through the DR-HVDC link, resulting in an initial increase of the DC voltage of the DR-HVDC link, as observed in Fig. 5.13 a). Due to the increased DC voltage, the transmitted power of the DR system decreases, leading to the reduction of the reactive power consumed by the DR station and thereby the offshore frequency. Thus, the output voltage of WTs is reduced by the proposed f-V droop control, as illustrated in Fig. 5.13 g), resulting in the power export to the DR-HVDC link drop to almost zero. Consequently, the DC

voltage of the DR-HVDC link stops increasing, and the maximum DC voltage reaches 653 kV as shown in Fig. 5.13 a). After the onshore fault clearance at t=4.14 s, the onshore AC grid recovers. The DC voltage of DR-HVDC link and offshore AC voltage exhibit slight disturbances during the fault but are quickly recovered to the pre-fault state as shown in Fig. 5.13 a), f) and g).

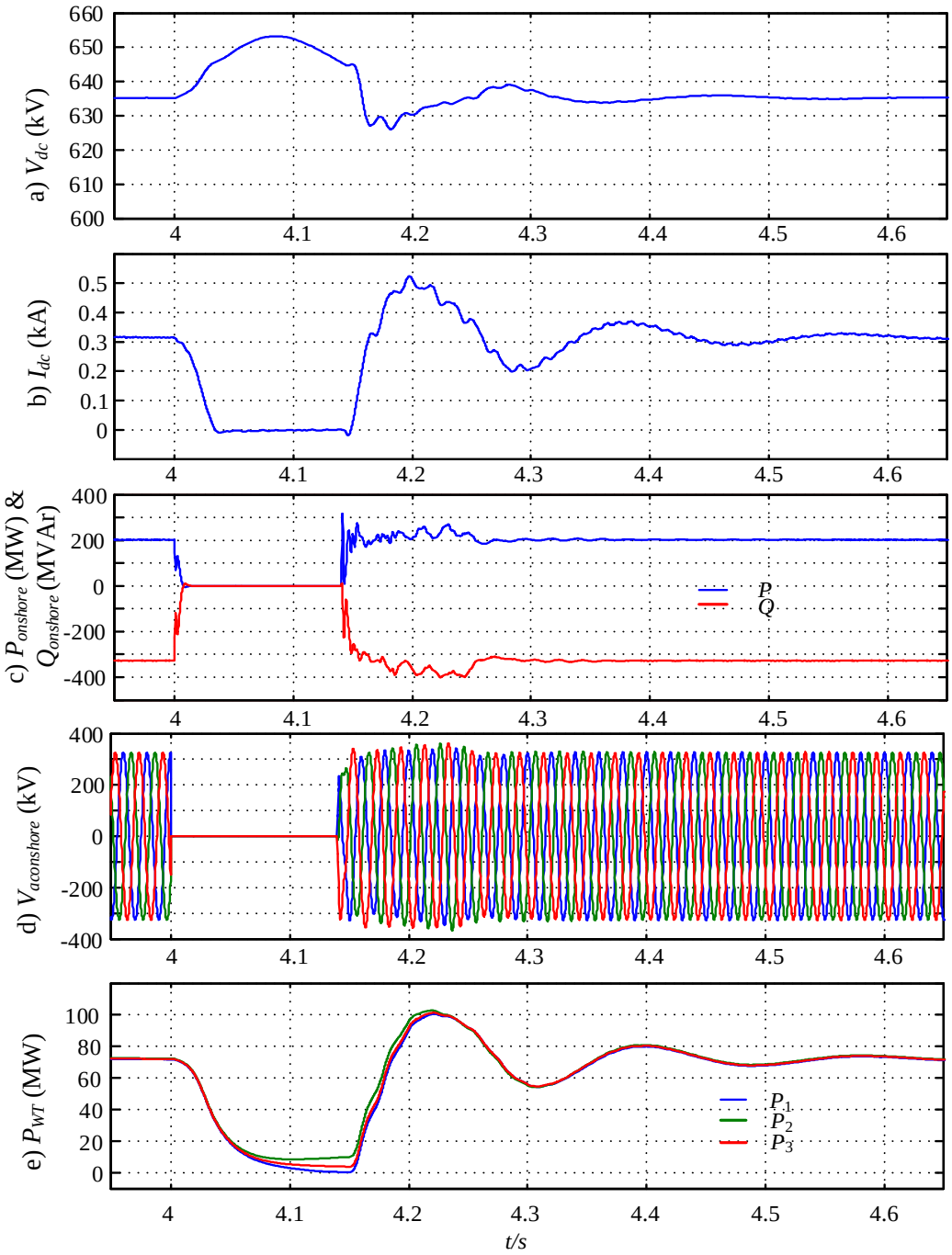

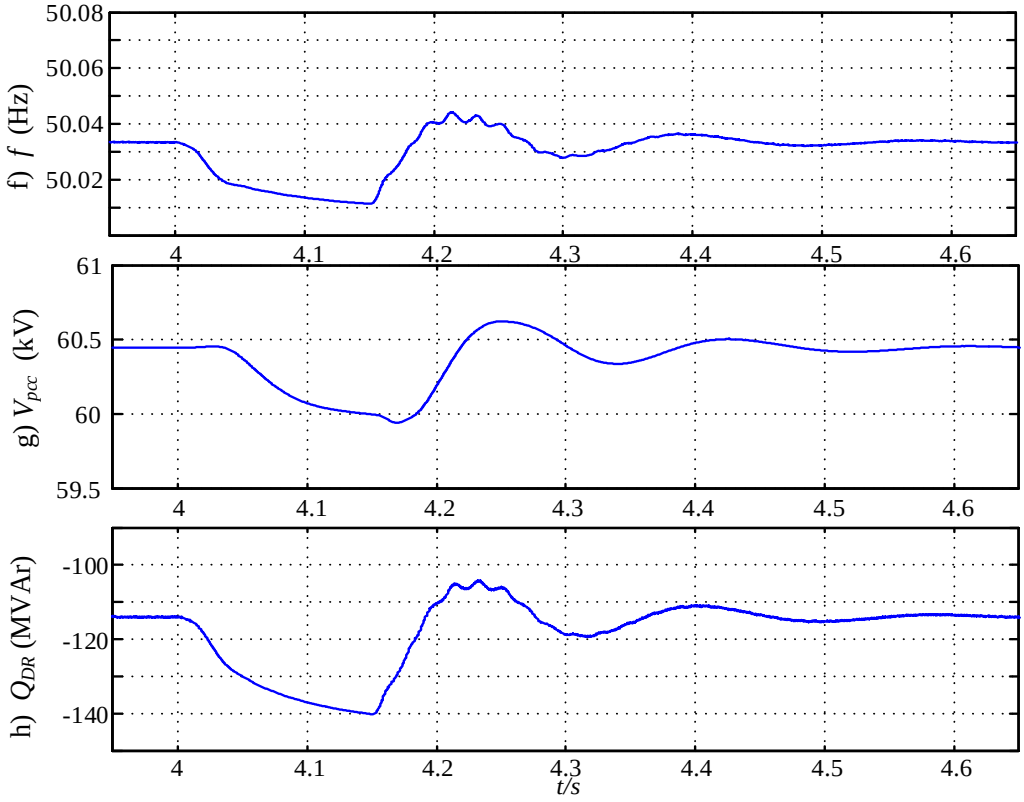

Fig. 5.13 Performance of the proposed black start scheme under onshore AC fault: a) DC voltage of DR-HVDC link, b) DC current of DR-HVDC link, c) onshore active and reactive power, d) onshore AC voltages, e) offshore WT power, f) offshore frequency, g) offshore PCC voltage and h) DR reactive power.

5.5.4 Offshore wind power redistribution

Practically, the maximum available power from each WT across a large offshore windfarm can vary due to exposure to different wind speeds. Some WTs' available wind power may be low such that the power controllers de-saturate, leading to deactivation of the *f-V* droop control during black start. Therefore, it is necessary to ensure that the WTs with low power can automatically change from the *f-V* droop control to MPPT control with the proposed scheme and the offshore AC voltage will be determined by other WTs to maintain a stable DC voltage.

Assuming that the onshore station supplies a 400 MW load while the available wind power of Cluster 2 is reduced to be less than the demand after t=5.02 s, as shown in Fig. 5.14 d), the output of the WT active power controller in Cluster 2 reduces and becomes less than the upper limit set by the f-V droop control. The active power controller of Cluster 2 WTs, thus de-saturates and regulates the output power to follow the reference set by the MPPT algorithm. The reactive power consumed by the DR station and offshore frequency slightly changes, leading to an increase of the output power of Cluster 1 and 3. Thus, the generated power of the entire offshore windfarm remains largely unchanged, as displayed in Fig. 5.14 c) and d). The power is redistributed among the three clusters and the DC voltage of DR-HVDC link and offshore PCC voltage are largely unaffected, as illustrated in Fig. 5.14 a) and f).

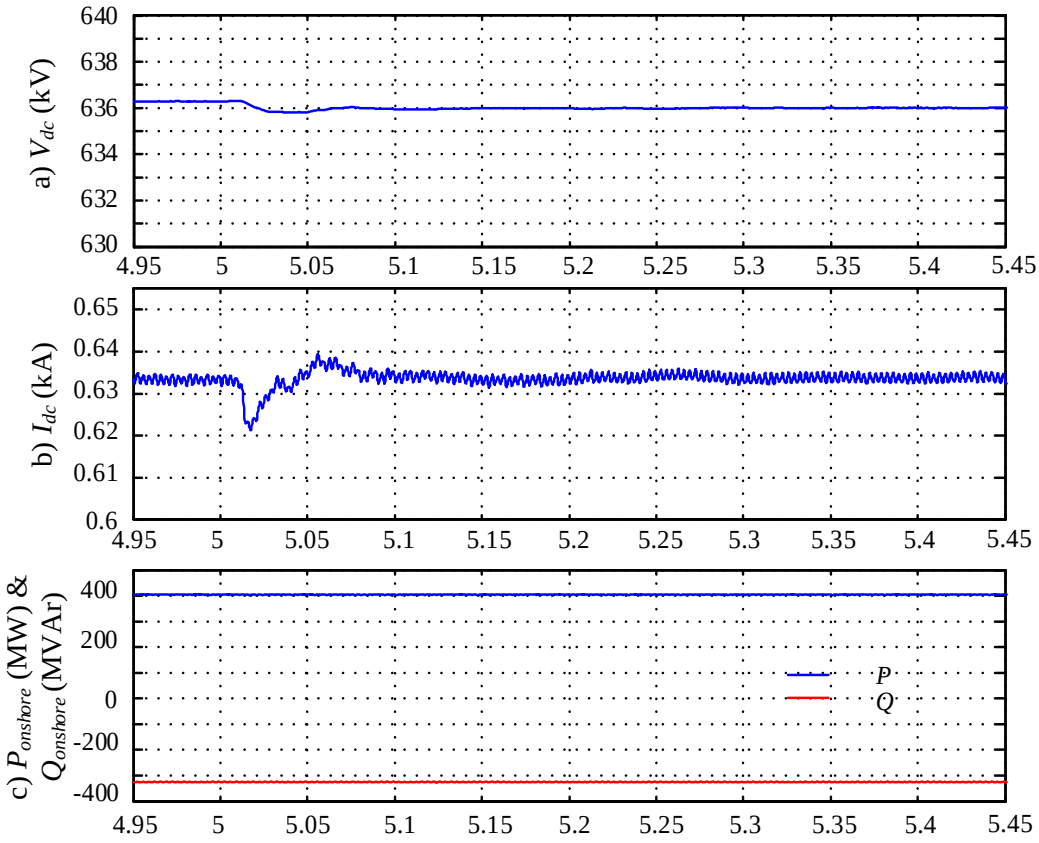

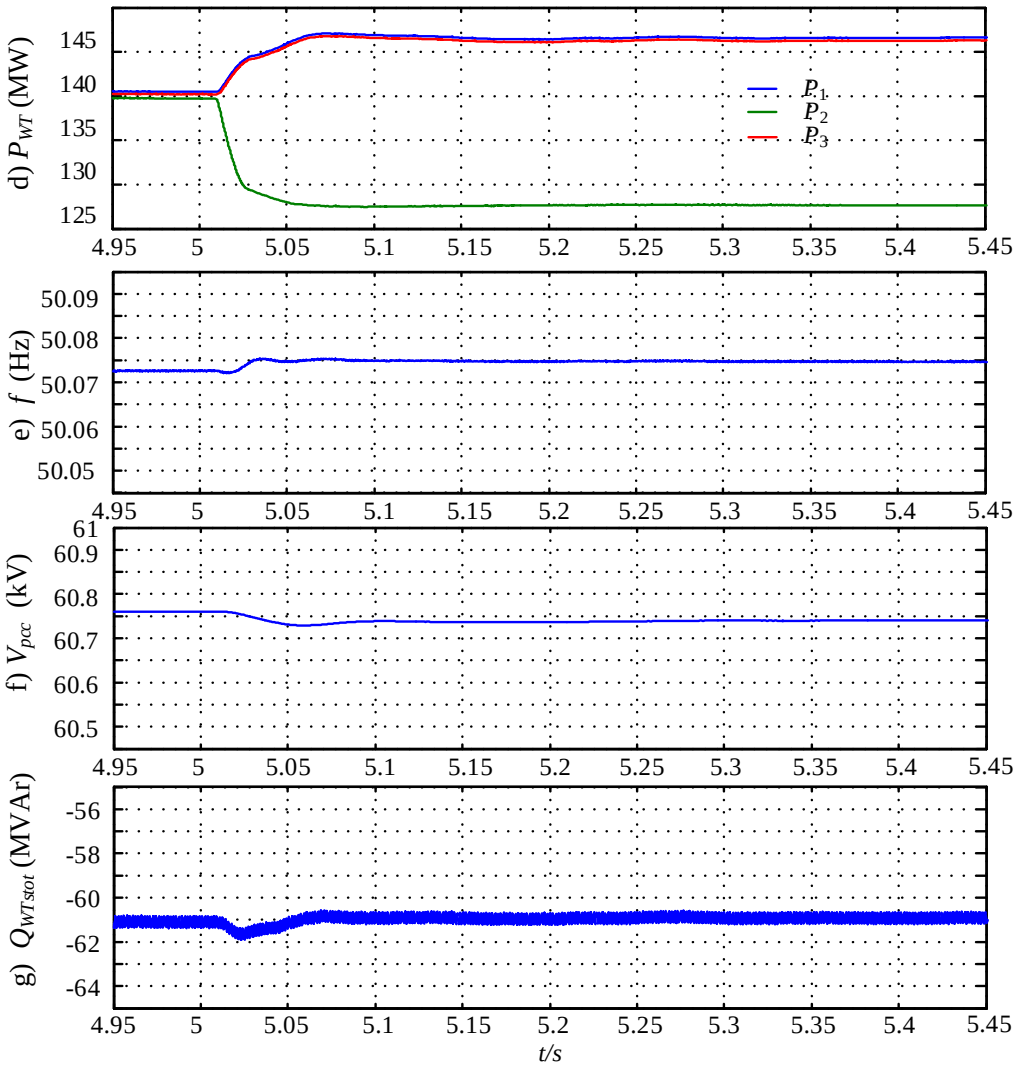

Fig. 5.14 Performance of the proposed black start scheme in low wind speed scenario: a) DC voltage of DR-HVDC link, b) DC current of DR-HVDC link, c) onshore active and reactive power, d) offshore WT power, e) offshore frequency, f) offshore PCC voltage and g) DR reactive power.

5.6 Summary

In this chapter, the use of DR-HVDC connected offshore wind farms for black start of an onshore AC network is studied. To address the issue of large DC voltage

variation during black start when the onshore loads vary, an enhanced control which utilizes the offshore frequency to dynamically regulate the offshore AC voltage is proposed aiming to maintain the DC voltage of the DR-HVDC link within the safety range. The active power-reactive power-frequency (*P-Q-f*) coupling characteristics of DR-HVDC systems are studied and subsequently used in the proposed control to enable WTs to automatically sense the operation condition of the DR-HVDC link without communication and ensure offshore and onshore power balance. In the event of onshore grid faults, the proposed control can also automatically reduce the offshore AC voltage and potential overvoltage of the HVDC link is thus limited. Considering different wind conditions across a large offshore wind farm, e.g., when certain WTs' available wind power is low, the power required by onshore loads during black start can be automatically redistributed among WTs with the proposed control and the system operation is unaffected. In addition, the detailed energization process of the DR-HVDC link and onshore MMC station, as well as onshore AC load pick up are investigated and demonstrated through simulations. The proposed control scheme provides a feasible solution to use DR-HVDC systems for black start of onshore AC grid.

Chapter 6
Conclusions and Future Work

6.1 General conclusion

MMC connected offshore windfarm systems exhibit different characteristics during offshore AC faults when compared with typical onshore AC systems with conventional synchronous generators. The situation becomes more challenging in the events of asymmetrical faults since the best practice of considering converters' capability in negative sequence control, converter hardware constraints, and the requirements of the offshore network during and after faults, have not been well defined and understood. For instance, detailed sequential analysis and simulation validation reveals that, the negative sequence current can be completely suppressed to prevent the overcurrent of the offshore MMC station during asymmetrical faults. However, after fault clearance, the induced negative sequence voltage does not allow the automatic recovery of the AC voltage to the pre-fault condition. Such behaviour could also make the protection system unable to distinguish between fault and post-fault conditions. Based on the observation of case study and the finding from sequential analysis, a new modified control scheme for the offshore MMC that employs negative sequence voltage controller to facilitate controlled injection of negative sequence currents is proposed. The additional outer negative sequence AC voltage control regulates the negative sequence voltage to zero during normal operation and while during offshore asymmetrical AC faults, controlled negative sequence currents are injected into the offshore AC network due to the saturation of the negative sequence AC voltage controller. The proposed scheme can not only define a safe level of fault current during different fault scenario but also enable quick

recovery of the AC voltage following clearance of AC faults. In addition, the proposed scheme takes the induced negative and zero sequence voltages into consideration to manipulate the setting of the positive sequence voltage reference in order to prevent any excessive overvoltage in the healthy phases. Simulation results have verified the effectiveness of the proposed asymmetrical fault management scheme.

Studies on the use of multi-terminal HVDC (MTDC) networks for interconnection of large offshore wind farms and onshore power networks have shown good potentials though significant technical and economic challenges exist, e.g. system protection and control during DC faults. Partially selective DC fault protection schemes for offshore MTDC networks may provide good balance between performance and cost, in which the expensive and bulky DCCBs are only used in limited cable locations while the cheap ACCBs and DC disconnectors are installed in most places. However, such protection schemes can cause problems such as overvoltage and frequency deviation in an AC offshore grid when the offshore MMC station is suddenly blocked during DC faults or the ACCBs in offshore AC grid suddenly open for fault clearance operation. Detailed analysis reveals that, the conventional WT power control will saturate its controllers due to the remaining power and reactive power reference and potentially lead to the shutdown of the offshore windfarm. Thus, to avoid the collapse of the offshore AC voltage, an enhanced WT control is proposed which enables the WT converter control seamlessly transits between grid following and forming modes. In addition, a detailed fault ride through operation including fault clearance and system recovery process is designed for a 4-terminal MTDC system. Detailed simulation studies confirm the feasibility of the proposed WT control and DC fault ride through scheme.

The rapid increases of RES in power system introduces new challenges to maintain reliability, stability, and security of power supplies. In the event of system

blackout, the ability of RES to black start part of a large network could bring significant economic and technical benefits to system operators. Thus, a black start operation for DR-HVDC connected offshore windfarm system is investigated in this thesis to support onshore AC grid restoration after system blackout. As the onshore MMC must perform AC voltage regulation to provide black start service to the onshore network, the DC voltage of the DR-HVDC link needs be regulated by the offshore WTs, which is in contrast to the normal operation of DR-HVDC connected offshore windfarm system. A detailed analysis on system characteristics reveals that adjusting the offshore PCC voltage by WTs according to the DR transmitted active power can maintain the DC voltage of the DR-HVDC link in a safety range during black start. However, the offshore DR power is not local measurement for WTs and individual WT power capability is small compared with the whole DR transmitted power. Thus, to address the issues of DC voltage regulation, an enhanced control which utilizes active power-reactive power-frequency (*P*-*Q*-*f*) coupling characteristics of DR-HVDC system is proposed. Such control method enables WTs to automatically sense the operation condition of the DR-HVDC link without communication and ensures offshore and onshore power balance. The detailed energization process of the DR-HVDC link and onshore MMC station, and onshore AC load pick up are investigated and demonstrated. In addition, the performance of the system during onshore AC faults and the redistribution of power generation among WTs due to wind condition changes are studied and the results show satisfactory performance.

6.2 Author's contribution

The thesis contains the following main contributions:

- A detailed sequence analysis is performed to assist in the understanding of

converter-based network characteristics under asymmetrical faults. An enhanced offshore MMC control strategy is then proposed to keep the fault current and phase voltage in safety levels in offshore AC network while support AC voltage recovery following clearance of AC faults.

- The impact of DC faults and its fault clearance strategy on offshore windfarm system is studied. Based on the findings, an enhanced passive voltage control for offshore WT converters is proposed to deal with the situation when the control from the offshore MMC station is lost due to its blocking or sudden opening of the offshore AC circuit breakers during a DC fault. The proposed WT control is incorporated with the partially selective DC fault protection scheme for a 4-terminal meshed DC network, to ensure adequate system recovery and minimize potential disturbance during grid restoration.
- When DR-HVDC connected offshore windfarm s used for black start onshore grid, a new WT frequency-AC voltage (*f*-*V*) droop control is proposed to regulate the DR-HVDC link voltage in a safe range and maintain power balance between onshore and offshore grids. Such operation method is achieved by dynamically regulating the offshore AC voltage according to the system operation condition considering the DR system power and reactive power and frequency coupling characteristics.

6.3 Suggestions for future research

This thesis has investigated some specific issues related to HVDC connected offshore windfarm system, potential areas for future research include:

- All the WTs model adopted in this thesis are aggregated and only represented

by the LSC. It is important to investigate the potential implications of the proposed methods on the WTs, e.g. WT drive chain during black start. Thus, detailed WTs models considering the dynamics in the turbine, generator, drive chain and GSC.

- The onshore system studied in this thesis during offshore transient is represented by a Thevenin equivalent circuit. Thus, the impact of the offshore system transient on the onshore system dynamics can be further explored.

- The black start studies performed in this thesis can be further extended to the detailed synchronous generator start-up and AC system reconnection, etc.

- Hardware-in-the-loop simulation platform can be created to further demonstrate the effectiveness of the proposed fault ride through and black start methods under various operating conditions.

References

[1] REN21 Community, "Renewables 2020 Global Status Report."Available Online: https://www.ren21.net/wp-content/uploads/2019/05/gsr_2020_full_report_en.pdf Accessed: 07-12-2020).

[2] Eurostat.Available Online: https://ec.europa.eu/eurostat/statistics-explained/index.php/Renewable_energy_statistics Accessed: 07-12-2020).

[3] E. Commission, "Proposal for a DIRECTIVE OF THE EUROPEAN PARLIAMENT AND OF THE COUNCIL on the promotion of the use of energy from renewable sources " *Official Journal of the European Union,* pp. 1-116, 2017.

[4] I. Erlich, F. Shewarega, C. Feltes, F. W. Koch, and J. Fortmann, "Offshore Wind Power Generation Technologies," *Proceedings of the IEEE,* vol. 101, pp. 891-905, 2013.

[5] A. Korompili, Q. Wu, and H. Zhao, "Review of VSC HVDC connection for offshore wind power integration," *Renewable and Sustainable Energy Reviews,* vol. 59, pp. 1405-1414, 2016/06/01/ 2016.

[6] WindEurope, "Wind energy in Europe in 2019 - Trends and statistics."Available Online: https://windeurope.org/data-and-analysis/product/?id=59 Accessed: 07-12-2020).

[7] Orsted, "Hornsea One and Two Offshore Wind Farms."Available Online: https://hornseaprojectone.co.uk/document-library#0 Accessed: 07-12-2020).

[8] SIEMENS Gamesa, "SIEMENS Gamesa product and services."Available Online: https://www.siemensgamesa.com/products-and-services/offshore Accessed: 07-12-2020).

[9] Orsted, "Hornsea Project One-Project Overview," in *Presentation for Ofgem OFTO TR6 Launch Event*, 2018.

[10] A. Abdalrahman and E. Isabegovic, "DolWin1 - Challenges of connecting offshore wind farms," in *2016 IEEE International Energy Conference (ENERGYCON)*, 2016, pp. 1-10.

[11] O. E. Oni, I. E. Davidson, and K. N. I. Mbangula, "A review of LCC-HVDC and VSC-HVDC technologies and applications," in *2016 IEEE 16th International Conference on Environment and Electrical Engineering (EEEIC)*, 2016, pp. 1-7.

[12] P. Bresesti, W. L. Kling, R. L. Hendriks, and R. Vailati, "HVDC Connection of Offshore Wind Farms to the Transmission System," *IEEE Transactions on Energy Conversion,* vol. 22, pp. 37-43, 2007.

[13] Y. Zhang, J. Ravishankar, J. Fletcher, R. Li, and M. Han, "Review of modular multilevel converter based multi-terminal HVDC systems for offshore wind power transmission," *Renewable and Sustainable Energy Reviews,* vol. 61, pp. 572-586, 2016/08/01/ 2016.

[14] N. B. Negra, J. Todorovic, and T. Ackermann, "Loss evaluation of HVAC and HVDC transmission solutions for large offshore wind farms," *Electric Power Systems Research,* vol. 76, pp. 916-927, 2006/07/01/ 2006.

[15] X. Xiang, M. M. C. Merlin, and T. C. Green, "Cost analysis and comparison of HVAC, LFAC and HVDC for offshore wind power connection," in *12th IET International Conference on AC and DC Power Transmission (ACDC 2016)*, 2016, pp. 1-6.

[16] F. Blaabjerg and K. Ma, "Future on Power Electronics for Wind Turbine Systems," *IEEE Journal of Emerging and Selected Topics in Power Electronics,* vol. 1, pp. 139-152, 2013.

[17] J. Rocabert, A. Luna, F. Blaabjerg, and P. Rodríguez, "Control of Power Converters in AC Microgrids," *IEEE Transactions on Power Electronics,* vol. 27, pp. 4734-4749, 2012.

[18] L. Zhang, L. Harnefors, and H. P. Nee, "Power-Synchronization Control of Grid-Connected Voltage-Source Converters," *IEEE Transactions on Power Systems,* vol. 25, pp. 809-820, 2010.

[19] Y. Jing, R. Li, L. Xu, and Y. Wang, "Enhanced AC voltage and frequency control of offshore MMC station for wind farm connection," *IET Renewable Power Generation,* vol. 12, pp. 1771-1777, 2018.

[20] G. Ö, N. A. Cutululis, P. S⊘rensen, and L. Zeni, "Asymmetrical fault analysis at the offshore network of HVDC connected wind power plants," in *2017 IEEE Manchester PowerTech*, 2017, pp. 1-5.

[21] R. Adapa, "High-Wire Act: HVdc Technology: The State of the Art," *IEEE Power and Energy Magazine,* vol. 10, pp. 18-29, 2012.

[22] N. A. Belda, C. A. Plet, and R. P. P. Smeets, "Analysis of Faults in Multiterminal HVDC Grid for Definition of Test Requirements of HVDC Circuit Breakers," *IEEE Transactions on Power Delivery,* vol. 33, pp. 403-411, 2018.

[23] R. Li and L. Xu, "Review of DC fault protection for HVDC grids," *Wiley Interdisciplinary Reviews: Energy and Environment,* vol. 7, pp. e278-n/a, 2018.

[24] G. Chaffey and T. C. Green, "Low speed protection methodology for a symmetrical monopolar HVDC network," in *13th IET International Conference on AC and DC Power Transmission (ACDC 2017)*, 2017, pp. 1-6.

[25] A. Raza, X. Dianguo, S. Xunwen, L. Weixing, and B. W. Williams, "A Novel Multiterminal VSC-HVdc Transmission Topology for Offshore Wind Farms," *IEEE Transactions on Industry Applications,* vol. 53, pp. 1316-1325, 2017.

[26] L. Xu and L. Yao, "DC voltage control and power dispatch of a multi-terminal HVDC system for integrating large offshore wind farms," *IET Renewable Power Generation,* vol. 5, pp. 223-233, 2011.

[27] R. Dantas, J. Liang, C. E. Ugalde-Loo, A. Adamczyk, C. Barker, and R. Whitehouse, "Progressive Fault Isolation and Grid Restoration Strategy for MTDC Networks," *IEEE Transactions on Power Delivery,* vol. 33, pp. 909-918, 2018.

[28] P. Wang, X.-P. Zhang, P. F. Coventry, R. Zhang, and Z. Li, "Control and protection sequence for recovery and reconfiguration of an offshore integrated MMC multi-terminal HVDC system under DC faults," *International Journal of Electrical Power & Energy Systems,* vol. 86, pp. 81-92, 2017/03/01/ 2017.

[29] P. Ruffing, N. Collath, C. Brantl, and A. Schnettler, "DC Fault Control and High-Speed Switch Design for an HVDC Network Protection Based on Fault-Blocking Converters," *IEEE Transactions on Power Delivery,* vol. 34, pp. 397-406, 2019.

[30] E. Muljadi, N. Samaan, V. Gevorgian, J. Li, and v. s. Pasupulati, *Short circuit current contribution for different wind turbine generator types*, 2010.

[31] R. Irnawan, K. Srivastava, and M. Reza, "Fault detection in HVDC-connected

wind farm with full converter generator," *International Journal of Electrical Power & Energy Systems,* vol. 64, pp. 833-838, 01/31 2015.

[32] D. Boeck, V. Hertem, and P. Ejnar, "Review of Defence Plans in Europe : Current Status , Strengths and Opportunities Publication date : S . De Boeck ; D . Van Hertem , K . Das , P . Sørensen , V . Trovato , J . Turunen , M . Halat (2016), " Review of Conseil International des Grands Réseaux Electriques International Council on Large Electric Systems," 2016.

[33] Ö. Göksu, O. Saborío-Romano, N. A. Cutululis, and P. Sørensen, "Black Start and Island Operation Capabilities of Wind Power Plants," *16th Wind Integration Workshop,* pp. 25-27, 2017.

[34] J. N. Sakamuri, G. Ö, A. Bidadfar, O. Saborío-Romano, A. Jain, and N. A. Cutululis, "Black Start by HVdc-connected Offshore Wind Power Plants," in *IECON 2019 - 45th Annual Conference of the IEEE Industrial Electronics Society*, 2019, pp. 7045-7050.

[35] A. Jain, Sakamuri, J. N., Das, K., Göksu, Ö., and Cutululis, N. A, "Functional Requirements for Blackstart and Power System Restoration from Wind Power Plants," presented at the 2nd International Conference on Large-Scale Grid Integration of Renewable Energy in India, New Delhi, 2019.

[36] A. Bangar and V. Hamidi, "Control strategy requirements for connection of offshore windfarms using VSC-HVDC for frequency control," in *10th IET International Conference on AC and DC Power Transmission (ACDC 2012)*, 2012, pp. 1-6.

[37] J. He, M. Li, J. Yi, Q. Chang, T. Xu, and Y. Zhao, "Research on dynamic characteristics and countermeasures of AC-DC hybrid power system with large scale HVDC transmission," in *2014 International Conference on Power System Technology*, 2014, pp. 799-805.

[38] A. Lesnicar and R. Marquardt, "An innovative modular multilevel converter topology suitable for a wide power range," in *2003 IEEE Bologna Power Tech Conference Proceedings*, 2003, p. 6 pp. Vol.3.

[39] H. Lang, Y. Xu, X. Peng, Z. Fan, M. Xin, L. Tao*, et al.*, "The evolution and variation of sub-module topologies with DC-fault current clearing capability in MMC-HVDC," in *2017 IEEE 3rd International Future Energy Electronics Conference and ECCE Asia (IFEEC 2017 - ECCE Asia)*, 2017, pp. 1938-1943.

[40] B. J. Pawar and V. J. Gond, "Modular multilevel converters: A review on topologies, modulation, modeling and control schemes," in *2017 International conference of Electronics, Communication and Aerospace Technology (ICECA)*, 2017, pp. 431-440.

[41] "HVDC CONNECTION OF OFFSHORE WIND POWER PLANTS," Accessed: 2015).

[42] O. Kuhn, P. Menke, R. Zurowski, T. Christ, S. Seman, G. Giering*, et al.*, "2nd generation DC grid access for offshore wind farms: HVDC in an AC fashion," *CIGRE, Paris,* pp. 1-7, 2016.

[43] S. Seman, R. Zurowski, and C. Taratoris, "Interconnection of advanced Type 4 WTGs with Diode Rectifier based HVDC solution and weak AC grids," in *Proceedings of the 14th Wind Integration Workshop,Brussels, Belgium, 20th–22nd Oct.* , 2015.

[44] T. H. Nguyen, D. C. Lee, and C. K. Kim, "A Series-Connected Topology of a Diode Rectifier and a Voltage-Source Converter for an HVDC Transmission System," *IEEE Transactions on Power Electronics,* vol. 29, pp. 1579-1584, 2014.

[45] Cigré Session, "Parallelling offshore wind farm HVDC ties on offshore side," ParisAccessed: 2012).

[46] R. Li, L. Yu, L. Xu, and G. P. Adam, "Coordinated Control of Parallel DR-HVDC and MMC-HVDC Systems for Offshore Wind Energy Transmission," *IEEE Journal of Emerging and Selected Topics in Power Electronics,* vol. 8, pp. 2572-2582, 2020.

[47] D. Van Hertem and M. Ghandhari, "Multi-terminal VSC HVDC for the European supergrid: Obstacles," *Renewable and Sustainable Energy Reviews,* vol. 14, pp. 3156-3163, 2010/12/01/ 2010.

[48] S. Gang, P. Simin, C. Xu, C. Zhe, and H. Wei, "Grid integration of offshore wind farms and offshore oil/gas platforms," in *Proceedings of The 7th International Power Electronics and Motion Control Conference*, 2012, pp. 1301-1305.

[49] S. Sanchez, A. Garcés, G. Bergna-Diaz, and E. Tedeschi, "Dynamics and Stability of Meshed Multiterminal HVDC Networks," *IEEE Transactions on Power Systems,* vol. 34, pp. 1824-1833, 2019.

[50] H. Li, C. Liu, G. Li, and R. Iravani, "An Enhanced DC Voltage Droop-Control for the VSC--HVDC Grid," *IEEE Transactions on Power Systems,* vol. 32, pp. 1520-1527, 2017.

[51] F. Thams, R. Eriksson, and M. Molinas, "Interaction of Droop Control Structures and Its Inherent Effect on the Power Transfer Limits in Multiterminal VSC-HVDC," *IEEE Transactions on Power Delivery,* vol. 32, pp. 182-192, 2017.

[52] E. Prieto-Araujo, A. Egea-Alvarez, S. Fekriasl, and O. Gomis-Bellmunt, "DC Voltage Droop Control Design for Multiterminal HVDC Systems Considering AC and DC Grid Dynamics," *IEEE Transactions on Power Delivery,* vol. 31, pp. 575-585, 2016.

[53] F. Yan, G. Tang, Z. He, and M. Kong, "An improved droop control strategy for MMC-based VSC-MTDC systems," *Zhongguo Dianji Gongcheng Xuebao/Proceedings of the Chinese Society of Electrical Engineering,* vol. 34, pp. 397-404, 01/25 2014.

[54] X. Han, W. Sima, M. Yang, L. Li, T. Yuan, and Y. Si, "Transient Characteristics Under Ground and Short-Circuit Faults in a ${\pm \text{500}\,\text{kV}}$ MMC-Based HVDC System With Hybrid DC Circuit Breakers," *IEEE Transactions on Power Delivery,* vol. 33, pp. 1378-1387, 2018.

[55] J. Hu, K. Xu, L. Lin, and R. Zeng, "Analysis and Enhanced Control of Hybrid-MMC-Based HVDC Systems During Asymmetrical DC Voltage Faults," *IEEE Transactions on Power Delivery,* vol. 32, pp. 1394-1403, 2017.

[56] S. Bernal-Perez, S. Ano-Villalba, R. Blasco-Gimenez, and J. Rodriguez-D'Derlee, "Efficiency and Fault Ride-Through Performance of a Diode-Rectifier- and VSC-Inverter-Based HVDC Link for Offshore Wind Farms," *IEEE Transactions on Industrial Electronics,* vol. 60, pp. 2401-2409, 2013.

[57] R. Blasco-Gimenez, S. Anó-Villalba, J. Rodriguez-D'Derlée, S. Bernal-Perez, and F. Morant, "Diode-Based HVdc Link for the Connection of Large Offshore Wind Farms," *IEEE Transactions on Energy Conversion,* vol. 26, pp. 615-626, 2011.

[58] L. Yu, R. Li, and L. Xu, "Distributed PLL-Based Control of Offshore Wind Turbines Connected With Diode-Rectifier-Based HVDC Systems," *IEEE Transactions on Power Delivery,* vol. 33, pp. 1328-1336, 2018.

[59] D. Herrera, E. Galván, and J. M. Carrasco, "Method for controlling voltage and frequency of the local offshore grid responsible for connecting large offshore commercial wind turbines with the rectifier diode-based HVDC-link applied to an external controller," *IET Electric Power Applications,* vol. 11, pp. 1509-1516, 2017.

[60] B. Liu, J. Xu, R. E. Torres-Olguin, and T. Undeland, "Faults mitigation control design for grid integration of offshore wind farms and oil & gas installations using VSC HVDC," in *SPEEDAM 2010*, 2010, pp. 792-797.

[61] U. Karaagac, J. Mahseredjian, L. Cai, and H. Saad, "Offshore Wind Farm Modeling Accuracy and Efficiency in MMC-Based Multiterminal HVDC Connection," *IEEE Transactions on Power Delivery,* vol. 32, pp. 617-627, 2017.

[62] X. Lie, B. R. Andersen, and P. Cartwright, "VSC transmission operating under unbalanced AC conditions - analysis and control design," *IEEE Transactions on Power Delivery,* vol. 20, pp. 427-434, 2005.

[63] S. Alepuz, S. Busquets-Monge, J. Bordonau, J. A. Martinez-Velasco, C. A. Silva, J. Pontt*, et al.*, "Control Strategies Based on Symmetrical Components for Grid-Connected Converters Under Voltage Dips," *IEEE Transactions on Industrial Electronics,* vol. 56, pp. 2162-2173, 2009.

[64] C. H. Ng, L. Ran, and J. Bumby, "Unbalanced-Grid-Fault Ride-Through Control for a Wind Turbine Inverter," *IEEE Transactions on Industry Applications,* vol. 44, pp. 845-856, 2008.

[65] D. Roiu, R. I. Bojoi, L. R. Limongi, and A. Tenconi, "New Stationary Frame Control Scheme for Three-Phase PWM Rectifiers Under Unbalanced Voltage Dips Conditions," *IEEE Transactions on Industry Applications,* vol. 46, pp. 268-277, 2010.

[66] T. Neumann, T. Wijnhoven, G. Deconinck, and I. Erlich, "Enhanced Dynamic Voltage Control of Type 4 Wind Turbines During Unbalanced Grid Faults," *IEEE Transactions on Energy Conversion,* vol. 30, pp. 1650-1659, 2015.

[67] S. K. Chaudhary, R. Teodorescu, P. Rodriguez, P. C. Kjaer, and A. M. Gole, "Negative Sequence Current Control in Wind Power Plants With VSC-HVDC Connection," *Sustainable Energy, IEEE Transactions on,* vol. 3, pp. 535-544, 2012.

[68] Q. Tu, Z. Xu, Y. Chang, and L. Guan, "Suppressing DC Voltage Ripples of MMC-HVDC Under Unbalanced Grid Conditions," *IEEE Transactions on Power Delivery,* vol. 27, pp. 1332-1338, 2012.

[69] J. Wang, J. Liang, C. Wang, and X. Dong, "Circulating Current Suppression for MMC-HVDC under Unbalanced Grid Conditions," *IEEE Transactions on Industry Applications,* vol. 53, pp. 3250-3259, 2017.

[70] G. P. Adam, I. Abdelsalam, J. E. Fletcher, G. M. Burt, D. Holliday, and S. J. Finney, "New Efficient Submodule for a Modular Multilevel Converter in Multiterminal HVDC Networks," *IEEE Transactions on Power Electronics,* vol. 32, pp. 4258-4278, 2017.

[71] X. Shi, Z. Wang, B. Liu, Y. Li, L. M. Tolbert, and F. Wang, "Steady-State Modeling of Modular Multilevel Converter Under Unbalanced Grid Conditions," *IEEE Transactions on Power Electronics,* vol. 32, pp. 7306-7324, 2017.

[72] M. Guan and Z. Xu, "Modeling and Control of a Modular Multilevel Converter-Based HVDC System Under Unbalanced Grid Conditions," *IEEE Transactions on Power Electronics,* vol. 27, pp. 4858-4867, 2012.

[73] S. Li, X. Wang, Z. Yao, T. Li, and Z. Peng, "Circulating Current Suppressing Strategy for MMC-HVDC Based on Nonideal Proportional Resonant Controllers Under Unbalanced Grid Conditions," *IEEE Transactions on Power Electronics,* vol. 30, pp. 387-397, 2015.

[74] J. Jia, G. Yang, and A. H. Nielsen, "A Review on Grid-Connected Converter Control for Short-Circuit Power Provision Under Grid Unbalanced Faults," *IEEE Transactions on Power Delivery,* vol. 33, pp. 649-661, 2018.

[75] R. Li, L. Yu, and L. Xu, "Offshore AC Fault Protection of Diode Rectifier Unit-Based HVdc System for Wind Energy Transmission," *IEEE Transactions on Industrial Electronics,* vol. 66, pp. 5289-5299, 2019.

[76] J. N. Sakamuri, Z. H. Rather, J. Rimez, M. Altin, G. Ö, and N. A. Cutululis, "Coordinated Voltage Control in Offshore HVDC Connected Cluster of Wind Power Plants," *IEEE Transactions on Sustainable Energy,* vol. 7, pp. 1592-1601, 2016.

[77] P. M. Anderson, *Analysis of faulted power systems [by] Paul M. Anderson*. Ames: Iowa State University Press, 1973.

[78] S. Cao, W. Xiang, L. Yao, B. Yang, and J. Wen, "AC and DC fault ride through hybrid MMC integrating wind power," *The Journal of Engineering,* vol. 2017, pp. 828-833, 2017.

[79] J. Maneiro, S. Tennakoon, C. Barker, and F. Hassan, "Energy diverting converter topologies for HVDC transmission systems," in *2013 15th European Conference on Power Electronics and Applications (EPE)*, 2013, pp. 1-10.

[80] S. K. Chaudhary, R. Teodorescu, P. Rodriguez, and P. C. Kjær, "Chopper controlled resistors in VSC-HVDC transmission for WPP with full-scale converters," in *2009 IEEE PES/IAS Conference on Sustainable Alternative Energy (SAE)*, 2009, pp. 1-8.

[81] M. J. Hossain, H. R. Pota, V. A. Ugrinovskii, and R. A. Ramos, "Simultaneous STATCOM and Pitch Angle Control for Improved LVRT Capability of Fixed-Speed Wind Turbines," *IEEE Transactions on Sustainable Energy,* vol. 1, pp. 142-151, 2010.

[82] M. Firouzi, G. B. Gharehpetian, and S. B. Mozafari, "Application of UIPC to improve power system stability and LVRT capability of SCIG-based wind farms," *IET Generation, Transmission & Distribution,* vol. 11, pp. 2314-2322, 2017.

[83] S. Nanou and S. Papathanassiou, "Evaluation of a communication-based fault ride-through scheme for offshore wind farms connected through high-voltage DC links based on voltage source converter," *IET Renewable Power Generation,* vol. 9, pp. 882-891, 2015.

[84] M. A. Ahmed and Y. C. Kim, "Hierarchical Communication Network Architectures for Offshore Wind Power Farms," in *2014 International Symposium on Computer, Consumer and Control*, 2014, pp. 299-303.

[85] G. Ramtharan, A. Arulampalam, J. B. Ekanayake, F. M. Hughes, and N. Jenkins, "Fault ride through of fully rated converter wind turbines with AC and DC transmission," *IET Renewable Power Generation,* vol. 3, pp. 426-438, 2009.

[86] B. Silva, C. L. Moreira, H. Leite, and J. A. P. Lopes, "Control Strategies for AC Fault Ride Through in Multiterminal HVDC Grids," *IEEE Transactions on Power Delivery,* vol. 29, pp. 395-405, 2014.

[87] R. Li and L. Xu, "Review of DC fault protection for HVDC grids," *WIREs*

Energy and Environment, vol. 7, p. e278, 2018.

[88] J. Yang, J. E. Fletcher, and J. O. Reilly, "Short-Circuit and Ground Fault Analyses and Location in VSC-Based DC Network Cables," *IEEE Transactions on Industrial Electronics,* vol. 59, pp. 3827-3837, 2012.

[89] X. Li, Q. Song, W. Liu, H. Rao, S. Xu, and L. Li, "Protection of Nonpermanent Faults on DC Overhead Lines in MMC-Based HVDC Systems," *IEEE Transactions on Power Delivery,* vol. 28, pp. 483-490, 2013.

[90] G. P. Adam, I. A. Abdelsalam, K. H. Ahmed, and B. W. Williams, "Hybrid Multilevel Converter With Cascaded H-bridge Cells for HVDC Applications: Operating Principle and Scalability," *IEEE Transactions on Power Electronics,* vol. 30, pp. 65-77, 2015.

[91] R. Marquardt, "Modular Multilevel Converter topologies with DC-Short circuit current limitation," in *8th International Conference on Power Electronics - ECCE Asia*, 2011, pp. 1425-1431.

[92] R. Zeng, L. Xu, L. Yao, and B. W. Williams, "Design and Operation of a Hybrid Modular Multilevel Converter," *IEEE Transactions on Power Electronics,* vol. 30, pp. 1137-1146, 2015.

[93] P. Ruffing, C. Brantl, C. Petino, and A. Schnettler, "Fault current control methods for multi-terminal DC systems based on fault blocking converters," *The Journal of Engineering,* vol. 2018, pp. 871-875, 2018.

[94] E. Kontos, R. T. Pinto, S. Rodrigues, and P. Bauer, "Impact of HVDC Transmission System Topology on Multiterminal DC Network Faults," *IEEE Transactions on Power Delivery,* vol. 30, pp. 844-852, 2015.

[95] T. Eriksson, Backman, M., & Halen, S., "A low loss mechanical HVDC breaker for HVDC grid applications," presented at the Proceedings ofCigré Session, Paris, France, 2014.

[96] J. Descloux, P. Rault, S. Nguefeus, J. B. Curis, X. Guillaud, F. Colas*, et al.*, "HVDC meshed grid: Control and protection of a multi-terminal HVDC system," *CIGRE 2012,* 08/27 2012.

[97] M. Callavik, Blomberg, A., Häfner, J., & Jacobson, B. (2012). "The hybrid HVDC breaker-an innovation breakthrough enabling reliable HVDC grids," *ABB Grid Systems, Technical paper,* 2012.

[98] X. Han, W. Sima, M. Yang, L. Li, T. Yuan, and Y. Si, "Transient Characteristics Under Ground and Short-Circuit Faults in a +-500 MMC-Based HVDC System With Hybrid DC Circuit Breakers," *IEEE Transactions on Power Delivery,* vol. 33, pp. 1378-1387, 2018.

[99] W. Sanusi, M. A. Hosani, and M. S. E. Moursi, "A Novel DC Fault Ride-Through Scheme for MTDC Networks Connecting Large-Scale Wind Parks," *IEEE Transactions on Sustainable Energy,* vol. 8, pp. 1086-1095, 2017.

[100] M. A. Parker, D. Holliday, and S. J. Finney, "DC protection for a multi-terminal HVDC network including offshore wind power, featuring a reduced DC circuit breaker count," *The Journal of Engineering,* vol. 2019, pp. 4511-4515, 2019.

[101] R. Li, L. Xu, and L. Yao, "DC Fault Detection and Location in Meshed Multiterminal HVDC Systems Based on DC Reactor Voltage Change Rate," *IEEE Transactions on Power Delivery,* vol. 32, pp. 1516-1526, 2017.

[102] M. H. Rahman, L. Xu, and L. Yao, "Protection of Large Partitioned MTDC Networks Using DC-DC Converters and Circuit Breakers," *Protection and Control of Modern Power Systems,* vol. 1, p. 19, 2016.

[103] Z. Suo, G. Li, R. Li, L. Xu, W. Wang, Y. Chi*, et al.*, "Submodule configuration of HVDC-DC autotransformer considering DC fault," *IET Power Electronics,* vol. 9, pp. 2776-2785, 2016.

[104] E. S. O. National Grid, "Technical Report on the events of 9 August 2019," pp. 2-38, 2019.

[105] E. S. O. National Grid, "Black Start from Non - Traditional Generation Technologies," 2019.

[106] M. Bahrman and P. Bjorklund, "The New Black Start: System Restoration with Help from Voltage-Sourced Converters," *IEEE Power and Energy Magazine,* vol. 12, pp. 44-53, 2014.

[107] J.-H. Ying, H. Duchen, M. Karlsson, L. Ronstrom, and B. Abrahamsson, "HVDC with voltage source converters - a powerful standby black start facility," in *2008 IEEE/PES Transmission and Distribution Conference and Exposition*, 2008, pp. 1-9.

[108] T. Midtsund, A. Becker, J. Karlsson, and K. A. Egeland, "A live black-start capability test of a voltage source HVDC converter," *Cigre Science &*

Engineering, vol. N°4, pp. 81-87, 2016.

[109] T. B. Sørensen, Kwon, J. B., and Jørgensen, J. M, "A live black start test of an HVAC network using soft start capability of a voltage source HVDC converter," in *CIGRE 2019 Aalborg Symposium*, 2019.

[110] I. Arana, A. Hernandez, G. Thumm, and J. Holboell, "Energization of Wind Turbine Transformers With an Auxiliary Generator in a Large Offshore Wind Farm During Islanded Operation," *IEEE Transactions on Power Delivery,* vol. 26, pp. 2792-2800, 2011.

[111] L. Cai, U. Karaagac, and J. Mahseredjian, "Simulation of Startup Sequence of an Offshore Wind Farm With MMC-HVDC Grid Connection," *IEEE Transactions on Power Delivery,* vol. 32, pp. 638-646, 2017.

[112] A. Jain, Das, K., Göksu, Ö., & Cutululis, N. A, "Control Solutions for Blackstart Capability and Islanding Operation of Offshore Wind Power Plants," in *Proceedings of 17th wind Integration workshop*, 2018.

[113] B. Li, D. Xu, Y. Zhang, R. Yang, G. Wang, W. Wang*, et al.*, "Closed-Loop Precharge Control of Modular Multilevel Converters During Start-Up Processes," *IEEE Transactions on Power Electronics,* vol. 30, pp. 524-531, 2015.

[114] L. Zhang, J. Qin, X. Wu, S. Debnath, and M. Saeedifard, "A Generalized Precharging Strategy for Soft Startup Process of the Modular Multilevel Converter-Based HVDC Systems," *IEEE Transactions on Industry Applications,* vol. 53, pp. 5645-5657, 2017.

[115] L. Yu, R. Li, L. Xu, and G. P. Adam, "Analysis and Control of Offshore Wind Farms Connected With Diode Rectifier-Based HVDC System," *IEEE Transactions on Power Delivery,* vol. 35, pp. 2049-2059, 2020.

[116] M. Hagiwara and H. Akagi, "Control and Experiment of Pulsewidth-Modulated Modular Multilevel Converters," *IEEE Transactions on Power Electronics,* vol. 24, pp. 1737-1746, 2009.

[117] S. Rohner, S. Bernet, M. Hiller, and R. Sommer, "Modulation, Losses, and Semiconductor Requirements of Modular Multilevel Converters," *IEEE Transactions on Industrial Electronics,* vol. 57, pp. 2633-2642, 2010.

[118] Q. Tu and Z. Xu, "Power losses evaluation for modular multilevel converter

with junction temperature feedback," in *2011 IEEE Power and Energy Society General Meeting*, 2011, pp. 1-7.

[119] R. Zhang, D. Boroyevich, V. H. Prasad, H. Mao, F. C. Lee, and S. Dubovsky, "A three-phase inverter with a neutral leg with space vector modulation," in *Proceedings of APEC 97 - Applied Power Electronics Conference*, 1997, pp. 857-863 vol.2.

[120] H. Yang and M. Saeedifard, "A Capacitor Voltage Balancing Strategy With Minimized AC Circulating Current for the DC–DC Modular Multilevel Converter," *IEEE Transactions on Industrial Electronics,* vol. 64, pp. 956-965, 2017.

[121] R. Zeng, L. Xu, L. Yao, and S. J. Finney, "Analysis and Control of Modular Multilevel Converters under Asymmetric Arm Impedance Conditions," *IEEE Transactions on Industrial Electronics,* vol. 63, pp. 71-81, 2016.

[122] X. Cheng, W. Lee, M. Sahni, Y. Cheng, and L. K. Lee, "Dynamic Equivalent Model Development to Improve the Operation Efficiency of Wind Farm," *IEEE Transactions on Industry Applications,* vol. 52, pp. 2759-2767, 2016.

[123] D. Xiang, J. C. Turu, S. M. Muratel, and T. Wang, "On-Site LVRT Testing Method for Full-Power Converter Wind Turbines," *IEEE Transactions on Sustainable Energy,* vol. 8, pp. 395-403, 2017.

[124] M. Nasiri and R. Mohammadi, "Peak Current Limitation for Grid Side Inverter by Limited Active Power in PMSG-Based Wind Turbines During Different Grid Faults," *IEEE Transactions on Sustainable Energy,* vol. 8, pp. 3-12, 2017.

[125] R. Blasco-Gimenez, S. A.-. Villalba, J. Rodríguez-D'Derlée, F. Morant, and S. Bernal-Perez, "Distributed Voltage and Frequency Control of Offshore Wind Farms Connected With a Diode-Based HVdc Link," *IEEE Transactions on Power Electronics,* vol. 25, pp. 3095-3105, 2010.

[126] *Power System Stability And Control*: McGraw-Hill, 1994.

[127] D. Guo, m. Rahman, G. Adam, L. Xu, A. Emhemed, G. M. Burt*, et al.*, *Detailed quantitative comparison of half-bridge modular multilevel converter modelling methods*, 2018.

[128] R. Zeng, L. Xu, L. Yao, and D. J. Morrow, "Precharging and DC Fault Ride-Through of Hybrid MMC-Based HVDC Systems," *IEEE Transactions on*

Power Delivery, vol. 30, pp. 1298-1306, 2015.

[129] N. R. Merritt, C. Chakraborty, and P. Bajpai, "New Voltage Control Strategies for VSC-Based DG Units in an Unbalanced Microgrid," *IEEE Transactions on Sustainable Energy,* vol. 8, pp. 1127-1139, 2017.

[130] K. Tahata, R. Uda, K. Kuroda, K. Kikuchi, R. Yamamoto, H. Ito*, et al.*, "Mitigation on requirement of DCCB by DC reactor for multi-terminal HVDC operation," in *12th IET International Conference on AC and DC Power Transmission (ACDC 2016)*, 2016, pp. 1-6.

[131] I. Erlich, A. Korai, T. Neumann, M. K. Zadeh, S. Vogt, C. Buchhagen*, et al.*, "New Control of Wind Turbines Ensuring Stable and Secure Operation Following Islanding of Wind Farms," *IEEE Transactions on Energy Conversion,* vol. 32, pp. 1263-1271, 2017.

[132] Y. Jing, R. Li, L. Xu, and Y. Wang, "Enhanced AC voltage and frequency control on offshore MMC station for wind farm," *The Journal of Engineering,* vol. 2017, pp. 1264-1268, 2017.

[133] I. Erlich, B. Paz, M. K. Zadeh, S. Vogt, C. Buchhagen, C. Rauscher*, et al.*, "Overvoltage phenomena in offshore wind farms following blocking of the HVDC converter," in *2016 IEEE Power and Energy Society General Meeting (PESGM)*, 2016, pp. 1-5.

[134] T. Neumann, I. Erlich, B. Paz, A. Korai, M. K. Zadeh, S. Vogt*, et al.*, "Novel direct voltage control by wind turbines," in *2016 IEEE Power and Energy Society General Meeting (PESGM)*, 2016, pp. 1-5.